Development of techniques for generation of multiple optical traps and utilization of these traps for different applications

By

RAVI SHANKER VERMA

PHYS03201104003

Raja Ramanna Centre for Advanced Technology

A thesis submitted to the

Board of Studies in Physical Sciences

In partial fulfillment of requirements

for the Degree of

DOCTOR OF PHILOSOPHY

of

HOMI BHABHA NATIONAL INSTITUTE

November, 2018

Homi Bhabha National Institute[1]

Recommendations of the Viva Voce Committee

As members of the Viva Voce Committee, we certify that we have read the dissertation prepared by Sh R. S. Verma entitled " Development of techniques for generation of multiple optical traps and utilization of these traps for different applications" and recommend that it may be accepted as fulfilling the thesis requirement for the award of Degree of Doctor of Philosophy.

Chairman – Prof. K. S. Bindra	20/09/2019
Guide / Convener – Prof. M. P. Joshi	20/9/19
Examiner - Prof. Asima Pradhan	3/10/19
Member 1- Prof. S. R. Mishra	
Member 2- Prof. A. Moorti	20/9/2019
Member 3- Prof. P. K. Mukhopadhyay	20/09/2019
Member 2- Prof. C. Mukherjee	20/9/19
Member 3- Prof. K. Divakar Rao	20/9/19

Final approval and acceptance of this thesis is contingent upon the candidate's submission of the final copies of the thesis to HBNI.

We hereby certify that we have read this thesis prepared under our direction and recommend that it may be accepted as fulfilling the thesis requirement.

Date: 20/9/19

Place: Indore

Signature
Co-guide (if any)

Signature
Guide

[1] This page is to be included only for final submission after successful completion of viva voce.

STATEMENT BY AUTHOR

This dissertation has been submitted in partial fulfillment of requirements for an advanced degree at Homi Bhabha National Institute (HBNI) and is deposited in the Library to be made available to borrowers under rules of the HBNI.

Brief quotations from this dissertation are allowable without special permission, provided that accurate acknowledgement of source is made. Requests for permission for extended quotation from or reproduction of this manuscript in whole or in part may be granted by the Competent Authority of HBNI when in his or her judgment the proposed use of the material is in the interests of scholarship. In all other instances, however, permission must be obtained from the author.

Ravi Shanker Verma

DECLARATION

I, hereby declare that the investigation presented in the thesis has been carried out by me. The work is original and has not been submitted earlier as a whole or in part for a degree / diploma at this or any other Institution / University.

Ravi Shanker Verma

List of publications arising from the thesis

Journals

1. "Optical guiding based cell focusing for Raman flow cell cytometer", **R. S. Verma**, S. Ahlawat and A. Uppal, Analyst 143, 2648-2655 (2018).

2. "Manipulation of microparticles and red blood cells using opto electronic tweezers", **R. S. Verma**, R. Dasgupta, N. Kumar, S. Ahlawat, A. Uppal and P. K. Gupta, Pramana J. Phy. 82, 433-437 (2014).

3. "Pattern matching based active optical sorting of colloids/cells", **R. S. Verma**, R. Dasgupta, S. Ahlawat, N. Kumar, A. Uppal and P. K. Gupta, J. Opt. 15, 085301 (2013).

4. "Microfluidic sorting with blinking optical traps", R. Dasgupta, **R. S. Verma** and P. K. Gupta, Opt. Lett. 37, 1739-1741 (2012).

Conference/Symposium

1. "An active optical sorting approach for low desired particle concentration in the sample using holographic optical tweezers", **R. S. Verma** and N. Kumar, Proceedings of National Laser Symposium-26 held at BARC, Mumbai, India, Dec. 20-23, 2017, CP-10.22.

2. "Opto electronic tweezers based smarts weeper for cells/micro-particles sorting", **R. S. Verma** and N. Kumar, Presented in internet session, Optics and Photonics 2017, Saratov Fall Meeting, Russia, Sept. 26-30, 2017.

Also selected for publications in the proceedings of SPIE

"Opto electronic tweezers based smart sweeper for cells/micro-particles sorting", **R. S. Verma** and N. Kumar, Proc. SPIE 10716, Saratov Fall Meeting 2017: Optical Technologies in Biophysics and Medicine XIX, 1071613.

3. "Separation of micro particles in a concentrated sample using opto electronic tweezers", **R. S. Verma**, N. Kumar, S. Ahlawat and P. K.

Gupta, Proceedings of National Laser Symposium-22 held at Manipal University, Manipal, Karnataka, India, Jan 8-11, 2014, CP-11-23.

4. "Image pattern based selection and sorting of micro particles using holographic optical tweezers", **R. S. Verma**, R. Dasgupta, S. Ahlawat, and P. K. Gupta, Proceedings of National Laser Symposium-20 held at Anna University, Chennai, India, January 9-12, 2012, pp. 904-907.

Ravi Shanker Verma

To my parents

For their unbiased support and

And to my lovely daughter

IRA

ACKNOWLEDGEMENTS

I am extremely thankful to my thesis guide *Prof. M. P. Joshi* for his valuable guidance, constant support, encouragement and motivation. I am grateful to him for critically reviewing and proofreading of the thesis.

I am also thankful to my previous thesis guide *Prof. P. K. Gupta* for his valuable guidance, constant support and encouragement. I am highly obliged to him for sharing his knowledge and providing constructive criticism and valuable suggestions during this work. His foresight and keen scientific intuition were vital for the progress of this work.

I am grateful to *Sh. R. Kaul* from Laser Materials Processing Division for his continuous support, encouragement and good wishes. I express my sincere thanks to my committee members, *Prof. K. S. Bindra, Prof. S. R. Mishra, Prof. A. Moorti, Prof. P. K. Mukopadhyay, Prof. C. Mukharjee* and *Prof. K. D. Rao* for their helpful suggestions. I would also like to thank the members of the previous thesis advisory committee *Prof. D. K. Palit, Prof. K. I. Priyadarshini, Prof. N. K. Sahu, Prof. Kaustav Das, Prof. Rama Chari* and *Prof. A. Dube* for their encouragement and insightful comments.

I would also like to thank *Dr. S. Ahlawat* and *Dr. R. Dasgupta* for their suggestions and continuous support in the planning of experiments, analysis of the experimental data and scientific interpretation of the results. I also thank to *Dr. A. Uppal* and *Sh. N. Kumar* for their support and co-operation during all my experiments.

I would also like to thank *Sh. H. S. Patel* for his continuous support and valuable suggestions throughout this work. I also take this opportunity to thank my colleagues *Dr. Y. Verma* and *Dr. M. K. Swami* for proofreading of various drafts of this thesis and

synopsis which helped me to present the research work in an effective manner. I also thank my colleagues *Dr. K. Sahu, Dr. B. Bose, Dr. M Sharma Dr. R. Srivastava* and *Smt. P. Patheja* for creating friendly environment during the work. I also express my thanks to friends from training school especially *Sh. H. Srivastava, Sh. Abdurrahim* and *Dr. B. S. Rao* for their constant encouragement.

I also express my sincere thanks to *Prof. D. S. Chitnis* and *Prof. S. K. Jaiswal* from Choithram Hospital and Research Centre, Indore for their valuable support during this work.

Thanks to my project trainee *Sh. S. Roy* and *Dr. A. Prasad* for participating in some of the studies included in this thesis. Thanks to Mr. V. Sharma for his support in getting the mechanical job done for our experimental setups.

A special thanks to my family members especially to my lovely daughter *Ira* for creating a cheerful atmosphere at home and being a consistent motivation in accomplishing this work. I would like to express my sincere gratitude to my parents and sisters for their encouragements, endless affection and moral support.

I am also thankful to all who have contributed in completing this work but I could not mention them personally - thank you all!

Last and certainly not the least, I am thankful to God, the almighty, for providing me this opportunity and granting me the capability to accomplish this work successfully.

Contents

SUMMARY 1

List of figures 3

1 Chapter 1: Introduction 7

1.1. Optical forces on spherical particles 8

1.3. Optical trap calibration 17

1.4. Multiple optical traps 19

1.4.1. Use of polarization beam splitters (PBS) 21

1.4.2. Galvo scanning mirrors 21

1.4.3. Acousto-optic deflectors 23

1.4.4. Spatial light modulators 25

1.5. Opto-electronic tweezers 30

1.6. Literature survey 36

1.7. Aim and outline of the thesis 40

2 Chapter 2: Optical guiding-based cell focusing for Raman flow cell cytometer 42

2.1 Introduction 42

2.2 Experimental methods 46

2.2.1 Sample preparation 46

2.2.2 Setup 46

2.2.3 Microfluidic chip fabrication 47

2.2.4 Data acquisition 50

2.3 Results and discussion 51

2.4 Conclusion 62

3 Chapter 3: Acousto-optic tweezers for passive sorting of colloids 63

3.1 Introduction 63

3.2 Materials and method 65

3.3 Results and discussion 67

3.4 Conclusion 74

4 Chapter 4: Active optical sorting using holographic optical tweezers 75

4.1 Introduction 76

4.2 Pattern matching based active optical sorting 78

4.2.1 Method 78

4.2.2 Materials and methods 86

4.2.3 Results and discussion 88

4.2.4 Multi particle sorting 93
4.3 Sorting of particles in low concentration 95
4.3.1. Method 95
4.3.1 Results 98
4.4 Conclusion 99
5 Chapter 5: Micromanipulation of cells/ microparticles using Opto-electronic tweezers 101
5.1 Introduction 101
5.2 OET chip development 104
5.3 Experimental setup 105
5.4 Results 109
5.5 Separation of polystyrene micro-particles based on their size 111
5.6 Opto-electronic smart sweepers for cell/microparticle sorting 113
5.6.1 Scheme 113
5.6.2 Results and discussion 115
5.7 Projector based OET setup for manipulation of cells 118
5.8 Conclusion 120
6 Chapter 6: Conclusion 121
REFERENCES 124

SUMMARY

Optical tweezers have received lot of attention because of their ability to perform contact-less manipulation of micro/nano particles. It has been at the centre stage of development of various techniques for generation of multiple optical traps to accomplish more sophisticated tasks like cells stretching, three dimensional orientation/arrangement etc. These techniques have also opened several new application areas such as guiding, sorting of microparticles and are particularly suitable for small sample volume and are easy to integrate with microfluidic devices like micro total analysis systems (μTAS), modern spectroscopic techniques such as micro Raman spectroscopy etc. In this thesis, we have presented different approaches for the development of multiple optical tweezers and explored their use. These include development of (i) Dual line optical tweezers (static), dynamically controllable optical traps as (ii) Acousto-optic tweezers (AOT-time sharing), and (iii) Holographic optical tweezers (HOT-power sharing) and (iv) Opto-electronic tweezers (OET) and their use for development of novel guiding and sorting approaches for cells/microparticle in varied sample conditions.

The dual line optical tweezers were used in microfluidic Raman flow cytometry for achieving cell focusing in microfluidic chip i.e. a single line flow of cells through the analysis region. In conventional hydrodynamic focusing of cells in microfluidics, the cell flow speed is inversely proportional to the cell stream width which leads to increase in the flow speed through observation volume if the channel width is narrowed to ensure single cell stream. This in turn requires more optical power to hold the cells for recording the Raman spectra. We proposed dual line optical tweezers arranged in the shape of 'Y' as an optical guide for focusing of the cells into a single cell stream in microfluidic chip. This arrangement decouples the width of the cell stream and the cell flow speed in the microfluidic chip and facilitates independent control of the cell flow speed. The suitability of this approach for cytometry was demonstrated by identifying red blood cells (RBCs) in their met and normal form in a mixture of met-RBC and normal RBC in the ratio of 1: 9 with a cell throughput of ~500 cells/hour.

The multiple optical traps created by the acousto-optic tweezers were used for optical sorting of micro particles in flow free medium. We developed a new approach

based on the dependence of diffusion constant on the size of the particles for development of optical sorting by suitably adjusting the on/off period of blinking optical traps generated using accousto optic deflector. The proof of the concept demonstration was presented by sorting of ~2 μm silica microspheres in a mixture consisting of 1 μm and 2 μm diameter silica spheres. While AOTs can manipulate objects in one plane, HOTs, in which spatial light modulator was used to generate multiple optical traps from a single beam, can manipulate objects in multiple planes simultaneously. Utilizing this feature of HOT, we developed two active sorting approaches. In one approach, pattern matching was used for particle selection and multiple trapping planes for parallel transportation of particles to the desired region allowing higher throughput. In another approach, desired particles were selected manually and transported to higher Z-plane allowing sorting of desired particles in multiple region of interests. This approach is suitable for very low density of desired particle concentration.

The aforementioned tweezers setup could handle up to a few 100s of particles. Further higher throughput is mainly limited by the laser power handling capability of spatial light modulator. Damage of cell due to high intensity of the laser (~MW/cm^2) used in the optical tweezers is also a concern. We, therefore, developed another interesting tweezers setup based on light driven electro kinetic approach known as Opto-electronic tweezers facilitating manipulations of 1000's particle at a time with lower optical power (~mW) over an area as large as ~10^6 μm^2. We used an array of suitably spaced circular intensity spots for sorting the particles based on their size. In another approach, we exploited the dependency of the DEP response of cell on the frequency of applied field for sorting of red blood cells from a mixture of RBCs and polystyrene microspheres. Further, we used digital light projector for generating the required light pattern for virtual electrode and demonstrated that micromanipulation such as guiding; focusing of cells could easily be implemented.

List of figures

Figure 1.1: Schematic representation of the scattering and the gradient forces on a microsphere due to a Gaussian beam. The thicker line ray 'a' compare to the 'b' shows the higher intensity close to the axis of the laser beam _____ *9*

Figure 1.2: *Three dimensional trapping using a Gaussian laser beam focused (a) before and (b) after the geometric centre of the particle (Adapted from [2])* _____ *10*

Figure 1.3: *Schematic geometry for calculation of the forces due to interaction of a single ray of power P with a microsphere, (adapted from [2])* _____ *11*

Figure 1.4: Schematic of the single beam optical tweezers, Laser after expansion using the beam expander is coupled to the back aperture of the objective by relaying the beam using mirrors. The dichroic mirror is used to couple the laser beam and the light used for illumination of the sample. CCD camera is placed at the focus of the tube lens (TL) to image the sample. _____ *15*

Figure 1.5: *Different schemes for generation of time sharing multiple traps by (a) splitting a single laser beam using PBS (b) using galvano scanning mirror (c) acousto-optic deflector (b) spatial light modulator; the dotted line are the conjugate planes.* _____ *22*

Figure 1.6: Schematic of acousto optic deflector working principle _____ *24*

Figure 1.7: Schematics of the reflective type parallel aligned nematic liquid crystal SLM (adapted from [55]) _____ *26*

Figure 1.8: Flowchart describing the GS algorithm _____ *27*

Figure 1.9: Schematics of the OET chip _____ *31*

Figure 1.10: Schematics representation of how heterogeneous cells can be simplified to a homogeneous cell. _____ *34*

Figure 1.11: *CM factor for (a) various situation of the conductivity of the medium and the particle* $\sigma_m=1x10^{-3}\ Sm^{-1}$, $\sigma_p=100x10^{-4}\ Sm^{-1}$ *(Red);* $\sigma_m=10x10^{-3}\ Sm^{-1}$, $\sigma_p=100x10^{-4}\ Sm^{-1}$ *(Blue);* $\sigma_m=1x10^{-3}\ Sm^{-1}$, $\sigma_p=1x10^{-4}\ Sm^{-1}$ *(Green);* $\sigma_m=10x10^{-3}\ Sm^{-1}$, $\sigma_p=1x10^{-4}\ Sm^{-1}$ *(Cyan),* $\varepsilon_m = 80\varepsilon_0$ *and* $\sigma_m = 10Sm^{-1}$*, (b) Model cell with* $\varepsilon_{\text{int}} = 45\varepsilon_0$, $\sigma_{\text{int}} = 0.5Sm^{-1}$, $\varepsilon_{mem} = 8\varepsilon_0$, $\sigma_{mem} = 1\times10^{-8}Sm^{-1}$, *d=8 nm,* $\varepsilon_m = 80\varepsilon_0$, $\sigma_m = 10Sm^{-1}$ *and R: 2μm (red), 5μm (green) and 10μm (blue).* _____ *35*

Figure 2.1: (a) Schematic of the experimental setup. PBS1-2: Polarizing beam splitters, CL1-2: cylindrical lenses, M1-7: mirrors, SM: switching mirror: switches the collected light between bright-field imaging CCD and Raman spectrograph, Obj1: for focusing the 1064 nm laser onto the sample plane and collecting the Raman spectra, Obj2: for focusing the Raman excitation beam onto the sample, P1-2: polarizer, HWP1-2: half-wave plates for adjusting the power of the Raman excitation beam and trapping beam, respectively, HWP3-4: half-wave plates for adjusting the power in the dual-line optical tweezers, NF: notch filter, DM1: dichroic mirror: reflects the 514.5 nm laser and transmits the rest of the light from the illumination source, TL: tube lens, Cml: compensatory lens for collimating the emission signal, DM2: 1064 nm laser line mirror, L1-2, L5-6: lens pairs as beam expanders, L3: coupling lens to complete 4f system, L4: lens coupling the Raman-scattered light to the spectrograph. (b) Schematic expanded view of the dual-line tweezers (black) in the sample plane guiding the cells (red). _____ *48*

Figure 2.2: PDMS-based microfluidic chip connected with inlets and outlets for Raman flow cell cytometer. Scale bar: 2.7 mm. _____ *50*

Figure 2.3: *Raw spectrum of an RBC recorded while it was passing through the Raman excitation beam in the micro-fluidic chip.* ____ *52*

Figure 2.4: (a) Schematic of the forces acting on a cell while the cell interacts with line 1 and 2 in fluid flow. F_{t1} *and* F_{t2} *are the transverse components of the optical forces due to line tweezers 1 and 2 respectively.* F_d*: Drag force.* θ*: Tilt angle of line tweezers with respect to fluid flow direction. (b) Transverse components of optical forces due to the line tweezers and the drag force on the red blood cell. Line tweezers.* ____ *53*

Figure 2.5: (a) Image of the dual-line optical tweezers arranged in the shape of the letter 'Y'. The green-coloured spot indicates the Raman excitation beam; the line tweezers have been labelled as LT1 and LT2. Scale bar: 10 μm. (b) A snapshot from a video showing cells being guided to the tail of the optical guide arrangement (multimedia view). The semi-transparent red region schematically shows the line profile of the dual-line optical tweezers. ____ *55*

Figure 2.6: Average Raman spectra of normal-RBCs (blue) and met-RBCs (red) recorded over 25 cells. The spectra shown are area-normalized to emphasize the relative changes in the intensities of various bands. ____ *57*

Figure 2.7: *(a) Score plot of normal-RBC (blue- squire shape) and met-RBC (red-circular shape) (b) loading plot of PC1* ____ *58*

Figure 2.8: Area-normalized average spectra of (a) normal-RBCs (blue) and (b) met-RBCs (red) in flow. The thicker lines show the mean spectra of the normal- and met-RBCs, and the shaded regions show the standard deviations of the recorded spectra. The vertical lines show the band at 1358 cm^{-1} ____ *61*

Figure 3.1: Schematic of setup, Lenses pairs L1, L2 and L3, L4: beam expander, M1, M2, M3, M4 and M5: mirrors, HWP: half wave plate, Dual Axis AOD: dual axis acousto-optic deflector, MO: microscope objective, DM: dichroic mirror. L5: lens to focus the light onto the CCD, A cut-off filter (F) was used to suppress the back scattered laser light onto the CCD. ____ *66*

Figure 3.3: (a) Escape probabilities of spheres against T_{OFF} *(b) Trajectories of a (i) 1 μm and (ii) 2 μm particle in trap.* ____ *69*

Figure 3.4: *(a) Time laps images from a video while scanning a set of four traps. Scale bar: 12μm, (b) Image frames showing the motion of the particles when the traps are moving toward the right. (c)Particle trajectories with dark lines and faded lines representing 2 μm and 1 μm spheres, respectively. Scale bar: 12μm.* ____ *70*

Figure 3.5: (a) The scanning pattern of the trap array for sweeping over an area. (b) Image frames showing sorting between 1 μm and 2 μm silica spheres. (c) Trajectories of the 1 μm (fade lines) and 2 μm (dark lines) spheres. Scale bar: 12μm ____ *71*

Figure 4.1: Flowchart of the sorting process ____ *79*

Figure 4.2: *Determination of particle position by use of pattern matching technique (a) an image of the sample consisting of mixture of particles of sizes ~3 μm and ~5μm, the rectangle (green) shows the region of interest and the rectangle at top left corner (blue) is the variable rectangular region selector, (b) and (c) the cross correlation matrix for the big and small particle, the insets show the kernel for the particles, (d) and (e) the binary images of the two particles after thresholding. Scale bar: ~5μm.* ____ *80*

Figure 4.3: Arrangement of particles and trap beams considered to illustrate computation of a suitable translation step of traps; (a) the trapped particles in the initial condition and (b) the position of the trap beam and particles if a translation step equal to the radius of the particle is chosen. The solid arrows show the direction of beam propagation. The direction of the translation is shown by dashed arrows. The leading particle with respect to the direction of propagation is marked as '1' and the trailing particle as '2'. ____ *82*

Figure 4.4: Trapping forces on particles of sizes (a) 2, (b) 3 and (c) 5 µm while two particles of the same size adjacent to each other are being translated in a direction along the common diameter. The force on the leading particle is shown by a 'red color' and on the trailing particle by a 'green color'. _____ *83*

***Figure 4.5:** A schematic of the setup used in the experiment.SLM: spatial light modulator, HWP: half wave plate, P:polariser, L1,L2:lens working as a beam expander, L3,L4: lens for making 4f arrangement, M1,M2: mirrors for relaying the beam to the microscope, DM: dichroic mirror, MO: microscope objective, TL: tube lens, M3: mirror for reflecting the visible light to the camera, SPF: short pass filter, CCD: charged coupled device.* _____ *87*

Figure 4.6: Optical sorting of 3 and 5 µm diameter silica particles from a mixture of the two. (a) Initial image of the sample plane containing particles of both diameters. (b) 3 µm particles were lifted into the upper plane and 5 µm particles were trapped in the sample plane. (c) Particles in both planes were translated in two opposite directions. (d) Particles in the upper plane were brought back to the bottom sample plane. The total time required for sorting is ~13 s. Scale bar: 5 µm. _____ *89*

***Figure 4.7:** Images showing the sorting of 2 and 3 µm silica particles from a mixture of the two (a) bright field image of the particles (b) particles of diameter ~2 µm are in the upper plane while the 3µm particles are in the bottom plane (c) sorted particles at the bottom plane. The total sorting time is ~27 s. Scale bar: ~5µm.* _____ *90*

***Figure 4.8:** Images showing the sorting of silica and glass microspheres (diameter ~5 µm) from a mixture of the two. (a) Bright-field image of the sample plane. (b) Glass particles were trapped and lifted to the upper plane while silica particles are in the bottom plane in the trap. (c) Sorted particles. The total time required for sorting is ~21 s and the movie is accelerated by 3×. Scale bar: ~5 µm, (movie 3)* _____ *90*

Figure 4.9: Sorting of RBCs and WBCs from a mixture of the two. (a) Cells in the sample plane, this image have been taken for the kernel selection. (b) The cells were trapped and translated in opposite directions in their respective planes. (c) The RBCs in the upper plane were brought back to the lower plane. (d) After releasing the cells from the trap the RBCs took some time (~20 s) to move from the vertical orientation to the natural horizontal orientation. The total sorting time is ~30 s. Scale bar: ~8 µm, (movie 4) _____ *92*

Figure 4.10: Snapshots from a video showing sorting of particles in sequential manner using two Z planes (a) particle before the start of the sorting process (b) 2µm silica microspheres trapped and lifted to higher Z plane and (c) after translation to the bottom side of the ROI brought down to bottom side (black arrow shows the sorted particles on the bottom plane (d) ~3µm polystyrene sphere after getting sorted to upper side of the ROI (e) ~6µm polystyrene microsphere lifted to higher Z plane (black arrow shows the lifted particle) (f) all the particles sorted at four sides of the ROI; Scale bar: 5µm _____ *94*

***Figure 4.11:** Snapshots from a video showing sorting of particles in sequential manner using four Z planes (a) particle before the start of the sorting process (b) all the particles have been lifted in multiple Z planes leaving only one type of particle in the bottom plane (~5µm silica) (c) after translation to the pre defined sides of the ROI in their respective Z planes, all the particles were brought to the bottom plane. Scale bar: 5µm* _____ *94*

Figure 4.12: Schematics of the (a) upper plane particle filling order and (b) bottom and upper plane appearance when three particles are in the upper plane while the fourth one is to be trapped. _____ *96*

***Figure 4.13**: Flow chart of the sorting process* _____ *98*

Figure 4.14: Snapshots from a video of sorting ~3µm silica micro-sphere from a mixture of the silica microspheres of sizes ~3 and 5 µm; first silica particle (a) at the desired

position in the field of view for getting trapped and translated (b) in the upper plane in the middle of its path (c) reached to the predefined location in the upper plane ; (d) third particle in the middle of its path to the predefined location in the upper plane while there are already two particle lying in the same plane (e) seven particles have been trapped and maintained in the upper plane in a predefined manner using optical traps (f) trapped particles in the bottom plane when the trap was off. The green colour '+' sign on the images is the location where the desired particle has to be brought during scanning of the sample. Scale bar: ~5μm. _____*99*

Figure 5.1: (a) Image of the slide prepared using spin coating, (b) using thermal evaporation in bright filed illumination; Scale bar: 100μm, (c) Schematics of the OET chip and (d) the absorption spectra of titanium oxide pthalocynine. _____*106*

*Figure 5.2: Schematic of the experimental setup, the enclosed part is illumination unit.*_____*107*

Figure 5.3: Sequential images showing the particle concentration using varying mode of LG beam. The rings showing the schematic LG beam intensity pattern for (a) LG_{25} (b) LG_{18} and (c) LG_{10}. Scale bar: 30μm. _____*110*

Figure 5.4: *Manipulation of RBCs (a) illumination intensity pattern, (b)-(d) RBCs getting attracted towards the illumination region (e) RBCs getting repelled from the illuminated region. Scale bar: 30 μm.* _____*110*

Figure 5.5: (a) Schematics of the sorting approach showing shorting process while the intensity pattern scanned across the sample (b) sequential microscope images showing separation of 6 μm Polystyrene microspheres (PMs) from a mixture of PMs of sizes 6μm and 15 μm, Scale bar: 30 μm _____*112*

Figure 5.6: Schematics of the OET setup having modified illumination scheme _____*114*

Figure 5.7: Clausius-Mossotti factor frequency response of RBC and PSM _____*114*

Figure 5.8: Schematically showing a PSM interacting with the spinning intensity profile and getting repelled; resulting in these to move to the periphery of the circular region. _____*116*

Figure 5.9: Snapshots from a video showing the sorting of RBCs in a mixture of RBCs and PSMs by spinning the line shaped intensity profile (a) before spinning (b) after completing two spin; the black circle shows the region of interest. Scale bar: ~30 μm _____*116*

Figure 5.10: Snapshot from a video demonstrating the operation of the Opto-electronic sweepers by sweeping out the PSMs and leaving only the RBCs in the region of interest by translating the shaped intensity profile across the sample, sample appearing (a) before scanning (b) after completing the scan; Scale bar: ~30 μm. ____*117*

Figure 5.11: Schematics of the OET setup using the DMD based multimedia projector _____*118*

*Figure 5.12: A power point projection slide for generating ladder type virtual electrodes to guide the micro particles using negative DEP.*_____*119*

Figure 5.13: *Demonstration of the Projector based OET setup for guiding, focusing and patterning of colo 205 cells. Scale bar 50 μm.* _____*119*

1 Chapter 1: Introduction

Optical tweezers is an instrument which makes use of tightly focused laser beam to trap micrometer sized object at the laser focus without physical contact. Since its invention in the late eighties by Authur Ashkin [1], optical tweezers have found wide range of applications from trapping of neutral particles [2], single cells [3-5] manipulation of bacteria and viruses[6-8] red blood cells [9-13] intracellular organelles [14] etc.

In the early 17th century, German astronomer Johannes Kepler observed that the tail of comet always pointed away from the sun and proposed that this is because of the radiation pressure of the electromagnetic radiation emitting from sun. Later on, in the late 19th century, origin of the radiation pressure was explained theoretically by J. C. Maxwell in his electromagnetic theory [15]. According to his theory; light carries momentum and thereby can exert force, or *radiation pressure.* The existence of the radiation pressure was proved with elaborate experimental arrangements by Lebedev [16] and Nichols and Hull [17, 18] even before the advent of lasers. After decades of these experiments, the invent of the lasers in 1960 enabled A. Ashkin of AT&T (Bell) Laboratories to experimentally demonstrate the radiation pressure on micron-sized particles by accelerating and trapping the particles from two Gaussian beam facing each other [19]. Later Ashkin along with Dziedzic demonstrated the optical levitation of the dielectric spheres in air and vacuum [20], and of liquid drops [21]. In 1986, Ashkin observed that dielectric particles could be stably trapped by the gradient force of a tightly focused single beam [1] and the technique was termed as optical tweezers. Thereafter this technique was applied for various applications such as manipulation of bacteria and viruses [6], estimation of force produced by the organelle transport *in-vivo*

[22], automated cell trapping and sorting [23] etc. S. M. Block et al. made the first calibrated measurement of the compliance of bacterial flagella [7]. The detailed theoretical framework in the ray optics [2] and Rayleigh regime [24] was also presented. Soon the technique grew up as a standard tool for manipulation in bio-photonics [4, 5, 25, 26]. Furthermore, the optical tweezers have also been integrated with different advanced spectroscopic techniques such as Raman spectroscopy to perform Raman spectroscopic measurements on optically trapped cells [27, 28, 29]. Optical tweezers forces can be used to exert forces exceeding ~100 pN with resolution as low as ~100 aN [30] which makes it a suitable tool for investigating the properties of molecular motors and other microscopic particles [31-34].

In this chapter we will provide an overview of the optical trapping phenomena followed by a description of multiple optical traps that provide more precise control and better handling of the trapped objects. We will also describe different ways of generating multiple optical traps using electro-optic devices along with opto-electronic tweezers. Next we present an overview of the research work carried out using multiple optical traps. At the end, the aim and outline of the thesis has been presented.

1.1. Optical forces on spherical particles

Optical trapping of microscopic dielectric particle by optical radiation can be understood in a simple way using Ray optics approach. In this case the size of the microsphere is much larger than the wavelength of the laser beam (size>>λ) and the light can be considered as rays. The interaction of light with an object is understood in terms of reflection and refraction (for non absorbing particle). A microsphere of refractive index n_p inside a medium of refractive index n_m is placed slightly offset from

the axis of the laser beam having Gaussian intensity profile as shown in figure 1.1. Refractive index of the particle is taken greater than that of the surrounding medium. To understand the forces acting on the particle, let us consider two rays (‘a’ and ‘b’) from two different intensity regions of the beam. When these rays interact with the particle, reflection and refraction occur. These results in the change of the direction of the rays ‘a’ and ‘b’, so there is a change in the momentum of these rays.

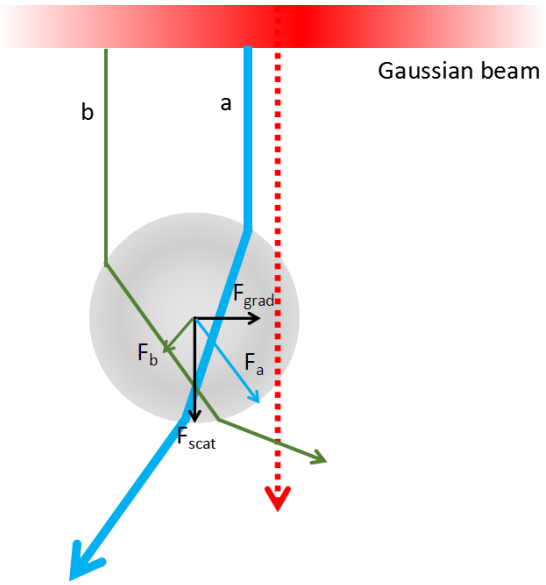

Figure 1.1: *Schematic representation of the scattering and the gradient forces on a microsphere due to a Gaussian beam. The thicker line ray ‘a’ compare to the ‘b’ shows the higher intensity close to the axis of the laser beam*

After interacting with the particle, ray ‘a’ bends towards left and ray ‘b’ bends towards right of its original trajectory. With help of vector theorem, it can be shown that F_a and F_b are the forces which work on the particle due to these rays. Here, it is assumed that the particle is weakly reflective and absorptive. Therefore the forces from these effects have been neglected and the forces F_a and F_b, arising due to the refraction of rays are only considered. Ray ‘a’ being in the high intensity region undergoes more momentum change as compare to the ray ‘b’ leading to $F_b < F_a$. The resultant force will have two

components. The transverse force is acting along the intensity gradient of the laser beam i.e. along the transverse direction towards central propagation axis (shown as dashed red color) and so referred as gradient force (F_{grad}). The axial force is acting along the propagation direction of the laser and referred to as Scattering force (F_{sct}). These forces push the particle towards the central axis and

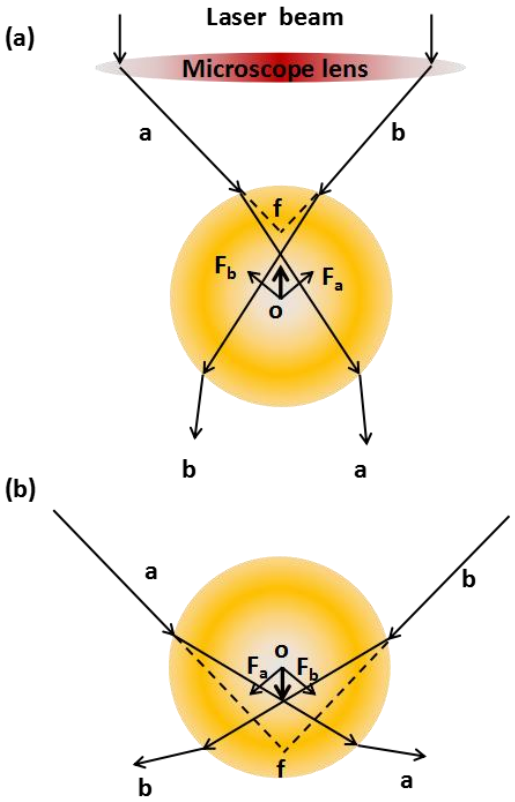

Figure 1.2: *Three dimensional trapping using a Gaussian laser beam focused (a) before and (b) after the geometric centre of the particle (Adapted from* [2]*)*

along the laser propagation direction respectively. When the particle is aligned to the axis of the laser beam, the net gradient force becomes zero while the scattering force is there to guide the particle in the direction of propagation. This phenomenon is called optical guiding. In case when the light is tightly focused, additionally there is an intensity gradient along the axis of the laser beam which is steep enough to make

axial gradient force exceed to the scattering force and the particle gets trapped at the focus (at equilibrium) i.e. particle is trapped in three dimension. Here, the dielectric particle has been considered as weakly refractive so the particle is trapped slightly off from the beam focus on the beam propagation axis where the axial gradient force balances the axial scattering force. In other situations as shown in figure 1.2 when the centre of the particle is away from the beam focus but lies at the beam propagation axis, a net gradient force acts on the particle to bring it back to the laser focus. It is to be noted that in this entire scenario the refractive index of the particle is taken as more than the refractive index of the medium. Whereas in the opposite situation, when $n_p < n_m$, the net gradient force will be having direction away from the positive intensity gradient resulting in the repulsion of the particle from the positive intensity gradient and thereby pushing the particle away from the laser focus.

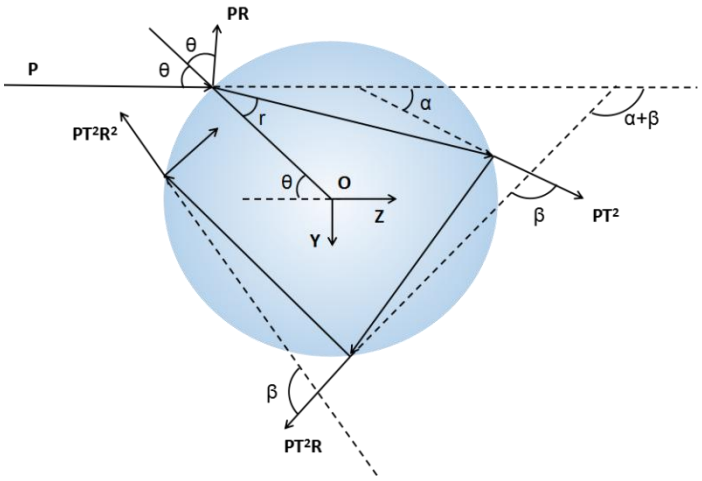

Figure 1.3: *Schematic for calculation of the forces due to interaction of a single ray of power P with a microsphere, (adapted from* [2]*)*

Figure 1.3 shows the schematic of the geometry of forces acting on the particle due to reflection and refraction. For a quantitative estimation of the forces, it is assumed that a single ray of optical power P interacts with the microsphere. The incident ray carries

initial momentum per second as $n_m P/c$. The total force on the sphere would be a vector sum of the contributions due to the successive reflections and refractions. Therefore the net forces acting on the particle is given by [2]:

$$F_z = F_s = \frac{n_m P}{c}\left\{1 + R\cos 2\theta - \frac{T^2(\cos(2\theta - 2r) + R\cos 2\theta)}{1 + R^2 + 2R\cos 2r}\right\} \tag{1.1}$$

and

$$F_y = F_g = \frac{n_m P}{c}\left\{R\sin 2\theta - \frac{T^2(\sin(2\theta - 2r) + R\sin 2\theta}{1 + R^2 + 2R\cos 2r}\right\} \tag{1.2}$$

where 'θ' and 'r' are the angle of incidence and the angle of refraction of light and R and T are the angle dependent Fresnel reflection and refraction coefficients at the interface. For a single beam gradient trap, the scattering and the gradient forces can be calculated by the vector sum of these forces from all the individual rays of the beam.

If the size of the particle is much smaller than the wavelength of the laser such that size < 0.1λ, the particle behaves as a point dipole and the instantaneous electric field over the extent of the particle can be considered as uniform. In this case also the force acting on the particle can be described by the two components; scattering force which is proportional to the intensity of the laser beam and the gradient force which is proportional to the gradient of the intensity. The scattering force is given by [24] ,

$$F_{scat}(\bar{r}) = \hat{z}\frac{n_m}{c}\frac{128\pi^5 a^6}{3\lambda^4}\left(\frac{m^2 - 1}{m^2 + 2}\right)^2 I(\bar{r}) \tag{1.3}$$

Where n_m is the refractive index of the medium and 'c' is the speed of light in vacuum, for a particle of radius of 'a' and $m = n_p/n_m$ being the relative refractive index of the

particle; *I(r)* is the beam intensity at some point from the beam focus and λ is the wavelength of the laser. The gradient force is given by [24]

$$\bar{F}_{grad}(\bar{r}) = \frac{2\pi n_m a^3}{c}\left(\frac{m^2-1}{m^2+2}\right)\nabla I(\bar{r}) \tag{1.4}$$

Therefore, as shown in eq. 1.4, the necessary condition for the stable 3D trapping is that the axial component of the gradient force should be more than the scattering force. In other words

$$R = \frac{F_{grad}}{F_{scat}} \geq 1 \tag{1.5}$$

We observe that the stability condition is independent of laser power. However, this is just a necessary but not the sufficient condition for optical trapping. We also have to consider the Brownian motion of the particles which leads to a sufficient trapping condition as

$$\exp\left(-U/k_B T\right) << 1 \tag{1.6}$$

where

$$U(\bar{r}) = -2\pi n_m a^3\left(\frac{m^2-1}{m^2+2}\right)I(\bar{r}) \tag{1.7}$$

At the trap focus $$U_0 = -2\pi n_m a^3\left(\frac{m^2-1}{m^2+2}\right)I_0 = -2\pi n_m a^3\left(\frac{m^2-1}{m^2+2}\right)\frac{2P}{\pi\omega_0^2} \tag{1.8}$$

Equation 1.8 states that a minimum power is required for optical trapping to happen in three dimensions. This condition can be basically argued as that the time required to pull the particle into the trap should be much smaller than the time required by the particle to diffuse out of the trap. As the instantaneous kinetic energy of the particle can

be larger than the average kinetic energy, the condition is set as $U/k_BT \geq 10$ for stable trapping.

The above description explains the optical forces acting on a particle when it is either very small or very large compare to the wavelength of the light. When the size of the object is comparable with the wavelength of light i.e. size ~λ, diffraction of light by the particle must be taken into consideration. Therefore, neither the Rayleigh approximation nor the Ray optics approach is valid. More complete electromagnetic theories where Maxwell's equations solved with appropriate boundary conditions are applied to get the full and formal solution. Lorentz Mie theory (LMT) describes the solution for scattering of an infinite plane wave by the spherical particle [35]. However, the plane wave approximation cannot be applied to the focused Gaussian beam. Therefore, a more general form of the LMT was presented by G. Gouesbet et al. and is known as Generalized LMT [36] which introduces an infinite set of beam shape coefficients in the form of partial wave expansion to describe the non planar nature of the Gaussian beam and therefore can be used for calculation of optical trapping forces [37].

1.2. Important components of optical tweezers system

A schematic of the single beam optical tweezers is shown in figure 1.4. The essential components of the system are the laser beam for trapping, a high numerical aperture objective, beam steering and expansion optics and an arrangement for the imaging the sample plane. The important parameters of these components are described below:

Laser: The choice of laser depends on several factors such as power, wavelength and the quality of the laser beam (like mode quality, power stability, pointing stability

etc.). As shown in eq. 1.8, a certain minimum laser power is required to trap an object, higher the power, easier the trapping. However, in optical tweezers the laser beam is very tightly focused resulting in intensity of ~MW/cm^2 at the trap focus. Such a high intensity may be a cause of concern while dealing with biological particles like cells as it may lead to photo damage of the cells [38-40]. Therefore, in case of biological particles like red blood cells (RBC), cancer cells, bacteria etc. laser wavelength is of significant importance due to their strong absorption effects.

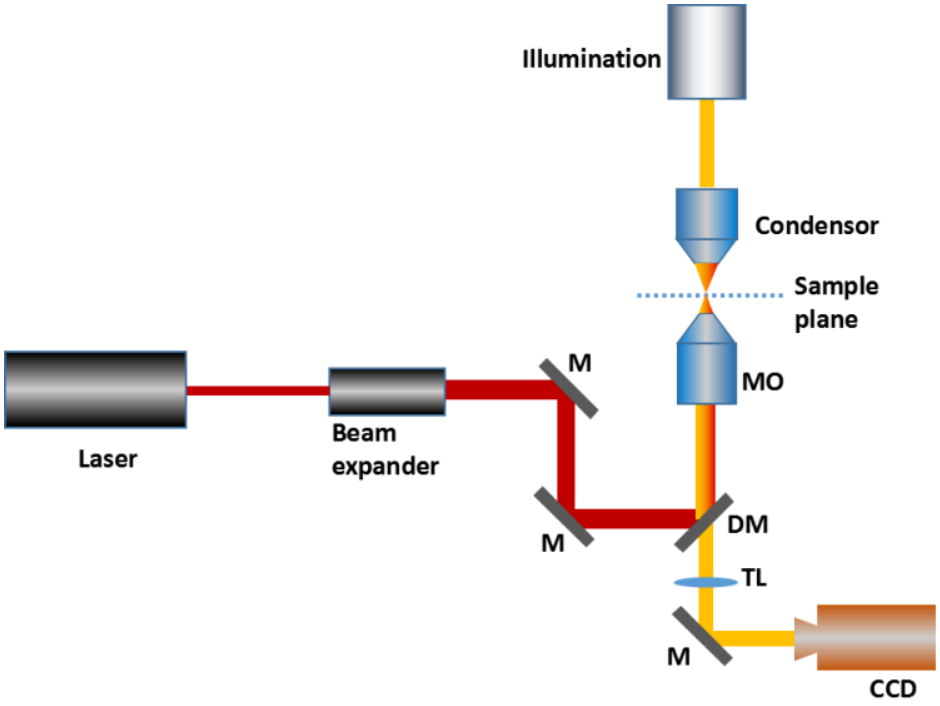

Figure 1.4: *Schematic of the single beam optical tweezers, Laser after expansion using the beam expander is coupled to the back aperture of the objective by relaying the beam using mirrors. The dichroic mirror is used to couple the laser beam and the illumination light used to the MO. CCD camera is placed at the focus of the tube lens (TL) to image the sample.*

The laser wavelength should be chosen such that the sub-cellular components like proteins, nucleic acids, chromophores etc. have minimal absorption at the wavelength used for laser trapping. Further, as the cells also contain a large amount of water, the laser wavelength should also have minimal absorption for water. The wavelength

range ~750nm to 1200 nm [41] provides a window with minimal absorption. The Neodymium: yttrium-aluminium garnet (Nd:YAG) laser (1064 nm) which is commonly available with good beam quality and high power, is most often used for biological experiments. The tunable cw Ti:Sapphire laser (~750nm to 950 nm) has also been employed for trapping. In order to achieve higher gradient force to trap a particle, tight focusing of the laser is important. As the fundamental Gaussian mode (TEM_{00}) can be focused down to diffraction limited spot, a laser with beam quality M^2 < 1.1 is desirable. Poor pointing instability leads to unwanted change in the trap position and the power fluctuation in the laser basically leads to an unwanted fluctuation in the trapping force. Therefore, the laser should have good pointing stability and stable power output.

Objective lens: Tight focusing of the laser beam is an important requirement of the optical trapping that allows achieving the high axial intensity gradient. The focal spot of an objective depends on the NA of the objective as given by $D_0=1.22f\lambda_0/n_mD=1.22\lambda_0/2NA$ Where '*f*' is focal length of the objective, '*D'* is the back aperture size (or input beam diameter when the beam size is less than D) and λ_0 is the wavelength of laser beam in air. Therefore the choice of the objective is dependent on the numerical aperture (NA). In general objectives with NA>1 can trap objects in three dimension. Therefore, oil immersion objectives are often used as these provide NA in the range of 1.2-1.4. Further, the spherical aberration is also a concern as this degrades the focusing of the property of the objective. Plan apochromat type objective with high level of spherical aberration correction are the preferred choice as these provide the best diffraction limited focusing of the laser beam. Oil immersion objectives have typical working distance of ~0.1 mm and with these objectives, going

deeper in the sample increases the spherical aberration significantly due to the mismatch between the refractive indices of immersion oil (n~1.52) and the trapping medium (n~1.34). For such requirements, water immersion objective is used which minimizes the spherical aberration.

Peripheral optics and imaging arrangement: Furthermore to get the tight focusing, the laser beam should completely fill the back aperture of the objective to utilize the full available NA of the objective. Generally the beam size of the output of the laser is less than the size of the back aperture of the objective. Therefore, a beam expander (combination of two convex lenses) with appropriate magnification is used such that the beam size matches with the back aperture of the objective. Mostly, the optical trapping setup is realized around an inverted microscope which provides a halogen lamp for sample illumination, suitable high NA objective and suitable ports for coupling the trapping laser beam and a CCD for imaging the sample. The CCD camera is coupled through a dichroic mirror (DM) which separates the imaging beam (visible light) from the trap (NIR laser) beam. These microscopes can also have feature for the fluorescence imaging of the sample, thus facilitating the studies involving the fluorescent spectroscopy. An additional benefit of using the microscope is that the bright field illumination is aligned in the Kohler illumination which also reduces the effect of the spatially in-homogeneous light source on the image of the sample.

1.3. Optical trap calibration

For small displacements of the trapped particle at equilibrium position near the focus, optical trap behaves like a Hookeian spring and follows $F=-k_t x$, where F is the applied force and x is the displacement of the particle and the 'k_t' is defined as trap stiffness which is proportional to the laser power. Calibration of the setup is involves

determination of the trap stiffness and computation of a position calibration. Equipartition method is one of the simplest ways for determining the trap stiffness. By Equipartition theorem, the average kinetic energy of a particle is $1/2k_BT$ where k_B is the Boltzmann constant and T is the absolute temperature. The potential energy of the trapped particle following the Hooke's law is given by $1/2k_t\langle x^2\rangle$. In thermal equilibrium these two energies will be equal [42] i.e. $1/2k_t\langle x^2\rangle = 1/2\ k_BT$. Thus by the measurement of the positional variance, the stiffness can be determined. For determining the position variance, video of the trapped particle is recorded using the CCD camera and digitized. Thereafter by using a centroid detection algorithm [43, 44], the position of trapped object can be determined. Alternatively, back focal plane imaging of the trapped objected on the quadrant photo diode can also be used for the calculation of the positional variance. Here, the trapped particle image is formed directly onto the quadrant photo diode detector which has four silicon photo diodes arranged in four quadrants of a square, mounted at the conjugate plane to the sample plane [45]. Thereafter, the output of the entire quadrants is summed up pair wise and a differential signal is generated for the displacement of the trapped objects.

Other methods for the trap stiffness calibration include drag force method and power spectrum analysis [41]. In drag force method, the trapped particle is subjected to viscous drag forces produced by the medium. The drag force is commonly produced by the triangular or sinusoidal motion of the stage while the particle is in trap. At equilibrium the drag force is equated to the trap force to determine the stiffness. Power spectrum approach is based on the measurement of corner frequency from the displacement power spectrum density (PSD) of the trapped particle. Here the corner

frequency f_0 can be determined by fitting a Lorentzian on the measured PSD. If the drag coefficient (β) of the particle is known, trap stiffness can be determined by $f_0 = \frac{k_t}{2\pi\beta}$.

Position calibration of the traps is achieved by first calibrating the CCD using standard like microscopy stage slide to get the conversion factor for pixel vs the real dimension and then the displacement of the trap is calibrated with respect to the parameter controlling the deflection angle of the laser beam.

In general, the objects are trapped close to the surface of the cover-slip, the boundary layer of the water close to the surface of the cover slip have a significant effect on the particle motion and leads to an increase in the hydrodynamic drag coefficient, which is given by the Faxen's law [41],

$$\beta = \beta_0 \frac{1}{1-\left(\frac{9}{16}\right)\left(\frac{a}{h}\right)+\left(\frac{1}{8}\right)\left(\frac{a}{h}\right)^3-\left(\frac{45}{256}\right)\left(\frac{a}{h}\right)^4-\left(\frac{1}{16}\right)\left(\frac{a}{h}\right)^5} \tag{1.8}$$

where h is the height of the center of microsphere from the surface, $\beta_0 = 6\pi\eta a$ where η is the viscosity of the medium.

1.4. Multiple optical traps

Single beam optical trap offers immense possibilities as non contact tool for micro-manipulation. However, shortly after the demonstration of the single beam optical trap [1], a need for multiple traps was apparent. For example, as the non spherical particle got trapped in a particular orientation in single beam trap, Ashkin used two static traps to control the orientation of rod like bacterium [3]. Optical tweezers could exert force on microscopic objects of the pico Newton order. In some of the initial experiments, protein molecules and filaments were tethered to the sample

base and the other end was attached to a microsphere to be trapped by the optical tweezers as a handle [7, 46, 47] for studying the dynamics of these molecules. To get multiple cells having these two handles at opposite ends was very difficult. Burn et al. [48] proposed an interference based approach to trap multiple particles in 2D and 3D. However, the approach had no control over the individual trap. Shortly afterwards, static pair of traps were introduced for such experiments [49, 50] to pull, wind and unwind such molecules. With these existing needs and more advanced application scenarios which could be realized with independently and dynamically controllable multiple traps, a number of advanced schemes employing various devices such as acousto-optic deflectors (AOD), galvo scanning mirrors (GSM), and spatial light modulators (SLM) etc. were proposed. These approaches used for generation of multiple optical traps can be categorised as; time sharing of single beam and power sharing i.e. simultaneous generation of all the traps by splitting of single beam. In time sharing mode, whole power of the single beam is available at one position in the specimen plane in 'on' and 'off' mode. The devices used to accomplish this job are galvo scanning mirrors, acousto-optic deflectors and electro-optic deflector (EOD). In the other case, the single laser beam is split into multiple beams and all the beams are simultaneously present at the sample plane and the power per trap is typically total power diffracted in the first order divided by the number of traps. The splitting of a beam can be achieved by simply using the polarization beam splitters (PBS), spatial light modulators, digital micro mirror etc. Here we describe those approaches which have been widely used in the generation of multiple optical traps, followed by an advanced tweezers approach known as Opto-electronic tweezers applicable for large field of view:

1.4.1. Polarization beam splitters

One of the easiest ways to generate multiple optical traps is to simply add multiple numbers of light sources or split a single source to multiple and then couple these to the microscope objective. For splitting a single beam, PBS is used to split the unpolarised or circularly polarized beam in two parts. These beams are again coupled to the objective using second PBS as shown in figure 1.5a. However, these traps are static in nature thereby allow very limited applications such as trapping of low index particle [51].

1.4.2. Galvo scanning mirrors

An alternative to the multiple static traps would be time sharing of a single beam at multiple positions in the sample plane. This could be achieved by using scanning galvano mirrors as shown in figure 1.5 b. The GSM is placed at the conjugate plane of the back aperture of the objective. The step response time of the GSM is typically ~0.3 -1 ms and is suitable for typically two traps with roll off frequency ~200-300 Hz [41]. Since these produce time sharing multiple traps by the mechanical movement of mirrors, wobbling, jitter and repeatability issues are there. Furthermore the problem is more pronounced when the traps are required to be

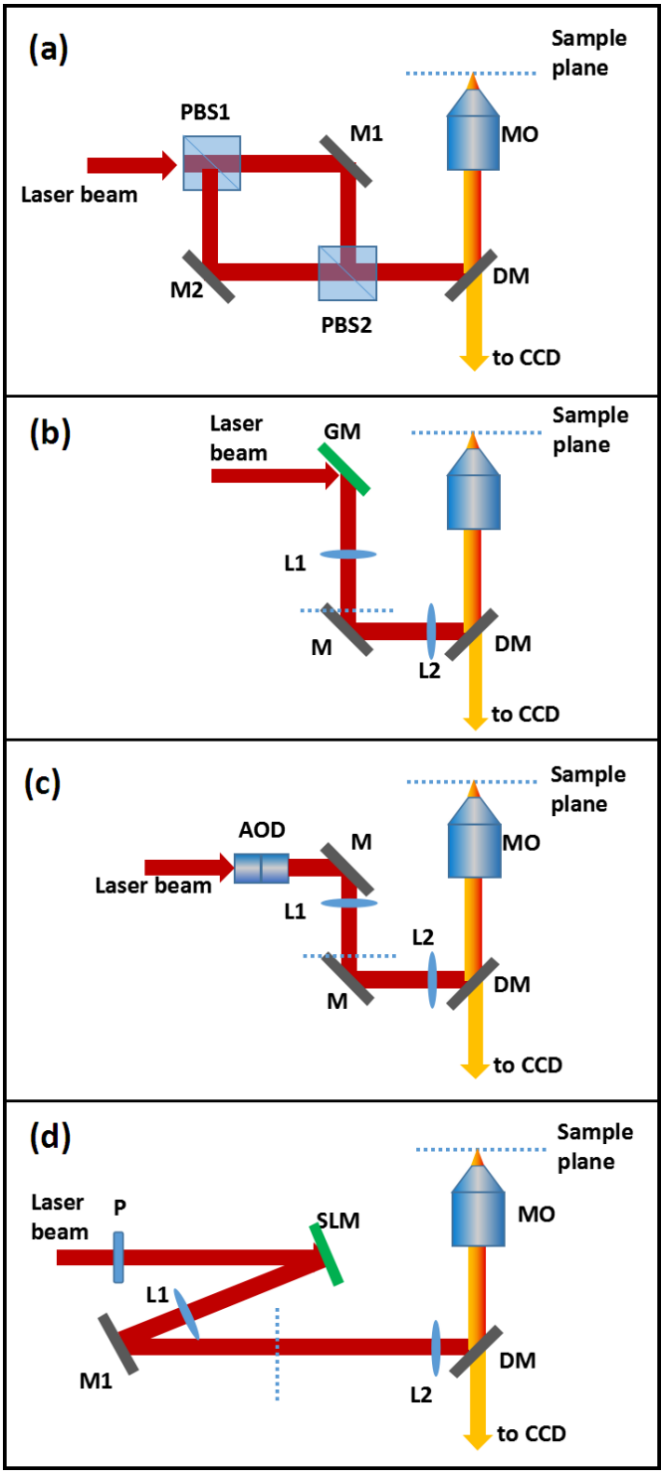

Figure 1.5: *Different schemes for generation of time sharing multiple traps by (a) splitting a single laser beam using PBS (b) using galvano scanning mirror (c) acousto-optic deflector (d) spatial light modulator; the dotted line are the conjugate planes.*

generated randomly in the sample plane. GSM is advantageous in respect of providing very large deflection angles at low cost and more uniform power deflection across the scan angle.

1.4.3. Acousto-optic deflectors

AOD is an electro-optic device with no mechanical movement. In AOD, the light is diffracted by sound waves generated in a suitable interaction medium like TeO_2. The schematic of the AOD setup is shown in figure 1.5 c. An RF amplifier is connected to the piezo electric transducer which is mechanically coupled to the acousto-optic material. Piezoelectric transducer exerts oscillating pressure on the acousto-optic material with the frequency of the applied RF field and in turn generates an acoustic wave (sound wave) which travels through the material and causes periodic variations of the refraction index. When a laser beam is incident on this disturbance, the beam is deflected partially similar to that is deflected by a diffraction grating. Two dimensional deflection of a laser beam is achieved by placing two AODs orthogonally as close as possible and their interface plane is imaged to the back aperture of the objective with the help of 4f optical arrangement. The setup is commonly known as acousto-optic tweezers (AOT) or time sharing optical trap (TSOT).

An incident laser beam passing through this grating generated by the sound wave will be diffracted into several orders. In an isotropic media, when the light incident at the Brag angle (θ_b), the light is only diffracted to the first order, in principle. The angle at which the light is diffracted is defined by [51]:

$$\phi = \lambda \frac{f_a}{V_a} \tag{1.9}$$

Where ϕ is the angle of deflection, λ is the wavelength of light in air, f_a is the applied acoustic frequency and V_a is the acoustic velocity of the material which does not

change for a given material. As the acoustic frequency of sound wave will be the same as that of the frequency of the applied RF voltage, variation of the acoustic frequency of the driver will thus change the acoustic wavelength, which in turn changes the periodicity of the refractive index variation.

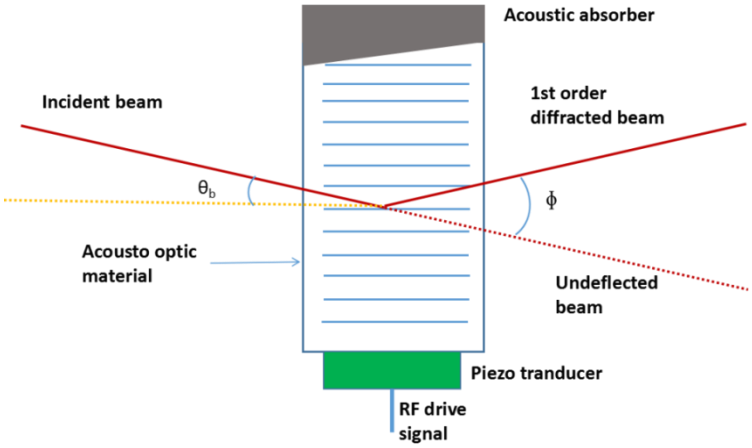

Figure 1.6: *Schematic of acousto optic deflector working principle*

Therefore, the angle tuning of the first-order diffracted beam is linearly proportional to changes in the frequency of the RF drive signal. As shown in figure 1.6, an acoustic absorber is placed at the end of the AOD is used to minimize the reflection. This is required to avoid formation of standing wave pattern which effectively increases the response time for the deflection of the laser beam. The RF drive signal is generated using a computer based digital frequency synthesizer board.

Another similar option for generation of the time shared traps is the use of the electro- optic modulators (EOD). Here an electric field is applied to the electro-optic material to generate the linear refractive index gradient which deflects the light. The EODs have typical diffraction efficiency of ~90% with the response time on ~100ns [41]. Though, EODs are much faster than the competing technologies like GSMs and AODs, these have some limitations too such as the maximum angle of deflection is

small (~2mrad) leading to a ~1 μm separation of traps which may not be suitable for most of the trapping applications [41]. Additionally the voltage required to operate the EODs is ~kV which is a safety concern.

All the above described techniques for generating dynamically controlled multiple optical traps have one drawback that the traps can be generated in one plane only. Use of diffractive optical elements like spatial light modulator overcomes this problem.

1.4.4. Spatial light modulators

SLM structure and functioning: SLM is liquid crystal (LC) based pixelated electronic device [52] as shown in figure 1.7. When light impinges on the SLM, the phase of the output beam is modulated such that the output beam splits into multiple beams travelling in different directions. These beams after coupled to the microscope objective to generate multiple optical traps at the sample plane.

Each pixel of the SLM consists of nematic liquid crystals sandwiched between the electrodes and aligned parallel to the electrode surface. SLM can be classified according to the liquid crystal alignment in the pixels as: Twisted LC-SLM in which the axis of the LC molecules twists to 90^0 while moving from the one electrode to the other in the pixel while the other one is parallel aligned (PL) type in which the LC molecules are aligned parallel to each other. In case of PL LC-SLM, when there is no field across the LC cell, all molecules align parallel to each other. On application of electric field, the LCs bends in the plane of orientation of LC. Therefore, the light undergoes phase only modulation while passing through these pixels provided the incident light is polarized in the plane of the orientation of the LC molecule [53]. In case of TN-SLM, each LC molecule layer has different plane of bending when the electric field is applied

and so these produces phase as well as the amplitude modulation to the incident light. As the amplitude modulation reduces the power in the diffracted beam, the SLM with phase only modulation is preferred. Hence, for trapping applications, the parallel aligned LCSLM are used in general. SLMs can also be classified as reflective type and transmissive type. Reflective type SLM is preferred over the transmissive type as they require half the LC thickness for a given phase delay due to the double pass in the reflection as compared to the transmissive type SLM.

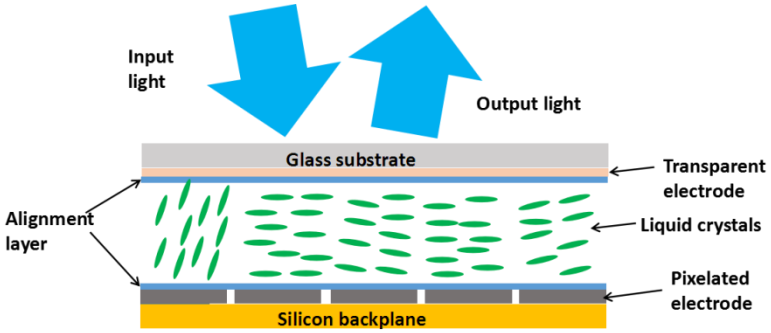

Figure 1.7: *Schematics of the reflective type parallel aligned nematic liquid crystal SLM (adapted from* **[52]***)*

Depending on the LC thickness, a SLM will have a maximum wavelength for which it can provide 2π phase delay. The control software and driver for the SLM are designed such that the possible range of voltage that can be applied to the liquid crystal cell is split to 256 levels so that these corresponds one to one 8 bit intensity image with 256 gray levels. Therefore, the SLM can generate phase modulation by simply using an intensity image or hologram. The important parameters determining the performance of the HOT are refresh rate of the SLM, uniformity of the generated traps and diffraction efficiency of the SLM. These parameters depend on the algorithm used to generate the hologram.

Phase hologram computation: The basic idea for hologram design is very simple. As we know that a diffraction grating diffracts the laser power to different higher diffraction orders. Each diffraction order corresponds to different angle. Therefore if a diffraction grating, corresponding to transverse position of a trap, is positioned at the back focal plane of the objective (Fourier plane w.r.t the focal plane of the objective [54]), a trap will be generated. So we only need to design a diffractive grating i.e. the computer generated hologram (CGH) which will have a defined number of diffraction orders corresponding to the number of traps.

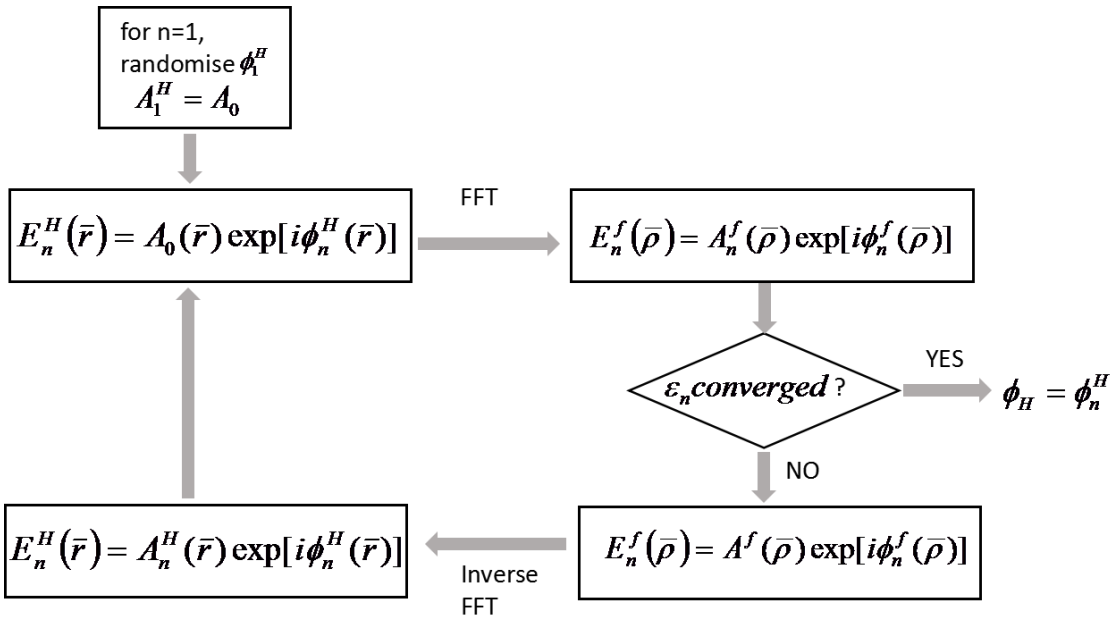

Figure 1.8: *Flowchart describing the GS algorithm*

Additionally each differently diffraction orders may have different divergence which will control the axial position of the trap in the specimen plane. A number of algorithms have been reported in literature such as lens and grating [55], direct search [56], iterative Fourier transform algorithms [54, 57] etc. for this. Each of these having its own

pros and cons when evaluated on the basis of diffraction efficiency, trap uniformity and the most important one is the computational speed [58].

Lens and grating algorithm: The easiest approach used is the grating and lens algorithm in which the analytical phase forms of the grating and lens are superposed. The grating phase provides the lateral shift while the lens phase profile provides the shift in Z plane. This algorithm is simple and fast but provides very poor uniformity of optical power in generated traps. Additionally when the generated traps has some symmetry like traps in four corner of a square, the generated traps are accompanied by some unwanted traps named as Ghost traps which consume a significant part of the diffracted laser power.

Direct search algorithm: Direct search algorithm, often used for the hologram refinement, starts with a good guess such as a primary level of hologram computed with lens and grating algorithm. Each pixel is picked up at random and its gray level is changes to all the 256 levels to examine that whether the new hologram is improving the amplitude in various traps. If there is improvement, the gray level is retained and similarly phase value for the other pixels is computed. The algorithm converges after several numbers of cycles when the error value reaches to a local minimum. This provides better uniformity over the traps. However, the number of cycles required to optimize the hologram is large and therefore makes the approach slow.

Gerchberg-Saxton (GS) algorithm: Another approach known as Gerchberg-Saxton (GS) algorithm [54, 59] is an iterative Fourier transform algorithm which exploits the fact that hologram plane and the sample plane are Fourier transform pair. Initially the computation is started with a random phase and the given amplitude of the input laser

beam. After each fast Fourier transform (FFT) of the complex input field, the amplitude of the output field is replaced with the desired field amplitude. Similarly, after the inverse FFT of this modified output field, the amplitude of the obtained complex field is replaced with the amplitude of the input laser beam as shown in the flowchart in figure 1.8.

The error between the computed intensity and the desired intensity is given by [54]

$$\varepsilon_1 = \frac{1}{m^2}\sum_{i=1}^{m^2}[I^f(\bar{\rho}_i) - I_1^f(\bar{\rho}_i)]^2 \qquad (1.10)$$

Where $I_1^f(\bar{\rho}_i) = \left|A_1^f(\bar{\rho})\right|^2$ and $I^f(\bar{\rho}_i) = \left|A^f(\bar{\rho})\right|^2$ are the computed and desired intensities in the trapping plane. The error ε reduces after each iteration step and after ~15 iterations it becomes < 0.0001.

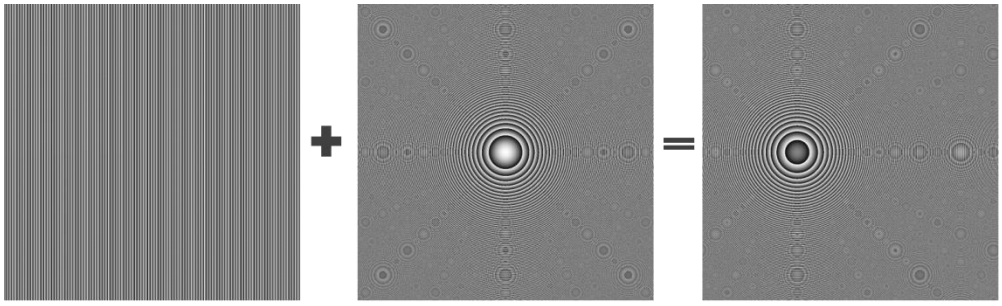

Figure 1.9: *Generation of combined hologram*

As the SLM can provide a phase delay of maximum of 2π for the specified operating wavelength, the obtained phase is phase wrapped with 2π. This wrapped phase pixel values are converted into 8 bit gray scale image whose phase ranges from 0 to 2π. This image when applied to the SLM, the incident light gets phase modulated to generate the desired array of traps. The typical diffraction efficiency of a SLM is

~40% and therefore a grating phase is superimposed onto the calculated phase to separate the desired pattern from the reflected beam (0^{th} order) as shown in figure 1.9. GS algorithm has several improved versions also such as Additive Adaptive algorithms [54], weighted GS [60] etc. where the uniformity and the number of iteration has been improved.

It is to be noted that too much laser power can affect the performance of the SLM by heating the liquid crystals. This essentially puts a limit to the optical power handling capacity of the SLM and results in the limitation of number of traps that can be generated. In this regard, digital micro-mirror device (DMD), a Micro Electro mechanical system manufactured [61-62] is another alternative to SLM, which modulates light by employing binary amplitude modulation mechanism. It has two dimensional arrays of micro rectangular moving mirrors working as pixels which are controlled by the underlying CMOS electronics [61]. These mirrors can be flipped individually in two tilt states so that light is reflected in a direction in one state (on state) and in the other direction in the other state (off state) at ~10kHz rate and can direct the light on to or away from an intended target. The reflective mirrors are less sensitive to the wavelength of the input laser beam and so can be used with pulsed lasers to generate special beams with high power.

1.5. Opto-electronic tweezers

Opto-electronic tweezers (OET) is an optically driven electro-kinetic approach which can manipulate ~1000s of particles over an area as large as ~1 mm^2 using optical intensity of ~nW/trap [63]. OET makes use of locally induced dielectrophoretic (DEP) forces controlled by light for trapping of microparticles. The heart of the system is

OET chip which consists of an indium tin oxide (ITO) coated glass substrate (top) and an ITO coated glass substrate (bottom) with a photo conductive layer separated by spacers as shown in figure 1.10.

An a.c. bias is applied between the electrodes and an intensity pattern is projected on the photo conductive layer which generates virtual electrodes resulting in a non uniform electric field between the electrode and the illuminated regions. This non uniform electric field induces DEP forces on particles in OET chip. Notably one electrode can be dynamically generated anywhere in the region of interest by illuminating the region allowing generation of complex electrode pattern for microparticle manipulation such as sorting [64-66] cell lysis [67], electroporation [68] etc.

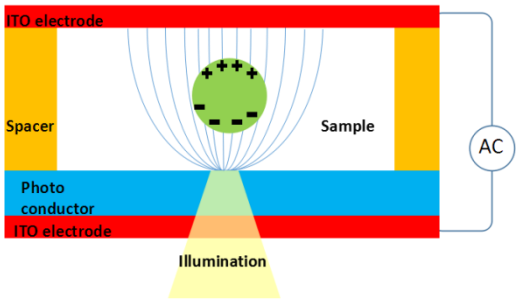

Figure 1.10*: Schematics of the OET chip*

The time averaged DEP force on a homogeneous spherical particle is given by [69]

$$F = 2\pi a^3 \varepsilon_m \,\mathrm{Re}[K^*(\omega)]\nabla E^2 \tag{1.11}$$

where

$$K^*(\omega) = \frac{\varepsilon_p^* - \varepsilon_m^*}{\varepsilon_p^* + 2\varepsilon_m^*} \tag{1.12}$$

$$\varepsilon_p^* = \varepsilon_p - j\frac{\sigma_p}{\omega} \qquad \varepsilon_m^* = \varepsilon_m - j\frac{\sigma_m}{\omega} \tag{1.13}$$

where *a* is the radius of the particle, ε_m is the permittivity of the media, ε_p is the permittivity of the particle, E is the electric field and Re[*k(ω)*] is the real part of the Clausius-Mossotti factor (CMF), σ_p and σ_m are the conductivty of the medium and the particle respectively, ω is the angular frequency of the applied electric field. Notably the DEP force depends on the square of the applied electric field, so the approach is useful in d.c. as well as in a.c. and the direction of force will not change with change in the direction of field as in case of electrophoresis. If particle has a large polarizability than the suspended medium, particle experiences net force in the direction of the higher electric field (positive-DEP or p-DEP). Accordingly when the particle has a lower polarizability than the medium, the DEP force pushes the particle in the direction of the lower electric field (negative-DEP or n-DEP).

Further the real part of the CMF lies in the range of +1 for $\varepsilon_p >> \varepsilon_m$ i.e. for the situations when the particle is much more polarisable than the medium and -0.5 for $\varepsilon_p << \varepsilon_m$ for the situations when the particle is very less polarisable than the medium. Thought CMF for the n-DEP can, at the maximum, be a half of the p-DEP, n-DEP is more commonly used for manipulation of the cells/ microparticles as compared to p-DEP. Since in p-DEP the particle gets attracted towards the electrode around which the electric field gradient is high and sticks there, leading to problem of congestion and clogging when used in dense sample. If we take the two extreme situations for the frequency of the applied electric field, the CMF factor at the lower frequency is given by

$$\underset{\omega \to 0}{CMF} \approx \frac{\sigma_p - \sigma_m}{\sigma_p + 2\sigma_m} \tag{1.14}$$

and at higher frequency by,

$$\underset{\omega\to\infty}{CMF} \approx \frac{\varepsilon_p - \varepsilon_m}{\varepsilon_p + 2\varepsilon_m} \tag{1.15}$$

Thus, at lower frequencies (<50 kHz), the CMF is governed by the conductivity values, while at higher frequencies (> 50 MHz) by the dielectric permittivity values of the particle and medium [70]. At the intermediate bias frequencies, both the conductivity and permittivity of the particle and the medium dictate the CMF value and polarity. The non-uniform electric field induces partial charges on the particle medium interface via - a process known as Maxwell Wagner (MW) interfacial polarization [70, 71]. There is a competition between the charging process in the particle and in the medium resulting in the charge build up at the particle-medium interface.

Unlike dielectric micro particles, cells are not homogeneous in nature. Simple cells like RBCs are modeled by single shell model whereas cells possessing nucleus are modeled using multi shell model. RBC is modeled as spherical particles with cytoplasm in core shell surrounded by a membrane as shown in figure 1.11. The effective complex permittivity of this single cell is calculated by [72]

$$\varepsilon_p^* = \varepsilon_{mem}^* \left(\frac{\left(\frac{a}{a-d}\right)^3 + 2\left(\frac{\varepsilon_{\text{int}}^* - \varepsilon_{mem}^*}{\varepsilon_{\text{int}}^* + 2\varepsilon_{mem}^*}\right)}{\left(\frac{a}{a-d}\right)^3 - \left(\frac{\varepsilon_{\text{int}}^* - \varepsilon_{mem}^*}{\varepsilon_{\text{int}}^* + 2\varepsilon_{mem}^*}\right)} \right) \tag{1.16}$$

Where $\varepsilon_{\text{int}}^*$ and ε_{mem}^* are the complex permittivity of the cytoplasm and cell membrane. Since the conductivity of the membrane is far less than the conductivity of the cytoplasm for MW relaxation time (~MHz) [72],

$$\left(\frac{\varepsilon_{\text{int}}^* - \varepsilon_{mem}^*}{\varepsilon_{\text{int}}^* + 2\varepsilon_{mem}^*}\right) \approx 1 \tag{1.17}$$

And if the thickness of the cell membrane d<<a (in general d~nm and a ~μm) [64]

then

$$\varepsilon_p^* = \frac{a}{d}\varepsilon_{mem}^* = C_{mem}^* \frac{3a\varepsilon_{\text{int}}^*}{3\varepsilon_{\text{int}}^* + 3C_{mem}^* a} \tag{1.18}$$

$$C_{mem}^* = \frac{\varepsilon_{mem}}{d} - \frac{j\sigma_{mem}}{d\omega}$$

Where C^*_{mem} is the complex conductance of the membrane and ε_{mem}, σ_{mem} are the dielectric permittivity and conductivity of the membrane.

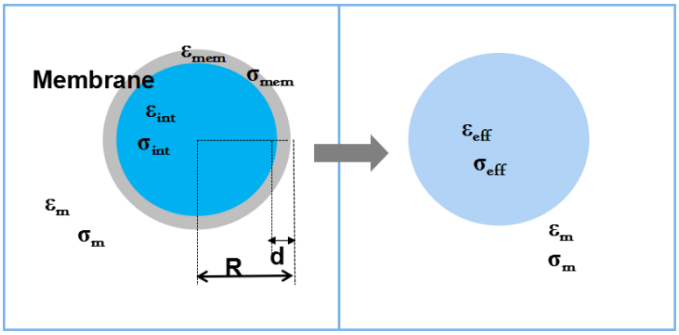

Figure 1.11: *Schematics representation of how heterogeneous cells can be simplified to a homogeneous cell.*

A plot of CMF for the uniform microsphere is shown in figure 1.12a showing how the conductivity of the particle and the medium affect the frequency dependence of the CMF. In figure 1.12 b, a model cell CMF frequency response has been shown with varying cell sizes. We observed that cells have DEP response as n-DEP or p-DEP depending on the frequency of the applied field. The frequency at which the CMF factor becomes zero is termed as cross over frequency.

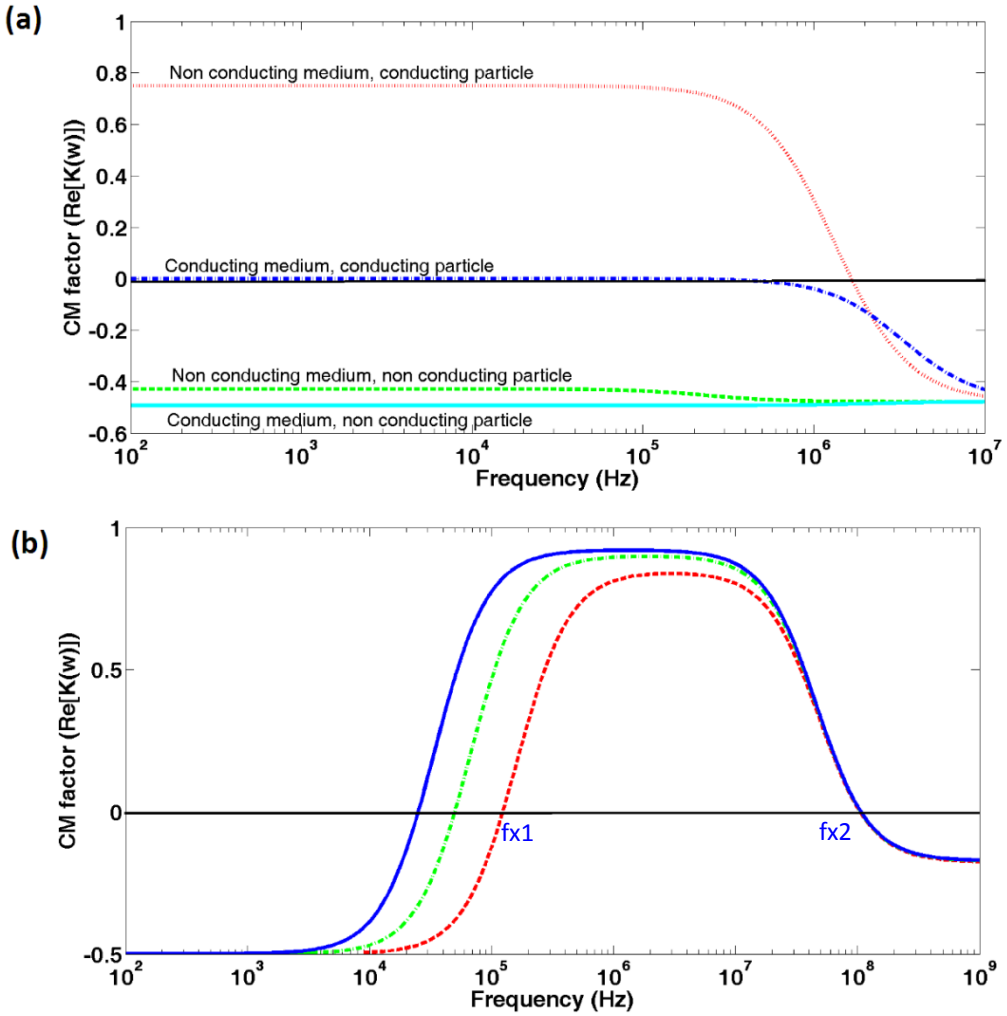

Figure 1.12: *CM factor for (a) various situation of the conductivity of the medium and the particle σ_m=1x10^{-3} Sm^{-1}, σ_p=100x10^{-4} Sm^{-1} (Red); σ_m=10x10^{-3} Sm^{-1}, σ_p=100x10^{-4} Sm^{-1} (Blue); σ_m=1x10^{-3} Sm^{-1}, σ_p=1x10^{-4} Sm^{-1} (Green); σ_m=10x10^{-3} Sm^{-1}, σ_p=1x10^{-4} Sm^{-1} (Cyan)* , $\varepsilon_m = 80\varepsilon_0$ *and* $\sigma_m = 10Sm^{-1}$, *(b) Model cell with* $\varepsilon_{\text{int}} = 45\varepsilon_0$, $\sigma_{\text{int}} = 0.5Sm^{-1}$, $\varepsilon_{mem} = 8\varepsilon_0$, $\sigma_{mem} = 1\times10^{-8}\,Sm^{-1}$, *d=8 nm,* $\varepsilon_m = 80\varepsilon_0, \sigma_m = 10Sm^{-1}$ *and a: 2μm (red), 5μm (green) and 10μm (blue).*

We see from the figure 1.12b that when the cross over frequency 'f_{x1}' is sensitive to the size of the cell while the f_{x2} does not change. At higher frequencies, the membrane capacitance effectively shorts out the high resistance of the cell membrane and therefore the CMF response depends on the relative differences of the dielectric permittivity of the cytoplasm and surrounding medium. As the crossover frequency

(f_{x1}) of cells of different sizes are different, this has been exploited for sorting of cells [67, 72].

In OET, apart from the optically induced DEP, several other electrokinetic (light induced a.c. electro-osmosis (LACE)) and thermal effects (electrothernal (ET) and buoyancy) also occur [73]. LACE is more like AC electro-osmosis in which the charges in the electrical double layer change polarity with change of applied ac field and therefore results in a motion of the ions in the fluid in one direction. The only difference is that instead of a metal electrode, a virtual electrode is used. Valley et al. [73] observed that LACE is a dominant effect at the applied frequencies below ~1 KHz. Similarly, when the light is illuminated on the photo conductive layer, it results in either generation of electron-hole payer or phonons. These phonons are a cause of concern being a localized heat source leading to a gradient in the permittivity and conductivity of the medium. Therefore higher the optical power, more dominant this effect would be due to higher heating. Additionally due to temperature gradient, there would be a gradient in the fluid density resulting in fluid flow and the particle will experience a force in this flow. Valley et al. [73] concluded that these thermal effect are more dominants at optical powers more that 1 $KW.cm^{-2}$. Therefore DEP to dominate among other effects, the operational frequency should be more than 1 kHz and applied power less than 1 $kWcm^{-2}$.

1.6. Literature survey

As a natural extension of the single beam trap, multiple tweezers can be constructed, in a most trivial way, by adding multiple lasers. Ashkin et al. had demonstrated the use of two lasers for levitation and orientation of non spherical particles [74]. Shortly afterward the demonstration of single beam optical trap [1], he used two independent

traps generated via two microscope objective one of which also worked as condenser [3] or through single objective through a beam splitter to trap rod like bacterium at the two end and orient them in controlled manner [74]. Here the number of traps is limited to the number of laser sources used and experimental complexities increase rapidly as more than two traps are attempted. Dual static optical traps generated by PBS were also reported [75, 76] for studies on single kinesin molecule mechanics. Burn et al. demonstrated that a large number of traps could be generated by interference of multiple beams and had demonstrated to generate periodic crystalline structures [48]. However, control of individual trap appears to be hard to implement. Over the period of time, fast and precise steering multiple optical trap systems using GSM and AOD were reported [26]. Sasaki and Misawa [77-80] reported the use of galvano scanning mirrors to generate multiple optical traps in time sharing mode for patterning of particles [77] [78] and trapping of metal particle [80]. These setups required that the scan rate of the scanning beam to be faster than the relaxation time of the particle being trapped [77]. Visscher et al. used acousto optic modulator (AOM) as a fast shutter to block the laser beam when the beam was scanned from one trap to the other by galvo scanning mirrors [81] and it was used for study on shape recovery of red blood cells [82]. Later on AOD based systems [49, 83] were reported which could control the position and power of individual trap and were having much faster scanning rate than the GSMs. These have been used for measurement of elasticity of RBCs for hemolytic disorders [84], direct measurement of colloidal forces [85], optical force clamp for single microtubules [86], RNA polymerase [87], DNA manipulation [88], stretching of RBCs [89] etc.

The above mentioned time shared optical traps could generate dynamically controlled multiple traps but in 2D only. To further have control in 3D, holographic

approaches were proposed [54, 55, 90, 91]. The initial efforts used static phase holograms to generate the traps while later on use of spatial light modulators revolutionized the field of micro-manipulation in two and three dimensions [58, 92, 93]. These allowed spatial tailoring of the light field for specific applications ranging from generation of special beams like Laguerre Gaussian (LG) beam [94, 95], Bessel beam [96-98] which found variety of applications such as cell rotation and orientation [99], trapping of low index particles [100] and spermatozoa [101], long distance guiding [102] to generation of complex structures for studies on lattice dynamics [103-109]. Not only these, several new application areas such as guiding/sorting of microparticles [110-130] were also explored. One of the major advantages of these optical techniques for guiding/sorting is that these are particularly suitable for small sample volume and are easy to integrate with microfluidic devices like micro total analysis systems (μTAS), modern spectroscopic techniques such as micro Raman spectroscopy etc. [131, 132]. Sorting approaches can be broadly categorized as active sorting and passive sorting; Passive sorting techniques [123, 127,128, 130, 133] exploit the difference in the intrinsic optical properties (such as refractive index and size) of the particles to result in different trajectories for the particles when these interact with optical field landscape generated by interference [133, 134], hologram [121, 123] or AOD [135] based approaches. On the other hand, in active sorting techniques [115, 118, 125] the desired particles are first identified by any external technique (e.g. fluorescence, size) and thereafter an optical force is used to deflect/guide these to the output channel.

Among these sorting approaches the ones which are suitable for flow less medium have an added advantage as they do not require the flow generation arrangement of syringe pump, microfluidic chips etc. Therefore, recently, the use of multiple optical

tweezers for development of various micro-scale sorting approaches suitable for flow less medium has gained a lot of research interest. Passive flow less sorting can be achieved by using the optical potential of a Bessel beam [126, 127]. Particles placed within the outer rings of the beam move toward the bright central core at a rate that depends on their size and refractive indices. However, since the sorted fraction is guided along the axis of the central core, the extraction of the sorted articles is not easy. Other types of flow less sorting are based on moving light interference fringe patterns that are swept over the sample [136, 137]. But since these techniques employ multiple beam interference, these methods may be sensitive to vibration instabilities. On the other hand, in the absence of fluid flow, active sorting can be achieved by employing bright-field images based identification and subsequently use of holographic optical traps to move the particles to the desired region. To avoid collisions among the moving particles an iterative path planning algorithm was used and the particle trajectories were kept sufficiently apart to avoid interference from the optical force field of other traps. These requirements reduce the throughput of the technique.

The aforementioned tweezers setup could handle up to ~100s of particles [57] limited by the laser power handling capability of SLM. This is a bottleneck for applications requiring further higher throughput. Damage of cell due to high intensity of the laser (~MW/cm^2) used in the optical tweezers is also a concern. To address these concerns, Opto-electronic tweezers (OET) which makes use of locally induced dielectrophoretic (DEP) forces controlled by light for trapping of microparticles were proposed [63]. This could manipulate ~15000 particles over an area as large as ~1.3 mm^2 using with optical intensity that is 10^5 times less that that used in conventional

optical tweezers.These have been used for manipulation of variety of microscopic objects such as cell separation [64], selective cell lysis [67], cell electroporation [68], flow cell cytometry [138, 139], nanoparticle ac electroosmosis [140], separation of metallic and semiconductor nanowires [66] etc. In OET, for generation of illumination pattern to create the virtual electrode, commercially available projectors [141], Spatial light modulators or Digital micro mirror devices with incoherent light sources [63, 142] have been used. Initially the amorphous Silicon was used as a photo conductive material. However, due to complicated process for coating a layer of a:Si, alternatively layer of organic materials such as P3HT:PCBM [143], TiOPc [142] by spin coating was also explored. TiOPc has been an alternative promising candidate as a photo conductive material but getting a uniform coating by solution based approaches takes lots of effort as this has low solubility in organic solvent.

1.7. Aim and outline of the thesis

The aim of the thesis was to develop the advanced multi trap techniques and utilizing these for development of novel approaches for sorting/separation in flow less medium and guiding of cells and microparticles.

In chapter 2 we describe the development of dual line optical tweezers and present the results on use of this as optical guide for focusing of cells in microfluidic channels for Raman spectroscopy based cell cytometry. In chapter 3 we present the development of AOD based multiple optical tweezers setup and thereafter its use for the development of optical sorting approach that relies on dependence of diffusion constant on the size of the particles. In chapter 4, we present the use of holographic optical tweezers for development of two active optical sorting approaches based on use of multiple planes for trapping of microscopic objects. Chapter 5 describes the development of

opto-electronic tweezers setups and their use for manipulation and sorting of micro particles in dense sample. At last the conclusion and outline of the future work has been discussed.

2 Chapter 2: Optical guiding-based cell focusing for Raman flow cell cytometer

In this chapter we describe our results on the use of dual line optical tweezers aligned in the shape of 'Y' as optical guide to produce a stream of single cells in a line for single-cell Raman spectroscopic analysis. The Raman excitation beam at 514.5 nm was positioned in the tail region so that the cells could be analyzed as they passed through. As a proof of concept, it was shown that red blood cells (RBCs) could be guided to the tail of the optical guide and the Raman spectra could be recorded in a continuous manner without trapping the cells. The recorded spectra were used to distinguish between RBCs containing hemoglobin in the normal form (normal-RBCs) and the met form (met-RBCs) from a mixture of RBCs comprising of met-RBCs and normal-RBCs in a ratio of 1:9.

2.1 Introduction

Flow cell cytometers play very important role in current cell biology research. Commercially available cell cytometers/ sorters such as fluorescence-activated cell sorters and magnetically assisted cell sorters are suitable for a wide variety of applications [144]. However, in addition to the requirement for a large sample volume, these systems are too expensive [144, 145]. Therefore, there is an interest in developing micro-fluidic based approaches, which provide advantages such as the requirement for a very small sample volume, being inexpensive and requiring low

Work discussed in this chapter has resulted in the following publication:

1. **R. S. Verma**, S. Ahlawat and A. Uppal, "Optical guiding based cell focusing for Raman flow cell cytometer", Analyst, 143, 2648-2655 (2018).

maintenance (disposable). A reduction in the size of equipment allows easy portability. Efforts have been made to develop Lab-on-a-chip type systems for point-of-care diagnostics [146] and to integrate various spectroscopic techniques with microfluidic for cytometry/sorting applications [145, 147, 148]. However, these fluorescence-based approaches require staining/tagging of cells which in addition to photo bleaching of the fluorescence signal, may also suffer from the lack of availability of an appropriate marker [149]. Therefore, techniques that obviate the need for staining/tagging and thus analyze the cells in their purest form are also gaining interest. In this context, impedance flow cytometry [150-154] has been demonstrated to be able to characterize cells in terms of size, morphology, membrane capacitance and cytoplasm resistance. Raman spectroscopy-based flow cytometry, which enables the recording of the intrinsic biochemical fingerprints of individual living cells in a label-free and non-invasive manner is another label free technique [155, 156] that is also gaining considerable interest. In microfluidics, there are two primary requirements for performing Raman spectroscopy on single cells: the first is to bring the cells into a single line, i.e., focusing of the cell stream, and the second is the immobilization of the cells during spectral acquisition to acquire signals of good quality, as Raman signals are inherently very weak in nature. The cell focusing arrangement should be such that it allows a single cell to flow past the Raman detection region with nearly identical velocity at a time. Conventionally, hydrodynamic focusing is used to bring the cells into a single line in a particular region of the microfluidic channel. Furthermore, for the immobilization of the cells one common approach has been to use optical tweezers [115,157-160]. To trap a cell in a flowing medium, the optical force on the cell should be greater than the

hydrodynamic drag force. Although hydrodynamic focusing has been widely used for cell focusing, it has one inherent drawback: as the central sample stream is sandwiched by the sheath fluid, the flow speed of the sample stream changes inversely with its width, which, in turn, is controlled by the flow speed of the sheath fluid. Therefore, when one requires a single-line flow of cells, i.e., a very narrow width (∼cell size) of the sample stream, the flow speed of the sample stream increases, which then requires the use of higher optical power to trap and hold the cells. Because optical trapping requires focusing a laser on a diffraction-limited spot and this results in very high intensity at the focus, and therefore the use of high optical power for trapping may cause damage to the trapped cells [28, 161, 162]. An alternative approach for achieving cell focusing at a desirable speed (typically less than ∼400 μm s^{-1} (ref. [115]), in which cells can be optically trapped in the detection region by a suitable optical power, makes use of a microfluidic channel containing a cavity [15, 157] in the detection region. The use of the cavity helps in reducing the flow speed in the trapping/detection region. A pinch flow fractionation approach to suddenly reduce the pressure of the liquid, leading to a reduction in cell flow speed, has also been reported [115] However, in both these approaches the cell stream becomes wider in the analysis region, and therefore many cells may be missed by the trapping and Raman excitation beams. Instead of focusing the cells into a single line to bring them to the detection region, another way could be the use of a programmable XY sample stage, so that by moving the sample stage the Raman excitation region inside the microfluidic channel could be adjusted according to the cell position [159]. However, the movement of the whole stage to bring the Raman excitation region to the cell position for recording the spectra requires an extremely dilute cell sample, which

results in very low throughput. Furthermore, these [115, 159, 160] optical trapping and release-based approaches always raise concerns regarding cell photo-damage, apart from having with low throughput. Although the concerns regarding damage raised by the use of a tightly focused trapping beam can be obviated by trapping the cells in the diverging fields of optical fibers [157, 158] or using DEP forces [163], the implementation of these techniques involves significant complexity. In addition, the use of a low conductivity buffer in dielectrophoresis based approaches may affect the cell viability [70, 164, 165]. Therefore, if the Raman signal can be enhanced so that the cells do not need to be stopped in the analysis region, this would serve both purposes: an increase in throughput and no concern regarding photo-damage due to the trapping laser. There are several techniques of signal enhancement, such as resonance Raman, surface-enhanced Raman scattering (SERS) [166], coherent anti-Stokes Raman spectroscopy (CARS)[167, 168] stimulated Raman scattering (SRS) [169, 170] etc. Of these, SERS requires the development of markers to tag the desired cells and therefore is not label-free [171-173]. CARS and SRS typically require expensive and bulky laser systems. Although, the signal enhancement in resonance Raman Effect is not very large, as compared to the other signal enhancement techniques, it is label-free and can be implemented using inexpensive laser systems.

Therefore we proposed a dual line optical tweezers based guiding arrangement for focusing the cells into a single line and making use of the resonance Raman Effect to analyze the cells as these pass through the Raman excitation region at the tail of the guiding arrangement. The major benefit of this approach is the decoupling of the width of the cell stream and cell flow speed, which enables independent control of the

cell flow speed. The detailed analysis of guiding of the cells using dual line optical tweezers and results of the proof of demonstration of the suitability of optical guide for cell focusing for Raman flow cell cytometry has been presented in this chapter.

2.2 Experimental methods

2.2.1 Sample preparation

For our experiments, the unused parts of blood samples, which were collected for screening and found to be healthy, were provided without disclosing the donors' identity by the blood bank of Choithram Hospital and Research Centre, Indore. The blood samples were collected by vein puncture from healthy volunteers in glass tubes containing EDTA (5.4 mg/3 mL) as an anticoagulant. RBCs were separated from the anticoagulated blood samples by centrifugation at 3000 rpm for ~3 min. The separated RBCs were then washed three times with ice-cold phosphate buffer saline (PhBS) and then suspended in PhBS containing 2% bovine serum albumin. Appropriate dilutions of the cells in the buffer solution were then used for experiments. To prepare met-RBCs, 10 μL of pelleted RBCs were suspended in 10 mL of PBS containing ~0.05% sodium nitrite and kept at room temperature for 20 min. The conversion from the oxygenated form of haemoglobin (Hb) to the met form was confirmed by the observation of a peak at 635 nm in the absorption spectra of the cells.

2.2.2 Setup

A schematic of the integrated microfluidics-Raman optical tweezers setup built on an Olympus IX83 inverted microscope is shown in figure 2.1a. Dual-line optical tweezers were generated by splitting a 1064 nm laser beam into two parts using a polarizing beam splitter (PBS1) and placing a cylindrical lens (CL) with a focal length of 100 mm

in the path of each of the split beams. These beams were then recombined using another polarizing beam splitter (PBS2) and passed through a spherical lens with a focal length of 200 mm before being coupled to a 60× oil immersion objective lens (Olympus, 1.35 NA). By rotating the cylindrical lenses, the 'Y' shaped arrangement of the tweezers could be generated at the focus of the objective. A 514.5 nm Raman excitation beam from Ar ion laser (Stellar-Pro-L Select 300, Modu Laser, USA) was focused through a 4× objective (Olympus, 0.28 NA) facing opposite the 60× objective. The use of the low NA objective resulted in a Raman excitation beam with a spot size of ~8 μm in the sample plane. This was done to obtain a Raman excitation region that can enable better interactions with a whole cell. Furthermore, this reduces the power density of the Raman excitation laser and hence the risk of photo-damage to the cells. The forward-scattered Raman light was collected using 60× objective and coupled to a spectrometer (ARC-SP 2356, Princeton Instruments, USA) after passing through a notch filter (Kaiser Optical Systems, Inc., USA). The spectrometer was equipped with a thermoelectrically cooled CCD detector (PIXIS 100B, Princeton Instruments, USA). A grating with a groove density of 1200 g per mm and blazing wavelength of 500 nm was chosen to disperse the Raman signal. A schematic of the dual-line optical tweezers focused at the sample plane in the microfluidic channel is shown in figure 2.1b. Of the two line tweezers; one was made longer in comparison with the other by adjusting the relative position and power of one of the line tweezers with respect to the other.

2.2.3 Microfluidic chip fabrication

For the fabrication of microfluidic chip, a master consisting of three input channels and one output channel was fabricated in polymethyl methacrylate (PMMA).

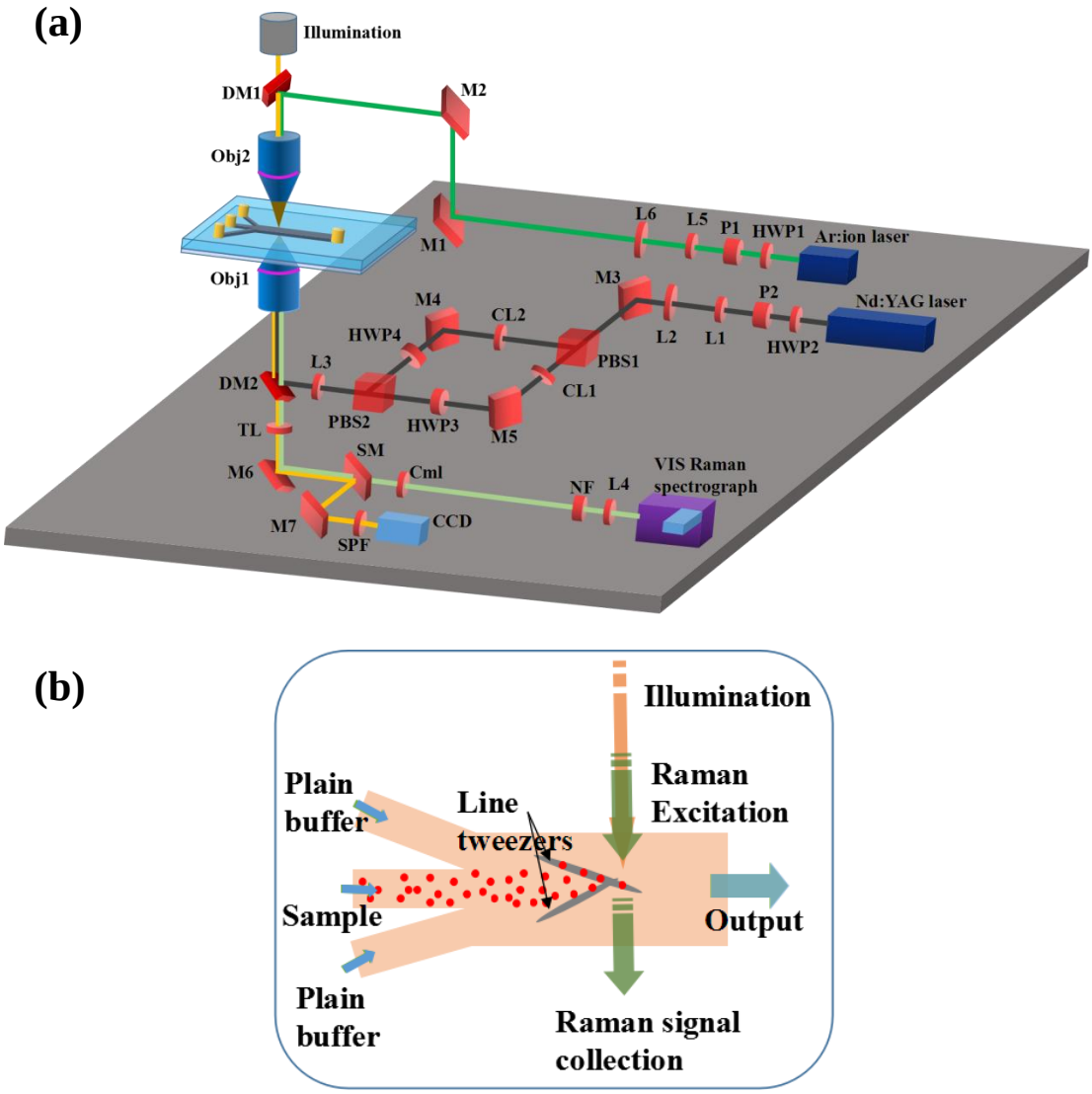

Figure 2.1: (a) *Schematic of the experimental setup. PBS1-2: Polarizing beam splitters, CL1-2: cylindrical lenses, M1-7: mirrors, SM: switching mirror: switches the collected light between bright-field imaging CCD and Raman spectrograph, Obj1: for focusing the 1064 nm laser onto the sample plane and collecting the Raman spectra, Obj2: for focusing the Raman excitation beam onto the sample, P1-2: polarizer, HWP1-2: half-wave plates for adjusting the power of the Raman excitation beam and trapping beam, respectively, HWP3-4: half-wave plates for adjusting the power in the dual-line optical tweezers, NF: notch filter, DM1: dichroic mirror: reflects the 514.5 nm laser and transmits the rest of the light from the illumination source, TL: tube lens, Cml: compensatory lens for collimating the emission signal, DM2: 1064 nm laser line mirror, L1-2, L5-6: lens pairs as beam expanders, L3: coupling lens to complete 4f system, L4: lens coupling the Raman-scattered light to the spectrograph. (b) Schematic expanded view of the dual-line tweezers (black) in the sample plane guiding the cells (red).*

Ultrasonic treatment was used to remove any debris. Sylgard 184 polydimethylsiloxane (PDMS) elastomers (pre-polymer and curing agent, Dow Corning Corporation) were mixed in a ratio of 10 : 1, poured onto the master and kept for ∼48 h at room temperature. The cured PDMS was peeled off the master, and connecting holes were punched using a 0.5 mm biopsy plunger. The structured PDMS was finally bonded with a microscope cover glass following treatment with oxygen plasma using Harrick plasma cleaner. The PDMS mould was pressed manually against the cover glass and further kept at 65 °C for ∼10 min for improved bonding. All the inlet channels in the microfluidic chip had a width of ∼100 μm, and the height of the microfluidic chip throughout the channel was ∼75 μm. The fabricated chip is shown in figure 2.2. The inlets were connected with the syringes via micro-tubing (Tygon). The syringes containing the sheath fluid were mounted on one syringe pump (New Era NE-4002X), and the syringe containing the cell sample was mounted on another syringe pump. The chip was first rinsed with 1% sorbitol, then with 1% Tween-80 to make the channels free of any debris, and finally with PBS to make the chip bio-compatible. Each rinsing step was carried out for 5 min at a flow rate of 20 $\mu L\ min^{-1}$. This process made the surface of the microfluidic channels hydrophilic and reduced cell adherence to the channel walls. Although cell focusing for Raman excitation was achieved using optical guiding, the purpose of using a sheath fluid to sandwich the sample was to keep the side walls of the chip away from the cell sample, which helps in attaining a more uniform velocity profile of the cells in the transverse plane, as also shown by Lei et al. [174] that microfluidic chips with a channel height: width ratio of ∼0.20 (close to the value of ∼0.25 for our chip) enable an almost uniform velocity in the central region in comparison with channels with a height:

width ratio of close to 1. Therefore, in our case (microfluidic channel height: width ratio of ~0.25) the region of uniform velocity would extend for at least ~100 μm (i.e., the width of the central sample region). The microfluidic chip design comprising three inlet channels (of which two side channels serve for sheath fluid flow) was therefore preferred over that with a single inlet channel. Furthermore, as the width of the sample stream was large (~100 μm) in comparison with approaches [157, 158] using hydrodynamic focusing (~10 μm) for the flow of cells in a single line, the effect of any fluctuations in pressure due to the syringe pumps was mitigated in the detection region.

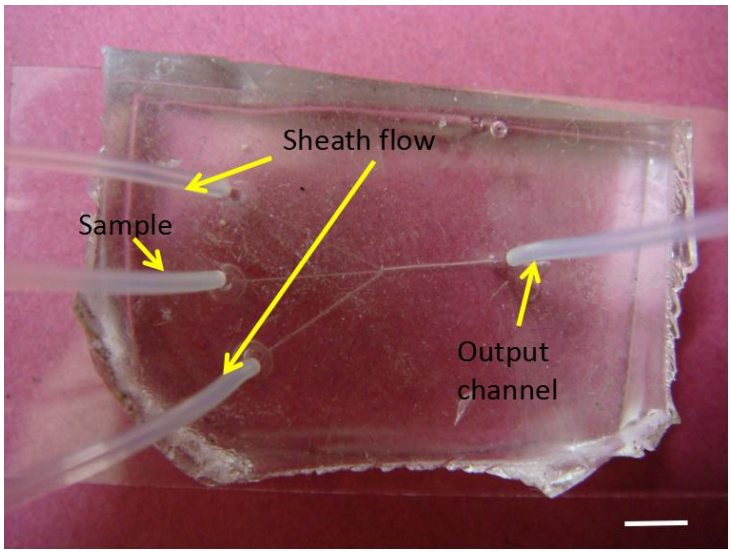

Figure 2.2: *PDMS-based microfluidic chip connected with inlets and outlets for Raman flow cell cytometer. Scale bar: 2.7 mm.*

2.2.4 Data acquisition

Continuous Raman spectra were recorded for single RBCs passing through the Raman excitation region with an acquisition time of 1s. The spectrometer was set to continuously acquire the resonance Raman spectra with an acquisition time of 1 s at an excitation power of ~5 mW. This allowed the Raman spectrum of a single cell to

be recorded in a single acquisition with good signal quality without trapping the cell. Figure 2 shows a typical raw Raman spectrum recorded for RBC while it was passing through the Raman excitation beam in the microfluidic chip. It can be observed that all the major spectral features are visible in the raw spectrum. During analysis, all the Raman spectra were smoothed using Savitzky–Golay filters and background subtracted. The background was corrected by iterative polynomial fitting using a Matlab program [175] before subtraction. One major problem with PDMS based microfluidic chips is the spectral contribution of the PDMS material to the cell spectra [176]. In the present case, the cell height remained in the transverse focal plane of the tweezers, which was closer to the bottom of the chamber in comparison with the top side of the channel, and the PDMS spectra therefore did not appear in the cell spectra. Furthermore, the background contribution from the glass bottom was much smaller as compared to the strong resonance Raman scattering from the RBCs and hence could be ignored.

2.3 Results and discussion

All the parameters of the cell focusing arrangement are governed by the time that a cell is required to spend in the Raman excitation beam to record a spectrum with a good signal to noise ratio. For a given experimental setting, if the acquisition time is t, the cells should cross the Raman excitation region at a rate of $(A + d)/t$ μm s^{-1}, where A is the diameter of the excitation beam spot and d is the diameter of the cell. Thus, the fluid flow velocity should be $R = ((A + d)/t) \cos\theta$, where θ is the angle by which the tweezers of the optical guide are tilted with respect to the fluid flow direction. The value of R for our experimental parameters (A = 8 μm, d = 7.76 μm [177], t = 1 s and θ = 30°) should be ~13.65 μm s^{-1}.

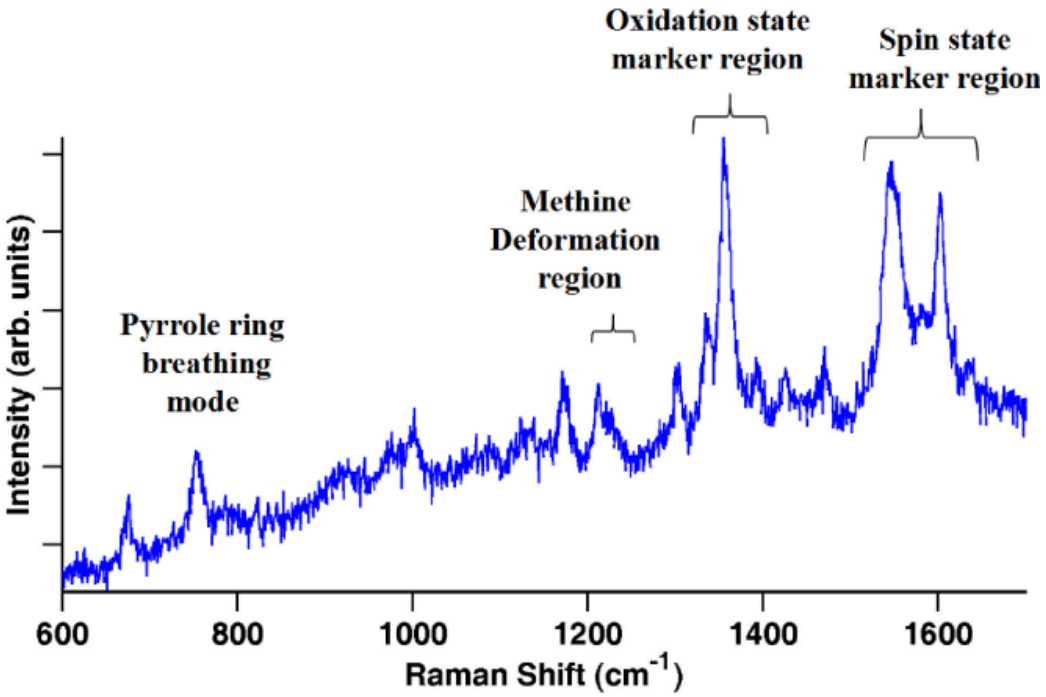

Figure 2.3: *Raw spectrum of an RBC recorded while it was passing through the Raman excitation beam in the micro-fluidic chip.*

In our experiments we used a flow speed of ~15 μm s^{-1}, which is very close to the desired value. Thus, the optical guiding arrangement was developed so that a single cell stream flowing at the above mentioned speed passed through the Raman excitation region. The guiding arrangement consisted of dual-line optical tweezers arranged in the shape of the letter 'Y'. The cells enter through the open side of the guiding arrangement. To focus the cells in the tail region, two conditions need to be satisfied. The first condition is that the cells arriving in the vicinity of the optical field should be confined; and move along the longer axis of the tweezers. This can be expressed as F_{t1}, $F_{t2} > F_d \sin\theta$, where F_{t1} (F_{t2}) is the component of the optical force transverse to the longer axis of the line tweezers 1 (2), F_d is the drag force acting on the cells and θ is the angle at which line tweezers are inclined with respect to the fluid flow direction (figure 2.4a). The second condition is that the cells moving along the

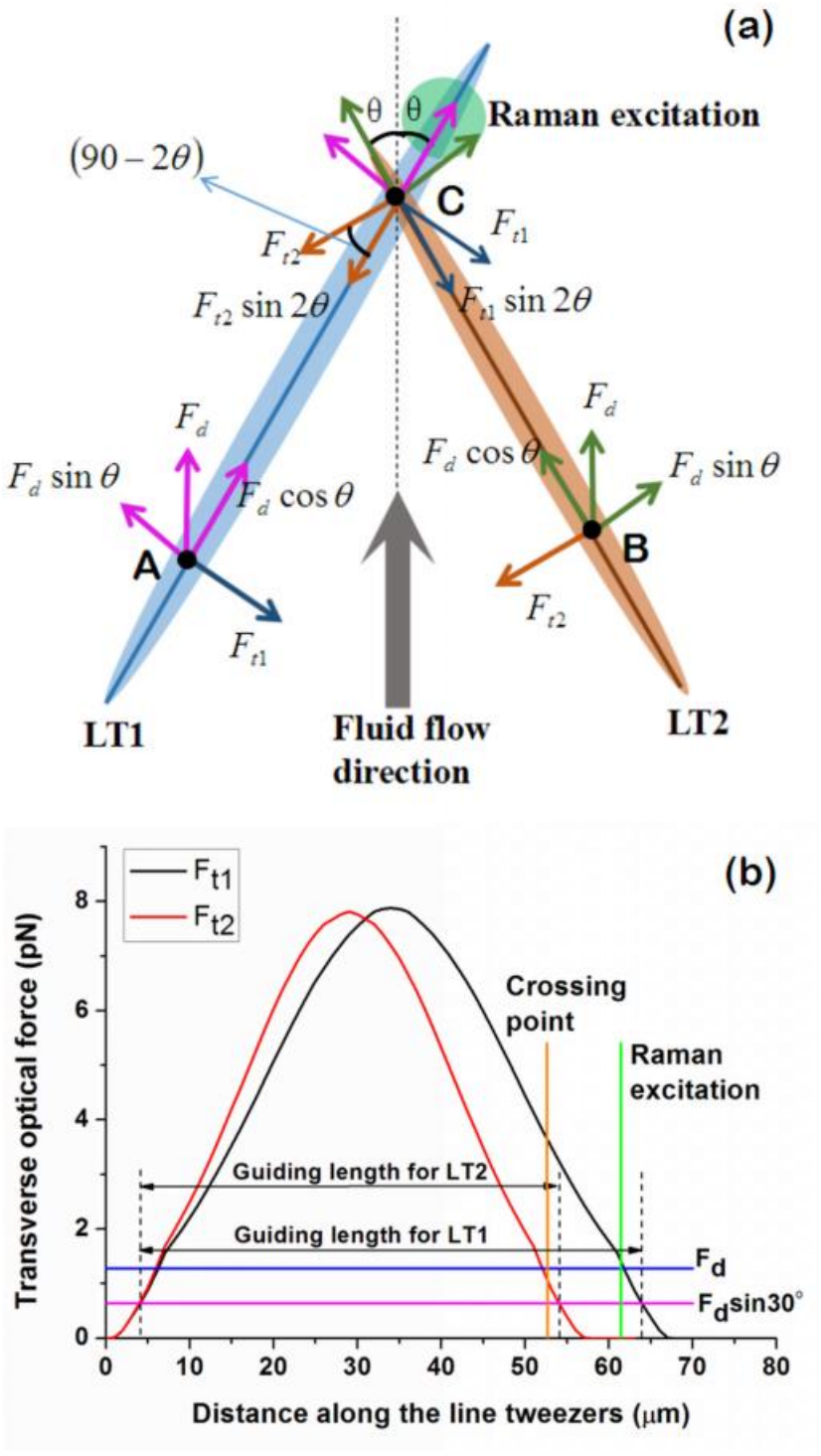

Figure 2.4: *(a) Schematic of the forces acting on a cell while the cell interacts with line tweezers 1 and 2 in fluid flow. F_{t1} and F_{t2} are the transverse components of the optical forces due to line tweezers 1 and 2 respectively. F_d: Drag force. θ: Tilt angle of line tweezers with respect to fluid flow direction. (b) Transverse components of the optical forces due to the line tweezers and the drag force on the red blood cell. LT: Line tweezers.*

shorter line tweezers (LT2) should switch to the longer line tweezers (LT1) at the crossing point of the two line tweezers, and the cells in line tweezers 1 should keep moving, i.e., after the crossing point all the cells flow only along the longer line tweezers (LT1). At the crossing point, cells moving in each respective line of the tweezers also experience a transverse confinement force due to the other line tweezers, which may act to trap the cells at the crossing point.

To avoid this, the drag force component along the axis of line tweezers 1 should exceed the transverse confinement force due to line tweezers 2, i.e., $F_{t2} \sin 2\theta < F_d \cos \theta$. Furthermore, the cells in line tweezers 2 also need to be switched to line tweezers 1, i.e., at the crossing point the component of the transverse confinement force due to line tweezers 1 along line tweezers 2 should exceed the drag force component along the axis of line tweezers 2, i.e., $F_d \cos \theta < F_{t1} \sin 2\theta$, which leads to $F_{t2} < F_d < F_{t1}$ for $\theta = 30°$. To achieve this condition, the optical power in line tweezers 1 was kept higher than the power in line tweezers 2 and, furthermore, line tweezers 2 was aligned to make the dual-line optical tweezers of almost equal length before the crossing point. The optical forces acting on the cells were calculated using ray optics theory [178]. For the power values of ~240 mW for line tweezers 1 and ~200 mW for line tweezers 2 used in the experiment, the transverse component of the optical forces for line tweezers 1 and 2 along the length of these tweezers is plotted in Figure 2.4b. For these calculations, the RBCs were considered to be spherical particles with a radius (r) of 3.3 μm and a refractive index of 1.37 [179]. The viscous drag force on the cells $F_d = 6\pi\eta r v$, where v is the speed of the fluid flow along the channel in the detection region and η is the dynamic viscosity of the fluid (0.001 Pa.s), was estimated to be 1.28 pN for the flow speed used in our experiments, i.e., ~15 μm s^{-1}. The Faxen law [180] was

also taken into consideration for calculating the drag force (height of the plane of focus of the laser tweezers ~5 μm from the glass bottom of the microfluidic chip). Thus, the first condition, i.e., F_{t1}, $F_{t2} > F_d \sin\theta$, is met up to a length of ~60 μm in line tweezers 1 and ~50 μm in line tweezers 2, as can be seen from figure 2.4b. At point C, the values of F_{t1} and F_{t2} are ~3.7 pN and ~1 pN, respectively. Therefore, the second condition, i.e., $F_{t2} < F_d < F_{t1}$, is satisfied. Furthermore, it should be noted that line tweezers 2 should be capable of guiding up to the crossing point (C), and the guiding length for line tweezers 1 should extend beyond the crossing point up to the location of the Raman excitation beam.

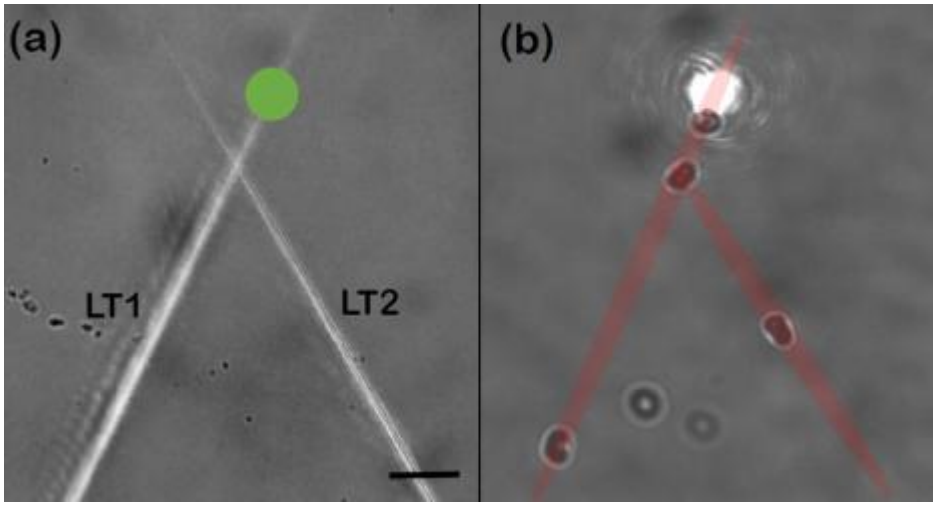

Figure 2.5: *(a) Image of the dual-line optical tweezers arranged in the shape of the letter* 'Y'. *The green-coloured spot indicates the Raman excitation beam; the line tweezers have been labelled as LT1 and LT2. Scale bar: 10 μm. (b) A snapshot from a video showing cells being guided to the tail of the optical guide arrangement (multimedia view). The semi-transparent red region schematically shows the line profile of the dual-line optical tweezers.*

It may be noted that in order to unambiguously record the spectrum of each individual cell, the cells should arrive in the Raman excitation region at intervals of at least 2t s. Therefore, the cells should enter the optical guide at this rate. For a width W of the capture region, i.e., the open side of the optical guide, fluid flow rate R and

depth of the microfluidic channel D, the cell density should be one cell per volume of fluid equal to 2WDR. This gives the maximum permissible cell density, which was estimated to be one cell per volume of fluid of 2.25×10^{-4} μL for our experimental parameters of W = 100 μm, D = 75 μm, R = 15 μm s^{-1} and t = 1 s, which resulted in a cell density of ∼4.44×10^{3} cells per μL. Because the cells flow randomly in the channel and enter the optical guide in a similar fashion, maintaining such a strict time gap between cells is difficult. Therefore, in our experiments we used an even lower cell density, namely, ∼2×10^{3} cells per μL.

A two-dimensional intensity image of the dual-line optical tweezers is shown in figure 2.5a. The location of the Raman excitation beam is indicated by the green circle. A snapshot from a video showing the guiding of RBCs by these dual-line optical tweezers is shown in figure. 2.5b. It can be observed that the RBCs, upon entering the guiding arrangement, are oriented vertically upon interaction with the tweezers, as this allows them to maximize their interaction with the highest-intensity region of the beam [99]. The video clearly shows that the RBCs are captured by both the line tweezers and are subsequently channeled within line tweezers 1, and thus a single-line flow of cells could be obtained. These cells were later analyzed by the Raman excitation beam located at the end of line tweezers 1.

It may be noted that damage to the cells during optical trapping is a concern, and several studies [131, 181] have reported damage to RBCs caused by the 1064 nm laser beam on the basis of changes that appeared in the Raman spectra of the trapped RBCs. It has been reported [131] that cells start to become damaged beyond a trapping power of ∼40 mW (peak power density of ∼10 MW cm^{-2}, considering the size of the focal spot to be of the order of ∼λ). To be on the safe side, the laser power in line tweezers

1, i.e., the line tweezers with higher power, was kept at ~240 mW, which resulted in a peak power density of ~0.5 MW cm^{-2}, considering the length and width to be ~60 μm and ~2 μm, respectively.

The Raman excitation wavelength was chosen close to the Q-band absorption region of Hb, which is the main constituent of RBCs, to resonantly enhance the Raman spectrum. We could record good quality Raman spectra of single cells with a power of ~5 mW and an acquisition time of 1 s. With these exposure conditions, no damage to the cells was observed, as was also noted from their Raman spectra. At a fluid flow velocity of ~15 μm s^{-1}, a cell typically spends ~1 s in the excitation region, and hence the Raman spectra of single cells could be recorded with a good signal-to-noise ratio without trapping the cells, as shown in figure 2.3.

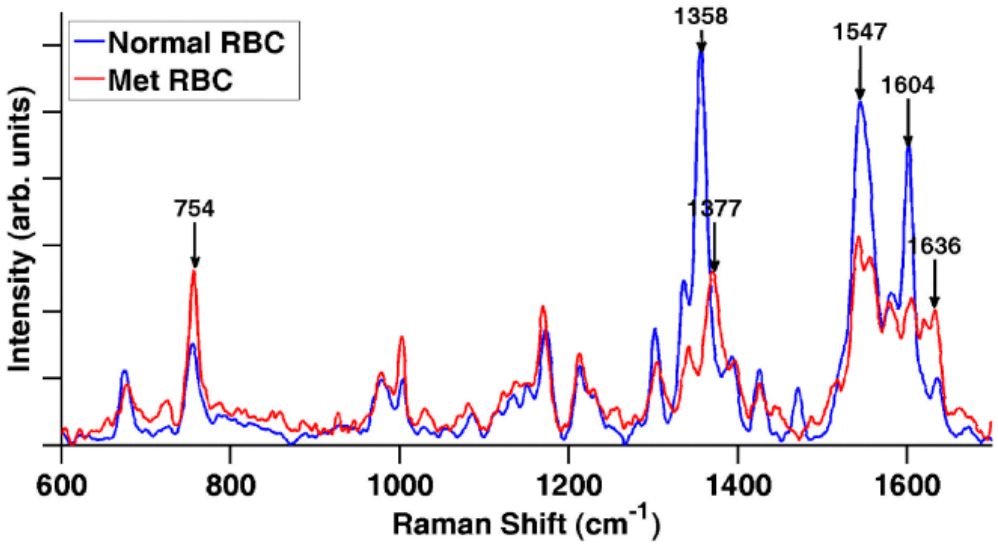

Figure 2.6: *Average Raman spectra of normal-RBCs (blue) and met-RBCs (red) recorded over 25 cells. The spectra shown are area-normalized to emphasize the relative changes in the intensities of various bands.*

Because each cell needs to spend ~1 s in the Raman excitation region to record good-quality spectra, this puts a limit on the throughput that can be achieved using the proposed arrangement. Thus, in a scenario in which the next cell arrives after a gap of

one acquisition period (~1 s), a throughput of ~1800 cells per h can be achieved, considering the fact that the spectrum of one cell should not overlap that of the next cell. However, in an actual situation the cells flow randomly in the channel, and therefore it is difficult to maintain a strict time gap between cells.

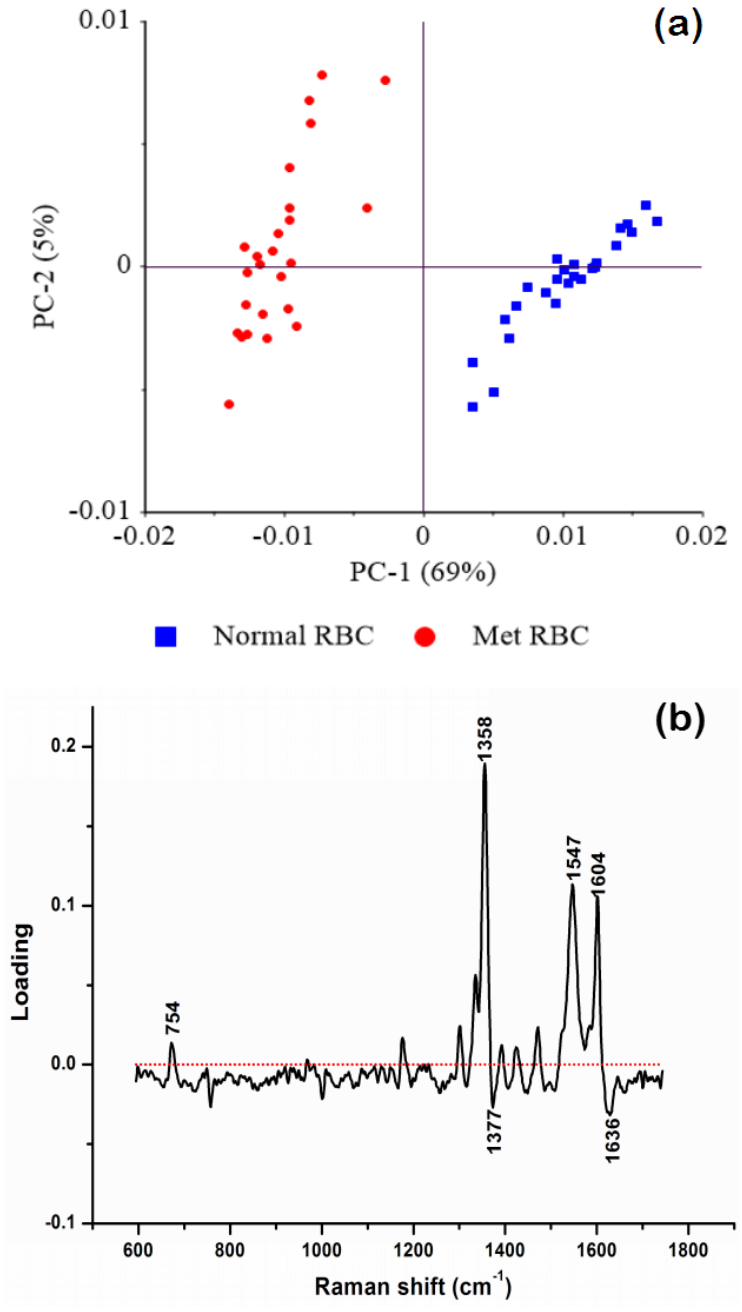

Figure 2.7: *(a) Score plot of normal-RBC (blue- squire shape) and met-RBC (red-circular shape) (b) loading plot of PC1*

With a fluid flow rate of ~400 nL h^{-1}, we could achieve a throughput of ~500 cells per h. To further increase the throughput, the acquisition time needs to be reduced, which in turn would require an increase in the Raman excitation power, but a higher Raman excitation power poses a threat of cell damage. However, a system with even higher throughput can be obtained by using advanced Raman scattering techniques such as coherent anti-Stokes Raman spectroscopy (CARS) [182, 183] stimulated Raman scattering (SRS) [184] etc., in which the signal level is several orders of magnitude higher than that in resonance Raman spectroscopy.

We further show that by using this scheme we could distinguish between normal-RBCs and met-RBCs from a mixture of these RBCs. To emphasize the spectral differences between the normal-RBCs and met-RBCs, we initially recorded the Raman spectra of these cells in a stationary medium, as shown in figure 2.6. Each spectrum represents the average of those of 25 cells. It may be observed that at the power level that was used (~5 mW), normal-RBCs became deoxygenated owing to photo-dissociation of oxygen from haemoglobin [162] and therefore the spectrum of normal-RBCs shown in the figure is more like that of deoxygenated RBCs. It can be observed from figure 2.6 that the prominent changes include shifting of the band at 1358 cm^{-1} (ν_4, breathing mode of pyrrole rings in Hb) to 1377 cm^{-1}, decreases in the intensities of the bands at 1547 cm^{-1} (ν_{11}) and 1604 cm^{-1} (ν_{19}) and an increase in the intensity of the band at 1636 cm^{-1} (ν_{10}) upon the transformation of normal RBCs into met-RBCs. This shift is known to be associated with a change in the oxidation state of Fe in Hb from Fe^{2+} to Fe^{3+} [162, 185].

The Raman spectral data were further analyzed with principal component analysis using software (The Unscrambler, Camo) to find out the band undergoing most

significant changes which can be used for discrimination between normal-RBC to met-RBC. A plot between principal component 1(PC1) and principal component 2 (PC2) shown in figure 2.7a indicates that n-RBC and m-RBC get clustered in different groups along the first principal component. Further from the loading plot as shown in figure 2.7b, the maximum loading appears in the region 1350-1400 cm^{-1} and corresponds to a shifting of the band at 1358 cm^{-1} to 1377 cm^{-1}. Because the absolute intensity of a particular band may vary depending on the volume of the cell and its interaction time with the Raman excitation beam, a shift in a band is therefore a better basis for discriminating between cells without the need for any statistical analysis. Therefore, we used the peak position of the ν_4 band for the identification of the normal or met state of the RBCs flowing in the microfluidic chip.

As a demonstration of the efficacy of this approach as a label-free microfluidic flow cytometer, we aimed to discriminate between met-RBCs and normal-RBCs from a mixture consisting of met-RBCs and normal-RBCs in a ratio of 1: 9. The spectrometer was set to continuously acquire resonance Raman spectra with an acquisition time of 1 s at an excitation power of ∼5 mW. Data were recorded for a total of 1328 cells at a cell flow rate of ∼500 cells per h in multiple sessions, which took ∼162 min. The recorded spectra were then analyzed for the position of the ν_4 band to identify met-RBCs and normal-RBCs. The area normalized averaged spectra of all the cells identified as normal-RBCs or met-RBCs are shown in figure 2.8. A total of 114 and 1214 cells were identified to be met-RBCs and normal-RBCs, respectively, which yielded a ratio of 1: 10.7. Although this is close to the original mixing ratio, a better result could be expected if the experiments were performed on a larger number of cells. It may be noted that in our experiments we used RBC as sample, as their Raman

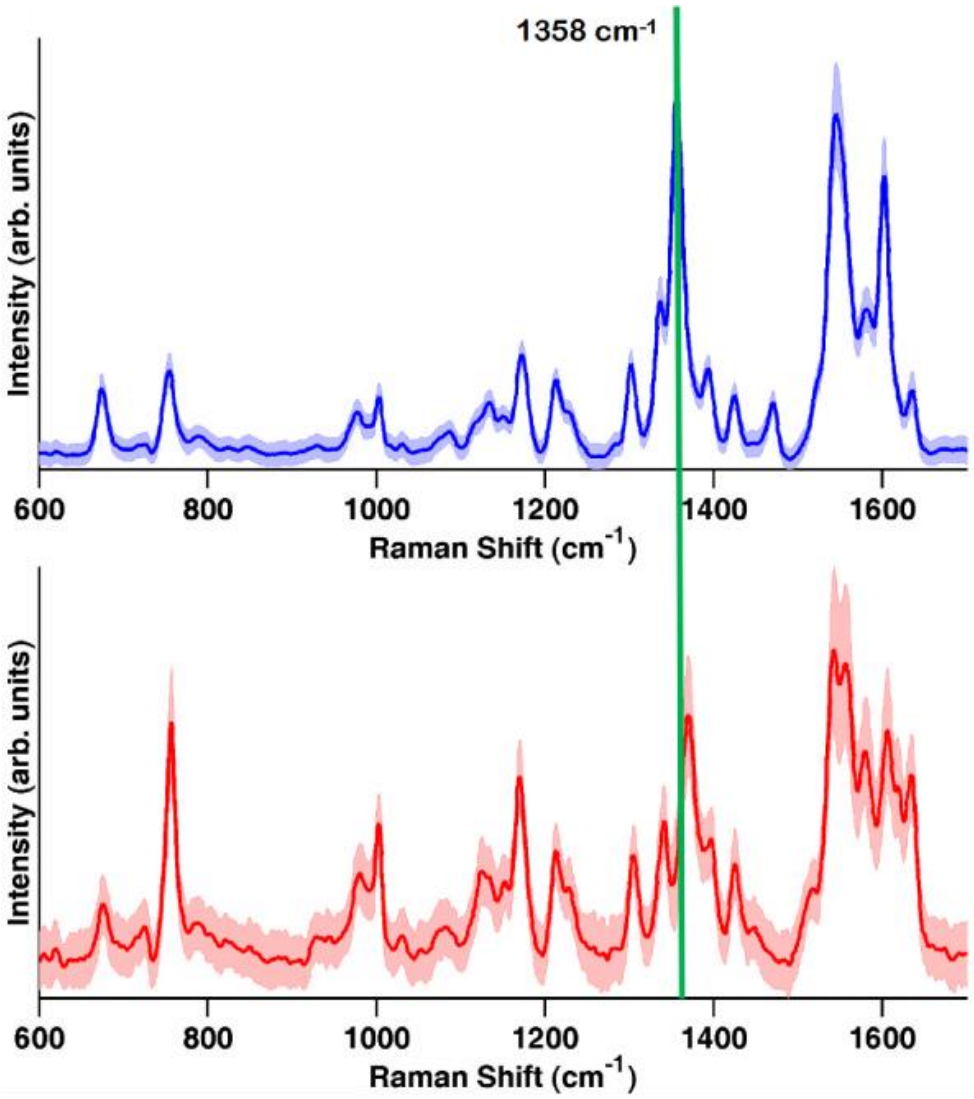

Figure 2.8: *Area-normalized average spectra of (a) normal-RBCs (blue) and (b) met-RBCs (red) in flow. The thicker lines show the mean spectra of the normal- and met-RBCs, and the shaded regions show the standard deviations of the recorded spectra. The vertical lines show the band at 1358 cm^{-1}*

spectrum can be resonantly enhanced using an excitation wavelength in the Soret or Q-band of the absorption spectrum of Hb. Similarly, molecules present in other mammalian cells, such as carotenoids, cytochromes, proteins, and nucleic acids, can also be investigated using the appropriate Raman excitation wavelengths. Furthermore, we used a weakly focused Raman excitation beam with a spot size close

to the size of the RBCs. By suitably adjusting the focal length or the distance between the lens (Obj 2 in figure 2.1) and the sample plane, the size of the Raman excitation spot can be varied and therefore cells such as white blood cells, tumor cells or other mammalian cells can also be investigated.

It is pertinent to note here that because the resonance Raman effect, which was used in our experiments, requires the presence of absorbing molecules to occur; its use cannot be generalized like the spontaneous Raman effect. However, there are other variants of Raman techniques such as coherent anti Stokes Raman scattering (CARS) [183] or stimulated Raman scattering (SRS) [184] that provide even stronger signals and do not require absorbing molecules. Hence, by integrating the proposed optical focusing technique with these coherent Raman techniques a faster and more generally applicable microfluidic Raman flow cytometer can be developed.

2.4 Conclusion

To summarize, we discussed development of a Raman spectroscopy based label free microfluidic cell cytometer in which dual-line optical tweezers were used for optical guiding of the cells to the Raman analysis region. Optical guiding facilitated the decoupling of the cell flow speed from cell focusing. The suitability of this approach for cytometry was demonstrated by identifying RBCs in their normal and met forms on the basis of the spectra recorded for single cells in flow. The throughput for detection was ~500 cells per h, which was limited by the acquisition time required for recording good-quality Raman spectra.

3 Chapter 3: Acousto-optic tweezers for passive sorting of colloids

In this chapter, we present the development of acousto-optic tweezers setup which makes use of AOD for generation of multiple optical traps. AOT works on time sharing mode and also known as blinking traps. By appropriately choosing the periodicity of these traps larger sized colloidal spheres can be selectively trapped out of a mixed population. This happens because smaller sized spheres being more agile escape out of the trap volume during the off period of the trap beam. Therefore, by scanning an array of blinking traps over a mixed sample bigger spheres can be forced to move with the traps and eventually could be taken to the output side. Experimental demonstration of sorting between 1 μm and 2 μm diameter silica spheres is presented.

3.1 Introduction

Optical techniques to sort heterogeneous samples for functional and biochemical analysis of various sub-populations are particularly useful for small sample volume or particle number, and can be integrated with micro-fluidic devices like micro total analysis systems (μTAS) [186]. The ability to generate spatially sculpted light fields, either generated holographically [128], multi-beam interference pattern [133], or by time sharing technique [135], has found significant application in this area. In these techniques, however, the particles are affected by colloidal traffic problems when flowing through the sorting region. These issues may be reduced to some extent by the use of a flashing or translating optical potential [134]. However, carrying out optical

Work discussed in this chapter has resulted in the following publication:

1. R. Dasgupta, **R. S. Verma** and P. K. Gupta, "Microfluidic sorting with blinking optical traps," *Opt. Lett.* **37**, 1739-1741 (2012).

sorting in absence of any fluid flow can largely minimize these issues. Further, the ability to separate particles in the absence of a fluid flow makes the technique usable with any sample chamber, without the need for complex microfluidic systems. Flow less sorting can be achieved by using the optical potential of a Bessel beam. Particles placed within the outer rings of the beam move toward the bright central core at a rate that depends on their size and refractive indices [127]. However, since the sorted fraction is guided along the axis of the central core, this scheme is not much suitable for planar microfluidic structure. Other types of flow less sorting are based on moving light interference fringe patterns that are swept over the sample [136, 187, 188]. But since these techniques employ multiple beam interference, these methods may be sensitive to vibrational instabilities. Another disadvantage of these methods is the need for laser sources delivering hundreds of mW of laser power, which makes it unsuitable to use low cost and compact diode lasers that can be conveniently integrated into the microfluidic structures. Here we show that blinking optical tweezers with appropriately chosen periodicity stably trap only the larger size fraction of the population when both smaller and larger particles are present in the medium. This occurs because the smaller particles are much more agile; if the time periodicity of the blinking trap is made suitably long, they have a high probability of escaping the trap volume during the off time. Therefore, in a flowless medium, when blinking traps were swept over a mixed sample, only bigger spheres follow the motion of the traps and are eventually taken to the output side. The technique requires only a few mW of power at each trap site and a small number of scanning traps was found to be adequate for sorting the particles. To understand the basic physical principle for selective trapping of particles by a blinking

trap, we may note that the mean square displacement of a Brownian particle is given by [189]

$$\left\langle \left| r^2 \right| \right\rangle = 6Dt \tag{3.1}$$

where 't' is the time interval for observation and D is the diffusion constant given by fluctuation dissipation formula as [189]

$$D = k_B T / 6\pi\eta R \tag{3.2}$$

where k_B is the Boltzmann constant, T is the temperature in °K, η is the dynamic medium viscosity, and R is the radius of the spherical colloid. It can be seen from eq. (3.2) that smaller spheres are more agile and move through a longer distance than larger spheres over a given time interval. Therefore, by tuning the time periodicity of the blinking traps, smaller particles can be made to have a higher chance of crossing the capture range of the trap and escape during the off time.

3.2 Materials and method

The schematic of the acousto-optic tweezers setup made on a home built microscope is shown in figure 3.1. The laser source was a cw, 1064 nm Nd:YAG laser (home built) which was collimated and expanded using lens pair L1(f=50 mm) and L2 (f=100 mm). The expanded beam passes through a dual-axis acousto-optic deflector (AOD) system (DTD-275HD6M, IntraAction Corp., USA) placed at conjugate plane to the back aperture of a 100x, NA=1.25 oil immersion microscope objective (Zeiss Acroplan). Lenses L3 (f=150 mm) and L4 (f=300 mm) along with the dichroic mirror (DM) were used to image the AOD onto the back aperture of the microscope objective. The dual-axis AOD system could be aligned to have an useful (1,1) order diffraction efficiency of approximately 60% and to obtain low power variation (<20%) of the (1,1)

diffraction order for complete range of driving RF frequencies (21 MHz to 33 MHz) ensuring similar trapping characteristics of the time shared traps. The iris was used to select the (1,1) diffraction order and block other light.

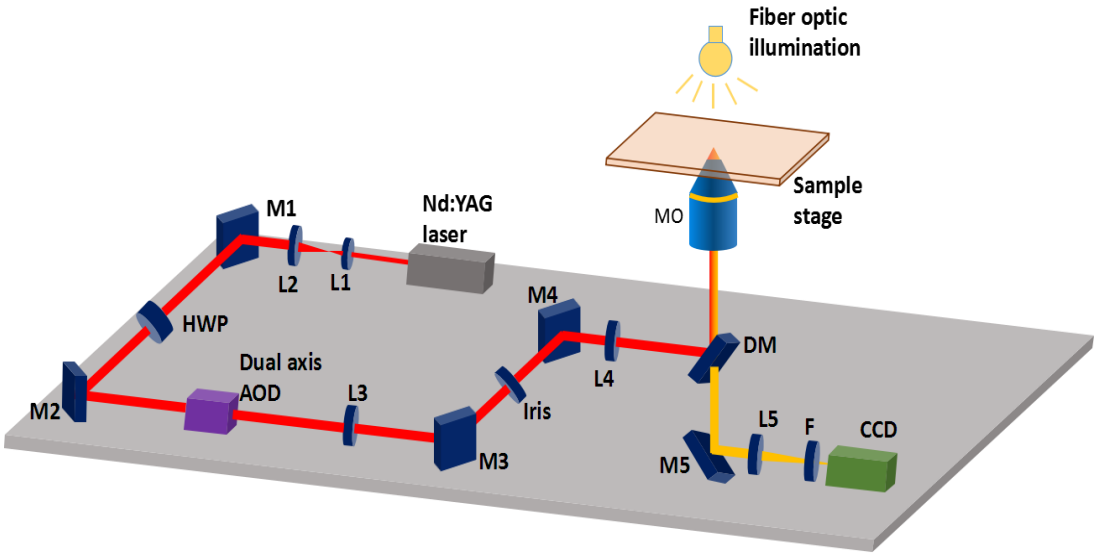

Figure 3.1: *Schematic of setup, Lenses pairs L1, L2 and L3, L4: beam expander, M1, M2, M3, M4 and M5: mirrors, HWP: half wave plate, Dual Axis AOD: dual axis acousto-optic deflector, MO: microscope objective, DM: dichroic mirror. L5: lens to focus the light onto the CCD, A cut-off filter (F) was used to suppress the back scattered laser light onto the CCD.*

A fiber optic illuminator was used to illuminate the sample and the sample was imaged onto the CCD camera using mirror M5 and lens L5 (f=150 mm). A cut-off filter (F) was used to suppress the back scattered laser light onto the CCD. After the alignment, the laser power of the Nd: YAG laser was adjusted to ensure a trapping power of ~ 5 mW at each trapping sites.

The AODs is controlled via direct digital synthesizers (DDS) (DVE 120, IntraAction Belwood, IL, USA) [190]. The DDS can generate sinusoidal waveforms with various frequencies, phases and amplitudes. The DDS sends the signal to RF power amplifier (DPA-502 Dual channel) which provides amplified RF power to piezoelectric materials bonded on Tellurium dioxide crystals placed perpendicular to

each other. The DDS can supply RF output up to 2 W of continuous wave power across 1MHz to 120 MHz band with an internal clock frequency of 300MHz. Since the AODs operate between 21 and 34 MHz, the bandwidth of the DDS is sufficient for controlling the AOD. A LabVIEW based program was developed to control of the angle of deflection and the amplitude in the deflected beam [191].

For AOT setup position calibration, the change in the displacement in the trapped object position was mapped with the change in the frequency shift of the applied RF. For this, we recorded the images of a polystyrene sphere of size ~2 μm in trap while changing the applied RF by 1MHz each time. The position of the particle was estimated by applying the centroid detection algorithm on the intensity thresholded image. From these images, 8 pixel shift of the trap was observed corresponding to the 1MHz frequency shift of the AOD. Further the CCD pixel image size was calibrated using the stage micrometer (Olympus) and was estimated to be 1 μm=9 pixel. These resulted in the position calibration value of 1 μm=1.125 MHz.

3.3 Results and discussion

First, we estimated the escape probabilities of the colloids with a change in the half period from 50 ms to 2 s. The single particle was trapped and observed for 30 s to see whether it remained in the trap or escaped. For each half period, observation was made over twenty particles of each size. Results presented in figure 3.2(a) show that for a half period of >500 ms, spheres of size 1 μm have 100% chance of escape. Whereas, 2 μm spheres have nearly zero escape chance up to a half period of ~1 s. Figures 3.2(b) (i) and (ii) show the trajectories of a 1 μm and a 2 μm sphere when trapped. The particles were tracked using cross correlation analysis method [43] on successive image frames

time separated by 40 ms. Briefly, a kernel image of a microsphere was selected out of a single image frame and thereafter cross correlation of the kernel with each frame in the sequence was performed. The centroid of the cross correlation peak in each image revealed the particle position. The precision of the method could be determined from the standard deviation of the estimated position coordinates over a series of images of a fixed microsphere on the cover slip as ~5 nm. We started tracking a particle only after it got trapped. The trapping range was estimated as the radius of the circle centered at the trap focus that encloses all the recaptured particle trajectories. The long trace with an open end extending beyond the capture range shows the escape path. Since presence of any nearby particle can cause error in the tracked trajectories or can influence its motion, dilute mono-dispersed suspensions of 1 μm and 2 μm spheres having concentrations of ~9.5×10^7 particles per ml and ~1.2×10^7 particles per ml respectively were used that ensures no other particles were present within the observation region. Also the setup was kept on an air floated table top (RS2000-36-8, Newport Corp) to suppress any environmental vibrations that could influence the particles. The observed trapping ranges were ~0.75 μm and ~1.5 μm for 1 μm and 2 μm spheres, respectively. The trapping ranges were larger than the radius of the trap beam (~0.5 μm); the trap range is approximately the sum of the radii of the beam and the particle itself. From Eq. (1), we calculated that the average time for the particles to diffuse through the trap ranges are ~200 ms and 1.53 s respectively. The values agree well with the results presented in figure 3.2(a). The above observation suggests that when an array of blinking traps with half period somewhat between 500 ms and 1 s is scanned towards an output side at a speed so that it takes ~30 s to complete each scan, it is likely only larger spheres will

follow the traps, whereas the smaller spheres will be left behind. We used a square trap array of four traps generated by time sharing the laser beam at a frequency of 1 kHz.

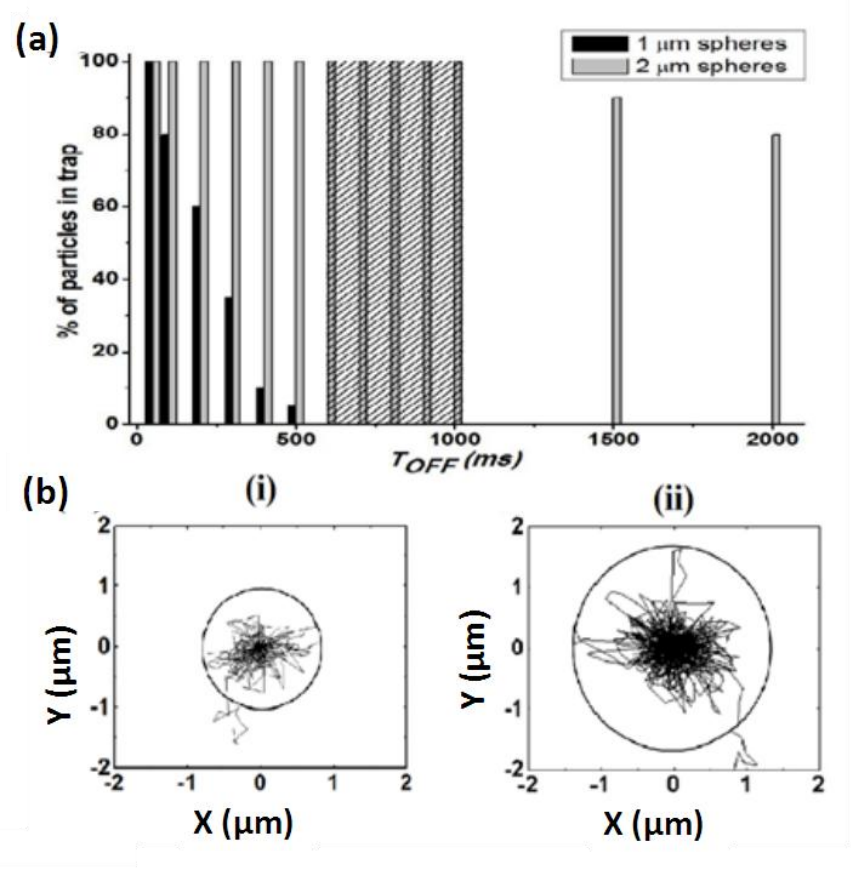

Figure 3.2: *(a) Escape probabilities of spheres against T_{OFF} (b) Trajectories of a (i) 1 μm and (ii) 2 μm particle in trap.*

As this scan rate is much faster for the Brownian motion of micrometer size colloids, we assumed that trapped particles only see a steady optical potential. Over this we superimposed an amplitude modulation to synchronously flash the traps on and off (half period 700 ms). Also, the blinking pattern was spatially scanned over a distance of ~12 μm to the right at steps of 1.2 μm⁄s as shown in figure 3.3(a).

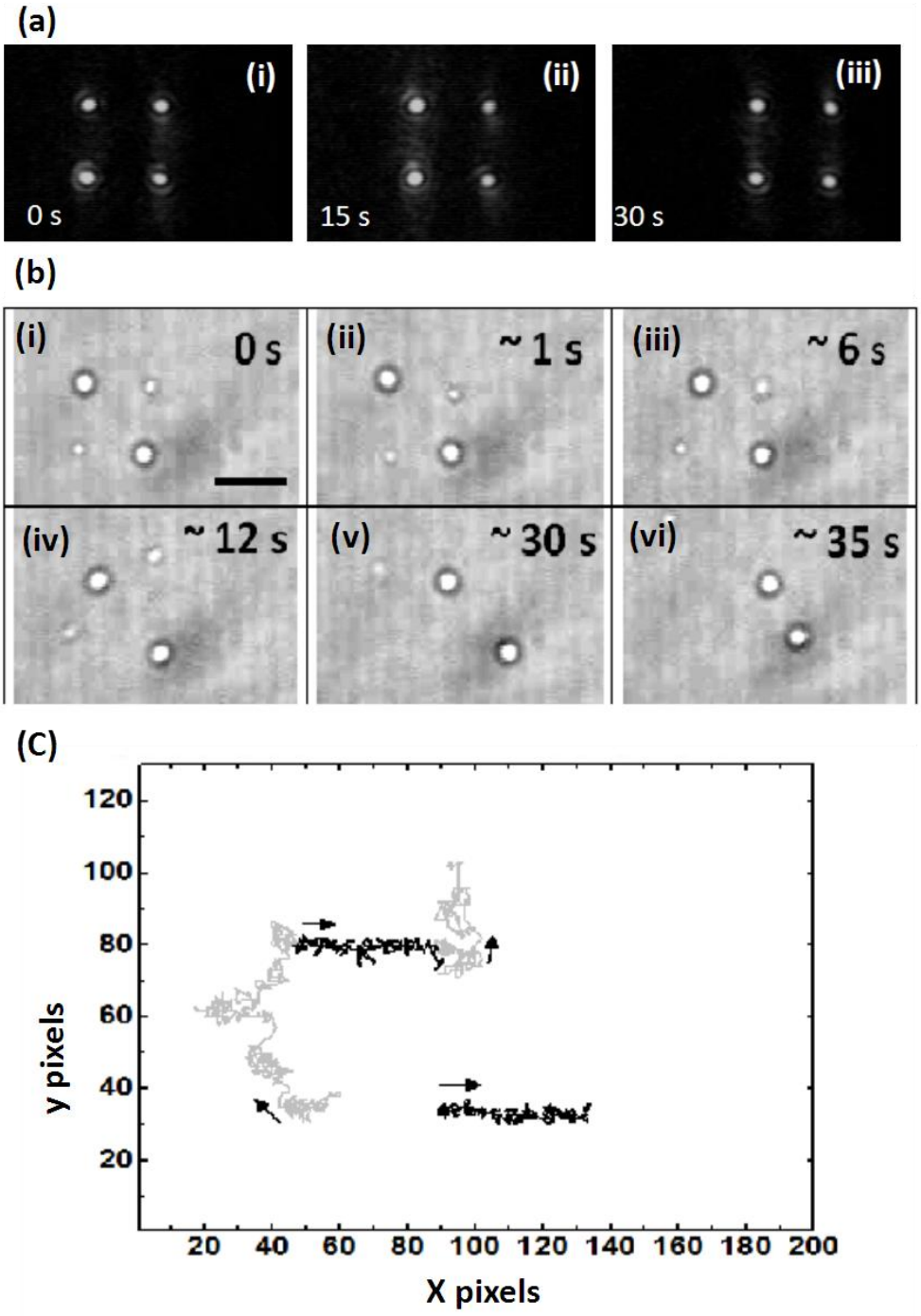

Figure 3.3: *(a) Time laps images from a video while scanning a set of four traps. Scale bar: 12µm, (b) Image frames showing the motion of the particles when the traps are moving toward the right.(c)Particle trajectories with dark lines and faded lines representing 2 µm and 1 µm spheres, respectively. Scale bar: 12µm.*

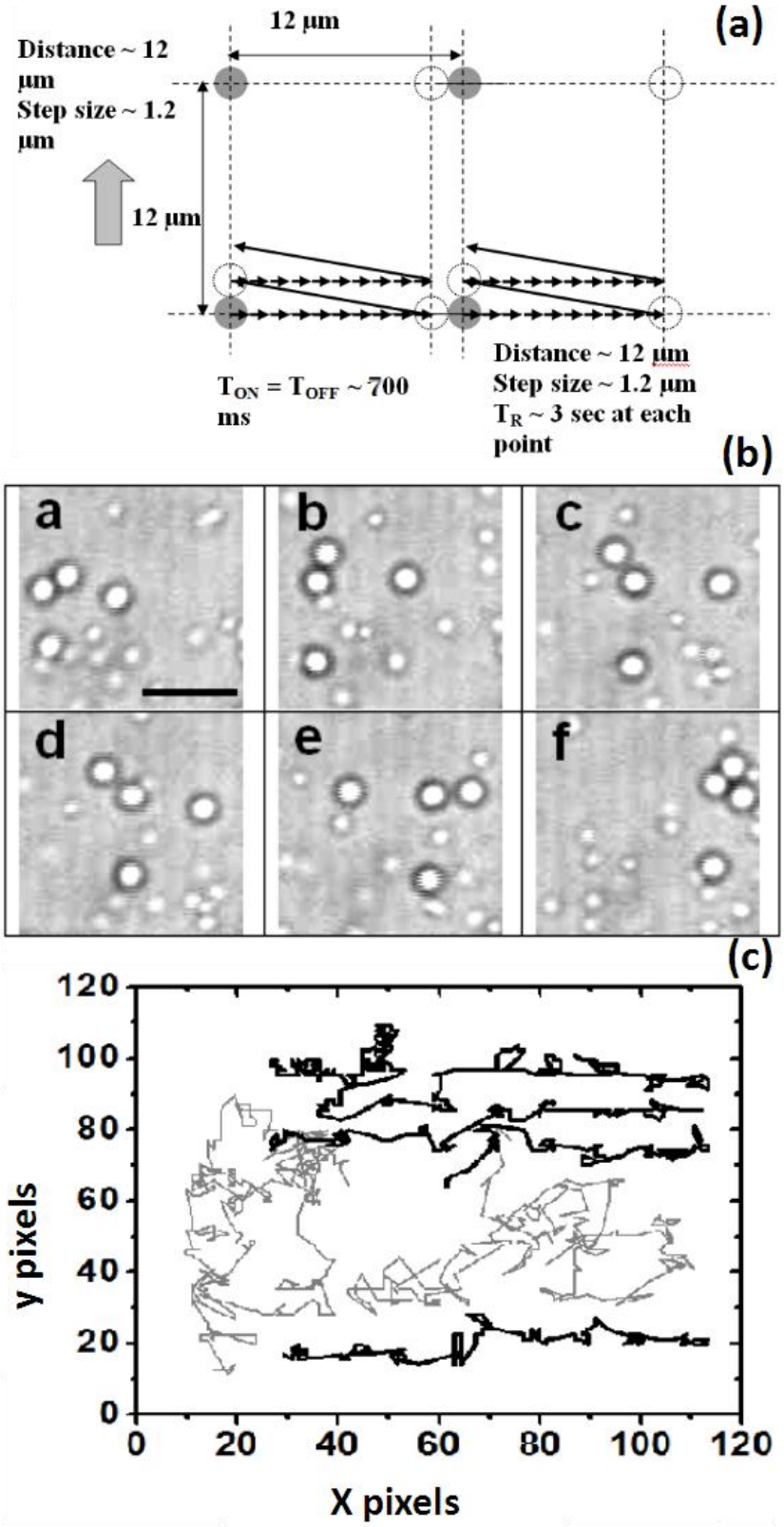

Figure 3.4: *(a) The scanning pattern of the trap array for sweeping over an area. (b) Image frames showing sorting between 1 µm and 2 µm silica spheres. (c) Trajectories of the 1 µm (fade lines) and 2 µm (dark lines) spheres. Scale bar: 12µm*

The traps were held at each spatial location for a residency period of 3 s, so that total time taken for one scan was ~30 s. To check whether the scheme works to produce selection between 1 μm and 2 μm spheres, we first trap two 1 μm and two 2 μm spheres in the four trapping sites and performed a scan toward the right. Results presented in figure 3.3(b) shows that at start (0 s) all the spheres are trapped at the four traps. The traps are off for 0.7 s–1.4 s and therefore at 1 s the distances between the spheres are not identical as these are free to move. At ~6 s the 1 μm sphere at bottom left corner escapes out and the second 1 μm sphere also escape the traps at ~12 s. The two 2 μm spheres stay on with the moving traps and at 30 s reach the right end. At 35 s the traps are off and the spheres have diffusional motion. Figure 3.3(c) shows the trajectories of the particles computed using a cross correlation algorithm. Whereas the 1 μm spheres did not have any directed motion toward the right end, the 2 μm spheres could be seen to get driven into the right end by the traps. It is pertinent to note here that since the capture range of traps depends on the size of the trap beam as well as on the particle size in a complicated fashion [192], and further, the time required for a particle to move through the trapping range can only be determined in a probabilistic fashion, it is therefore, difficult to predict the exact requirement on trap periodicity for effective separation between two given size fractions of colloids. We also did experiments with 0.5 μm and 1 μm spheres and it was observed that for a trap off period of 70 ms the spheres could be separated. Since the visibility of the 0.5 μm diameter particles was poor the measured trajectories were not very accurate and therefore data are not presented. The 70 ms T_{OFF} was chosen as we observed that for an off time of ~40 ms nearly 100% of 0.5 μm particles escape out of the trap during an observation time of 30 s and for an off time of ~80 ms nearly all the 1 μm size particles remained in trap for the same observation time.

Therefore, an intermediate value of 70 ms was chosen to selectively transport the 1 μm spheres. The result indicates that for going below particle sizes of 0.5 μm and 1 μm the required small T_{OFF} may become too stringent considering the typical delays associated with the hardware and software modules. On the other hand, at the larger size end the required off time may be a few seconds, and therefore, the approach may become much slower.

For sorting of particles over an area, we used raster scanning of the trap arrays. The trap array pattern moving toward the right end (output) was also made to shift in the perpendicular direction after each horizontal scan in steps of 1.2 μm/s over a distance of ~12 μm to perform an area scan as shown schematically in figure 3.4(a). Figure 3.4(b) demonstrates the sorting of 2 μm spheres toward the output. It is worthwhile noting that the scanning range can be varied by changing the focal lengths of the relay lenses (L3 and L4) that image the AOD to the input of the objective. A longer scanning range will help ensure a better accuracy of separation. It can be seen from figure 3.4(b) that out of the mixed population only 2 μm spheres were selectively taken toward the right. In the second frame, three spheres can be seen to be trapped at the corners of the square trap array. In the third frame, the sphere farthest to the right reaches the output, but the remaining two spheres, which are trapped at the left column of the array, only reach the halfway mark. In the fourth frame, these spheres are again trapped in the right column of the array when a new scan has started. Therefore, in the fifth frame these spheres are also taken to the output. In a similar fashion, the remaining one sphere was also taken to the output. Figure 3.4(c) shows the tracks of the particles. All 2 μm spheres were seen to get sorted to the right, whereas the trajectories for 1 μm spheres are largely seen to be

dominated by diffusional motion. A small number of 1 μm spheres were seen to enter the output side via diffusional process.

3.4 Conclusion

In summary, we have demonstrated a new optical method for sorting different sizes of colloids under flow less condition. The accuracy of the method may be further increased using microfluidic channels that will prevent entry of smaller spheres into the output side by diffusion. The method can also be applied in spatial light modulator based setups.

4 Chapter 4: Active optical sorting using holographic optical tweezers

In this chapter we have described the use of holographic optical tweezers for sorting applications suitable for different sample conditions in a flow less medium. For samples having small number of desired particles, an approach for active optical sorting of colloids/cells by employing a cross correlation based pattern matching technique for selection of the desired objects and thereafter sorting using dynamically controllable holographic optical traps is presented. The problem of possible collision between the different sets of objects during sorting was avoided by raising one set of particles to a different plane. Results obtained using this approach for some representative applications such as sorting of silica particles of two different sizes, of closely packed colloids and of white blood cells and red blood cells from a mixture of the two. Further it is shown that using multiple planes four different types of particles can be sorted in sequential or parallel manner. However, the approach is not suitable if the desired particles are in very small concentration. For such samples, an approach which can maintain separated particles from multiple ROIs was proposed and demonstrated by sorting of ~3 μm silica sphere in a mixture of ~3 and ~5 μm silica spheres.

Work discussed in this chapter has resulted in the following publication:

1. **R. S. Verma**, R. Dasgupta, S. Ahlawat, N. Kumar, A. Uppal and P. K. Gupta, "Pattern matching based active optical sorting of colloids/cells", *J. Opt.* **15,** 085301 (2013).
2. **R. S. Verma** and N. Kumar, "An active optical sorting approach for low desired particle concentration in the sample using holographic optical tweezers", Proc. of National Laser Symposium (NLS-26), held at BARC, Mumbai, CP-11-21, (2017).
3. **R. S. Verma**, R. Dasgupta, S. Ahlawat, and P. K. Gupta, "Image pattern based selection and sorting of micro particles using holographic optical tweezers", Proc. of National Laser Symposium-20 held at Anna University, Chennai, India, January 9-12, 2012, pp. 904-907.

4.1 Introduction

In recent years there has been considerable interest in the development of efficient optical sorting techniques because of the non-invasive and sterile nature of optical forces. Additionally, optical techniques can work with a very small volume of the sample and can be easily integrated on a lab-on-a-chip system. There are primarily two approaches for optical sorting; passive and active sorting. Passive sorting techniques [121, 127,133, 187, 193, 194] exploit the difference in the intrinsic optical properties (such as refractive index and size) of the particles to result in different trajectories for the particles when these flow over an optical field and escape. On the other hand, in active optical sorting techniques [115, 148, 195, 196] the desired particles are first identified and thereafter an optical force is used to deflect/guide these to the output channel. An example of active sorting scheme is the microfluidic version of the flow cytometer. Here the throughput is limited by the fact that the cells are identified and sorted one at a time. Parallel identification and sorting of a number of objects at a time is desirable for increasing the throughput. One approach to achieve this is to employ image analysis routines to identify objects and subsequently use holographic optical traps to sort them. An important advantage offered by this approaches is that the technique can work under a flow-free condition. Rodrigo et al. [119] were the first to demonstrate the use of real time arbitrary patterning of a holographic optical tweezers array for performing sorting tasks in a colloid suspension. However, their approach required human input for identifying and subsequently manipulating each individual particle and therefore was inherently slow. A significant improvement in the sorting speed was made by Chapin et al. [118], who used the bright-field images of objects for the identification and subsequently used an array of holographic optical traps to move

the particles to the desired region. To avoid collisions among the moving particles an iterative path planning algorithm was used and the particle trajectories were kept sufficiently apart to avoid interference from the optical force field of other traps. These requirements limited the applicability of the approach to dilute suspensions and also limited the speed of sorting. Typically, for a suspension of tens of particles over ~1600 sq μm of area, the time for calculating the optimized paths for all the particles were reported to be of the order of a few tens of seconds. Another possible approach to avoid collisions is to make use of multiple weakly focused laser beams to axially deflect one type of particle and then use a suitable fluid flow to deflect the particles present in a higher Z plane in one of the vertically stacked channels of a microfluidic system [125]. However, this approach has two drawbacks; first, it requires fluid flow for sorting, and second, a variation in the power of the multiple beams generated to trap particles results in a change in the position of the Z plane of the deflected particle, leading to a reduced accuracy of the sorting method. In this paper we report results of our studies on the use of computer controlled maneuvering of holographic traps to manipulate the particles in different Z planes and achieve sorting under a flow free condition.

Most of the approaches are limited for binary samples i.e. samples having mixture of two types of cells/particles. However, many a time, like in the blood samples, more than two constituents are present. In such samples it would be more useful for real life applications if the approach can be extended to more type of particles. To achieve this we investigated the possibility of using multiple planes in sequential or parallel manner. Furthermore, if the concentration of the desired particle in the sample is low as compared to the other, such as white blood cells in blood sample, it may so happen that many a time no white blood cell is visible in the field of view in a flow free medium. In

such cases, an approach which can be used for sorting of the desired particle for required number in multiple field of view would be useful.

In this chapter, we present the development of two active optical sorting approaches based on use of multiple planes for trapping using HOT. One approach makes use of pattern matching and the other makes use of manual selection of the target particles. We present results of sorting of different mixtures of different sizes of microparticles (such as polystyrene, silica, cells etc.) using these approaches.

4.2 Pattern matching based active optical sorting

In this approach, particles are first identified using a cross correlation based image pattern recognition technique. Thereafter these identified particles were trapped and one set of particles were moved in a higher Z plane using the holographic optical traps. These two set of particles maintained in trap but in different planes were translated parallel in opposite directions in respective planes. At the end the particles in the upper plane were brought down to the bottom plane. The approach naturally avoids particle–particle collision by using multiple planes for different types of particles. To demonstrate the applicability of the approach it was used to successfully sort particles of two different sizes or indices of refraction and for sorting human red blood cells from white blood cells.

4.2.1 Method

The main steps of the algorithm for optical sorting approach are shown by a flow chart as shown in the figure 4.1.

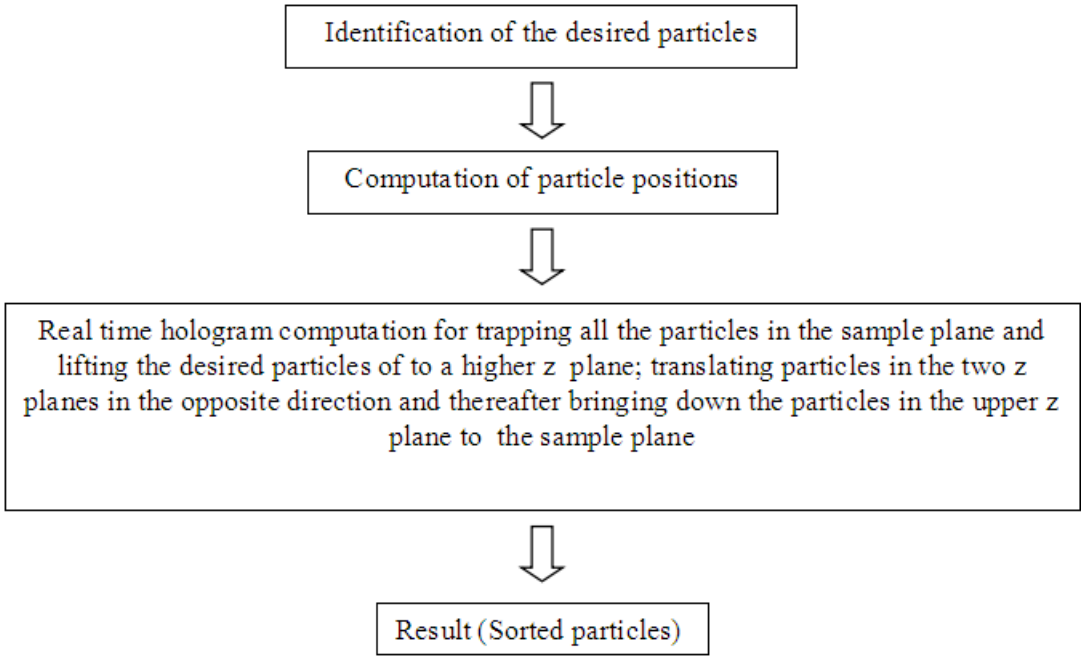

Figure 4.1: *Flowchart of the sorting process*

Identification of desired sets of particles in an image using the image processing algorithm:

The bright-field images of the sample were grabbed using a LabVIEW based camera interfacing program and analyzed in Matlab. Kernel images of the desired particles were marked by using a variable rectangular region selector (as shown by the blue rectangle at the top left corner of figure 4.2(a)), available in the GUI interface of Matlab, which can be moved on the whole image and be freely altered to any rectangular size. A cross correlation based pattern matching technique was used to identify the desired particles. As shown in figures 4.2(b) and (c), the cross correlation peaks at the locations of the desired particles are high as compared to those for other particles. To find the coordinates of these particles, the cross correlation image was thresholded and converted to a binary image by assigning the value 0 to pixels having values less than the threshold value and the value 1 to pixels having values equal to or more than the threshold value.

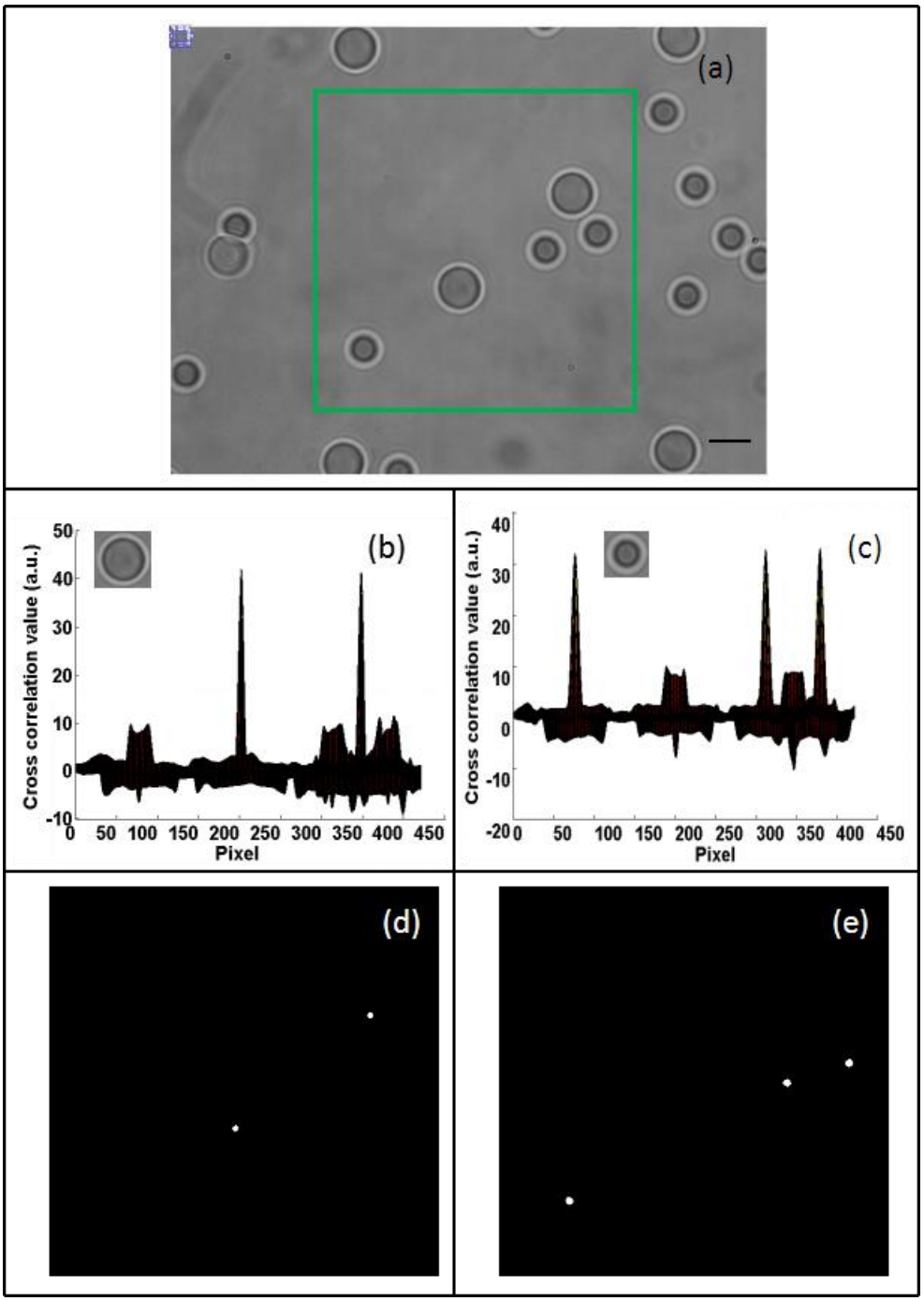

Figure 4.2: *Determination of particle position by use of pattern matching technique (a) an image of the sample consisting of mixture of particles of sizes ~3 μm and ~5μm, the rectangle (green) shows the region of interest and the rectangle at top left corner (blue) is the variable rectangular region selector, (b) and (c) the cross correlation matrix for the big and small particle, the insets show the kernel for the particles, (d) and (e) the binary images of the two particles after thresholding. Scale bar: ~5μm.*

The binary images are shown in figures 4.2(d) and (e). A weighted average method was used to locate the centre of the particle [197]:

$$X_c = \frac{\sum\sum I(x_i y_i) x_i}{\sum\sum I(x_i y_i)} \tag{4.1}$$

$$Y_c = \frac{\sum\sum I(x_i y_i) y_i}{\sum\sum I(x_i y_i)} \tag{4.2}$$

where x_i, y_i are the coordinates of the pixel and $I(x_i\ y_i)$ is the corresponding intensity. The particle positions thus estimated were thereafter used for computation of the phase hologram.

Choice of a suitable translation step size and an appropriate height for the upper Z plane:

In our approach once the position of all the particles in the region of interest is located, one set of particles are to be lifted to a higher Z plane and thereafter particles in the two planes are to be translated in opposite directions so that when the particles in the higher plane are brought back to the sample plane they are well separated from those trapped in the sample plane. The implementation of the approach requires determining a suitable translational step size and a proper height for the upper Z plane. To illustrate the need to select a proper translation step size, let us consider two identical particles adjacent to each other and assume the direction of translation to be along the common diameter as shown in figure 4.3(a). Initially holographic traps of identical strength are generated for trapping both particles. Now, if the trap beams are shifted by a translation step size equal to the radius of the particle (figure 4.3(b)), the leading particle '1' will lie symmetrically between the two traps and the trailing particle '2' will have an attractive force towards the direction of the translation. Since particle '1' is in a symmetric situation, it will remain there. Therefore, the translation of the trailing particles will be

hindered and could lead to jamming. To avoid such situations, all the particles in one given plane should remain in their respective trap during translation, which requires that the sequential movement of individual traps should be a fraction of the radius of the particle. The translation step size of the traps should be chosen to ensure that the particles in all the traps in one plane should remain in their respective traps during translation. For this, the optical trapping forces on the micro particles was calculated using generalized Lorentz Mie theory (GLMT), which is the most suitable for these sizes of particles as it does not make any approximation relating to the interaction wavelength and the particle size. The inter-trap separation was taken to be equal to the diameter of the particle (since this will correspond to the largest packing density in a linear chain).

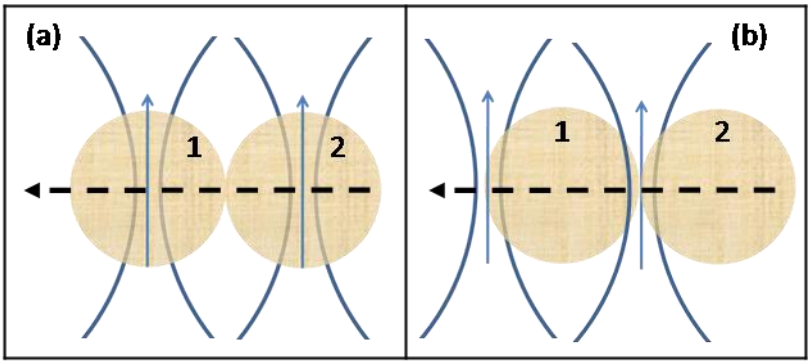

Figure 4.3: *Arrangement of particles and trap beams considered to illustrate computation of a suitable translation step of traps; (a) the trapped particles in the initial condition and (b) the position of the trap beam and particles if a translation step equal to the radius of the particle is chosen. The solid arrows show the direction of beam propagation. The direction of the translation is shown by dashed arrows. The leading particle with respect to the direction of propagation is marked as '1' and the trailing particle as '2'.*

In GLMT, the optical forces are expressed as [36, 37] ,

$$F(\bar{r}) = \left(\frac{n_m}{c}\right)\frac{2P}{\pi\omega_o^2}\left[\hat{x}C_{pr,x}(\bar{r}) + \hat{y}C_{pr,y}(\bar{r}) + \hat{z}C_{pr,z}(\bar{r})\right] \tag{4.3}$$

where $C_{pr;z}$ is the longitudinal radiation pressure cross-section along the direction of propagation of the trapping beam, $C_{pr;x}$, $C_{pr;y}$ are the transverse radiation pressure cross-sections, n_m is the refractive index of the medium, '*c*' is the speed of light in vacuum, *P* is the trap beam power and ω_0 is the waist radius of the focused beam in medium. The derivation and the expressions for these cross-sections can be found in [36, 37]. For the computation of the trapping forces on micro particles, the power of the trap beam was taken as 5 mW per trap and the beam waist at the focus was taken as ~0.8 μm, while the optical trapping forces were computed for particles of sizes 2, 3 and 5 μm.

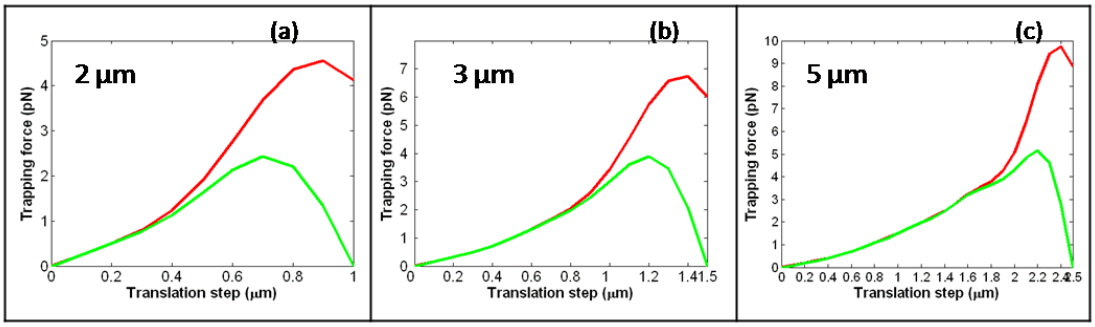

Figure 4.4: *Trapping forces on particles of sizes (a) 2, (b) 3 and (c) 5 µm while two particles of the same size adjacent to each other are being translated in a direction along the common diameter. The force on the leading particle is shown by a 'red color' and on the trailing particle by a 'green color'.*

Since the smallest separation between the positions of traps was kept equal to the diameter of the particle even for the smallest particle (2 μm), the interference between the trap beams in the focal plane can be ignored. The force on both the leading and the trailing particle was computed for different translation step sizes and is shown in figure 4.4. It was observed that the maximum trapping force on the two particles is achieved for a translation step corresponding to ~70–90% of the radius of the particle.

In experiments where particles of different sizes are used, the height of the equatorial planes with respect to the *Z* axis of the two particles will be different. If the *Z* plane corresponding to the equatorial plane of one size of the particles is imaged, the

size of the kernel for these particles will be equal to the diameter of the particle, but for the other size particles having an equatorial plane in the other *Z* plane, because of defocusing of the illumination beam, the kernel size will be larger than the actual size of the particle (by ~20% for particles in the size range 2–5 μm). To roughly take this factor into account, instead of choosing a translation step of 0.7–0.9 times the radius, we opted for a step size equal to R/2 for the particles. Thus a step size of 0.5, 0.75 and 1.25 μm was used for particles of diameter 2, 3 and 5 μm respectively.

The choice of the height of the upper *z* plane is affected by two competitive effects. First, the separation between the planes should be sufficiently large such that the motion of the particles in one plane does not affect the motion of particles in the other plane. Second, the trap strength decreases due to spherical aberration effects as we move deeper inside the medium [198]. Therefore the separation of the planes was chosen to be more than the sum of the diameter of the particles and was kept as 1.2 (R1 + R2). The total trap beam power used in the experiments was ~50 mW at the sample plane. It is to be noted that the upper plane height with respect to the sample plane can further be increased provided large optical trap beam power is needed.

Hologram computation

Various non-iterative techniques (lens and grating algorithm, random masking etc.) and iterative techniques (Gerchberg-Saxton algorithm, direct search algorithm) [59, 99-203] have been developed for phase hologram computation with a view to optimize aspects such as the hologram computation speed and the quality of the multiple trap beams. Since in our study we required 3D real time manipulation of the microscopic particles, the choice of algorithm is dictated by its speed. Random masking is the fastest method, but the diffraction efficiency of the hologram drops drastically as the number of traps

increases [204]. Another non-iterative approach (lens and grating algorithm) is also fast provided the number of particles to be manipulated is limited to ~8–10 particles. However, in situations such as in our experiment, where the number of particles could be higher than this, the computation time with the lens and grating algorithm increases significantly. Therefore, we used a simpler version of the GS algorithm, in which instead of using the iterative mode we used the phase part of the single inverse Fourier transform of the desired trap array at the focal plane as a phase hologram for 2D hologram computation to ensure higher speed [118] and added a lens phase function to translate the traps to higher planes.

The lens phase function for axial displacement from the focal plane is given by:

$$\varphi_{lens} = \frac{2\pi z}{\lambda f^2}\left(x_h^{\,2} + y_h^{\,2}\right) \qquad (4.4)$$

Where, x_h and y_h are grating hologram pixels, z is the axial displacement from the focal plane, λ is wavelength of the trapping laser beam and f is the focal length of the microscope objective. The total phase function is give by:

$$\varphi_{total} = \left(\left(\varphi_{lens} + \varphi_{gs}\right), \mathrm{mod}\, 2\pi\right) \qquad (4.5)$$

where, φ_{gs} is the phase hologram for the trap sites in the focal plane. In our case, computation of the hologram took ~600 ms for a 1024 pixel×1024 pixel size hologram on a computer with a Core 2 Duo, 2.66 GHz processor. To enhance the speed of computation we used hologram binning [199]. We computed the phase hologram for 512 pixels × 512 pixels and then assigned the phase value of one pixel to the corresponding four pixels in 1024 pixels × 1024 pixels, which reduced the computation

time by four times. Thus we could achieve computation of the phase-only hologram at a rate of about 7 Hz. Though the above technique reduces the range over which the traps can be steered in a sample plane, it was adequate for the sample area (~1325 μm^2) used in our experiments. It is to be noted that after addition of the lens phase function and thereafter performing the phase unwrapping, the final hologram display rate was about 6 Hz, and during the experiments the holograms were displayed at 5 Hz.

4.2.2 Materials and methods

A schematic of the setup used in the experiment is shown in figure 4.5. We used an inverted microscope (Olympus, IX-81) equipped with a motorized translation stage (Prior, H117). A liquid crystal based phase-only spatial light modulator (SLM) (Holoeye, PLUTO) was used for the generation of the holographic optical traps by diffracting a TEM00 1064 nm CW fiber laser beam (IPG Photonics, YLM-SC-20). The SLM has 1920 pixels × 1280 pixels and is computer controlled to provide 0 to 2π phase modulation in 256 gray levels. A pair of lenses (L1, L2) was used to suitably expand the laser beam to fill up the smaller dimension of the SLM. The diffracted beam was relayed using the lens pair L3 and L4 (~500mm) to the input pupil of a 100×, NA 1.4 Plan-apochromat oil-immersion objective lens (Nikon). The polarization of the incident laser beam was controlled by a combination of a polarizer and a half wave plate (HWP) placed before the beam expander. A halogen illumination source (12 V, 100 W) was used to illuminate the sample and the bright-field images were recorded using a monochrome CCD (Watec Inc.). A dichroic mirror was used to reflect the trapping laser beam (1064 nm) to the microscope objective and transmit the bright-field images to the CCD. A 800 nm short pass filter (SPF) was used to suppress the back scattered laser light from the different optics in the imaging path to the CCD.

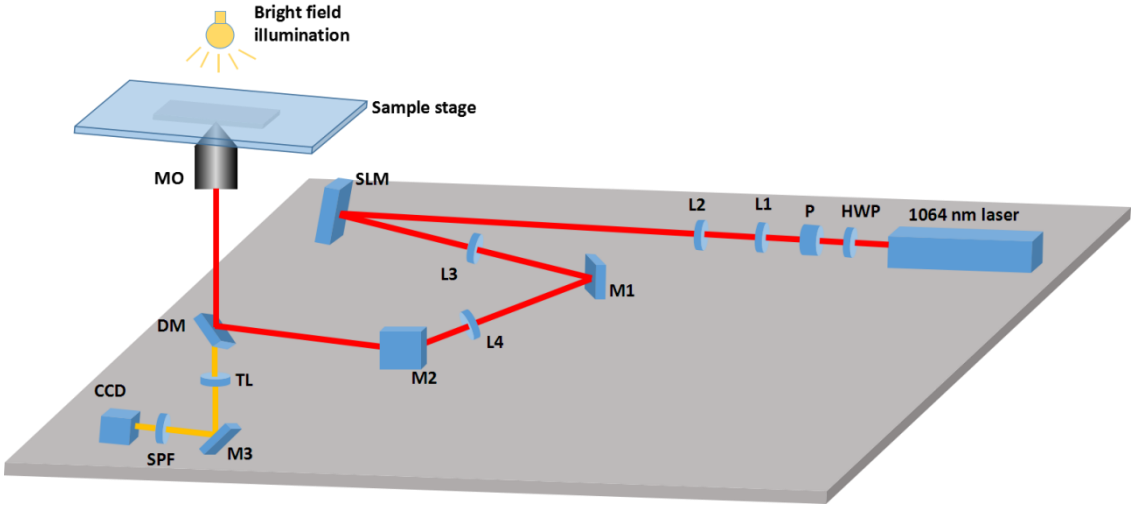

Figure 4.5: *A schematic of the setup used in the experiment.SLM: spatial light modulator, HWP: half wave plate, P:polariser, L1,L2:lens working as a beam expander, L3,L4: lens for making 4f arrangement, M1,M2: mirrors for relaying the beam to the microscope, DM: dichroic mirror, MO: microscope objective, TL: tube lens, M3: mirror for reflecting the visible light to the camera, SPF: short pass filter, CCD: charged coupled device.*

The CCD pixel image size was calibrated using the stage micrometer (Olympus) and was estimated to be 1 µm≡7 pixel. Further for experiments involving the translation of the trap requires the first order deflection of the SLM is scaled by a factor of 2.5 so that the change in the camera pixel value given to hologram computation is reflected in trap position translation. To align the trap laser to the centre of the SLM, a computer generated hologram required for generation of the Laguerre Gaussian beam was used. In case laser is not falling symmetrically to the centre of the SLM, the radial intensity pattern instead of being radially symmetric will be asymmetric. Thereafter, the 0^{th} order beam was allowed to pass from the periphery of the lens L3 and the first order deflected beam to pass through the centre of the lenses to the microscope objective.

The samples of silica microspheres of sizes 2, 3 and 5 μm (Poly Sciences Inc.) were prepared by mixing an aqueous suspension of these particles in 1 ml deionised water. The sample of borosilicate glass microspheres (Duke Scientific Corporation) of size ~5

μm was prepared by suspending glass microspheres in powder form in 1 ml deionised water. Binary samples of particles for the experiment were prepared by mixing appropriate volumes of the stock solutions. The blood sample (5 ml) was collected from a healthy volunteer in a glass tube containing EDTA (5.4 mg/3 ml) as an anticoagulant. The anticoagulated blood was mixed with an equal volume of Histopaque −1077 (Sigma Aldrich) and centrifuged at 2700 rpm for 30 min so that cells became layered in the tube. In the layered blood sample, the upper part of the plasma was aspirated and discarded from the sample. The ring portion containing mainly the white blood cells (WBC) was aspirated and suspended in RPMI-1640 growth medium (RPMI medium with 1 mM NaHCO3, 10% fetal bovine serum (FBS), HEPES (25 mM), glucose (5 mM), penicillin (50 U ml^{-1}), streptomycin (50 µg ml^{-1}) and nystatin (2.4 mM)) for further centrifugation at 2100 rpm for 10 min. The supernatant was aspirated and the pellet of cells was resuspended in RPMI medium. The centrifugation and washing of WBC portion was done thrice to get a highly enriched WBC sample. A few µl of palleted red blood cells were aspirated from the tube and suspended in RPMI-1640 growth medium. Both the sample of WBCs and RBCs were appropriately diluted and mixed for experiments.

4.2.3 Results and discussion

The approach was first used for sorting of 3 and 5 µm silica particles from a mixture of the two as shown in figure 4.5. Initially the positions of all the particles were determined using the cross correlation based image processing algorithm and traps were generated to trap all the particles. The particles of 3 µm size were then moved to a higher Z plane and, after translating the particles in the two planes in opposite directions to the edges of the region of interest (ROI), the 3 µm particles in the upper plane were

brought back to the bottom plane. In our experiments particles of the smaller diameter were lifted into the upper plane, but the reverse can also be performed.

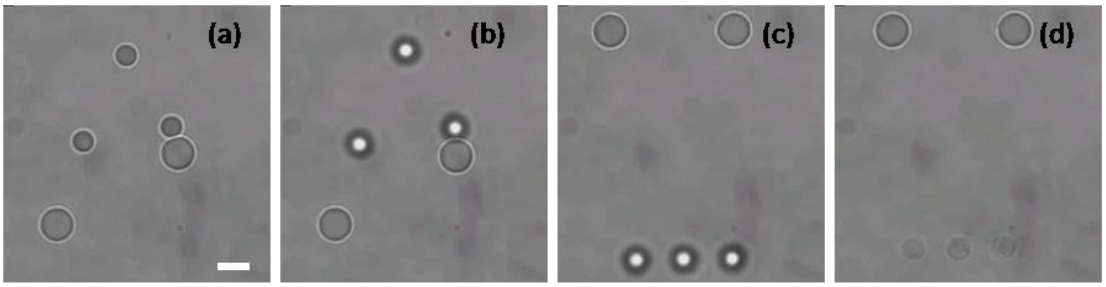

Figure 4.6: *Optical sorting of 3 and 5 µm diameter silica particles from a mixture of the two. (a) Initial image of the sample plane containing particles of both diameters. (b) 3 µm particles were lifted into the upper plane and 5 µm particles were trapped in the sample plane. (c) Particles in both planes were translated in two opposite directions. (d) Particles in the upper plane were brought back to the bottom sample plane. The total time required for sorting is ~13 s. Scale bar: 5 µm.*

The method could also be used for sorting a closely packed sample of silica particles of diameter 2 and 3 µm (particles covering ~28% of ROI). The results are shown in figure 4.6. For this packing density of particles, when a step size of R/2 was used, the accuracy of sorting of particles having diameters ~2 and 3 µm was ~70–80%. In general the ~2 µm particles were either getting deflected by other traps or not following the traps. We believe that this may arise due to the large variation in power of the different traps (as high as ~50%) due to the use of a non-iterative mode for computation of the holograms. This variation in individual trap beam powers will change the optical force on a particle, and may result in the deflection of particles in the other directions instead of getting translated in a desired direction, due to the effect of the other nearby trap beams. Experiments performed with smaller step sizes showed that as the step sizes were reduced the accuracy of sorting improved. With a step size of R/5 the particles could be sorted with an accuracy of 100%.

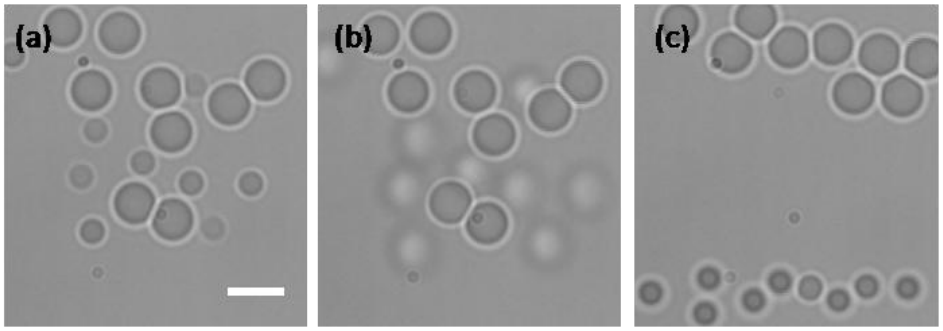

Figure 4.7: *Images showing the sorting of 2 and 3 µm silica particles from a mixture of the two (a) bright field image of the particles (b) particles of diameter ~2 µm are in the upper plane while the 3µm particles are in the bottom plane (c) sorted particles at the bottom plane. The total sorting time is ~27 s. Scale bar: ~5µm.*

Particles of the same diameter but with different refractive index will have a different distribution of intensity in its kernel and can be selected by using the pattern matching technique used in the approach. Therefore particles of silica and glass having the same diameter ~5 µm could be sorted as shown in figure 4.7. The glass microspheres were trapped and lifted to the upper plane while silica particles were in the trap in the bottom plane. The total time required for sorting is ~21 s.

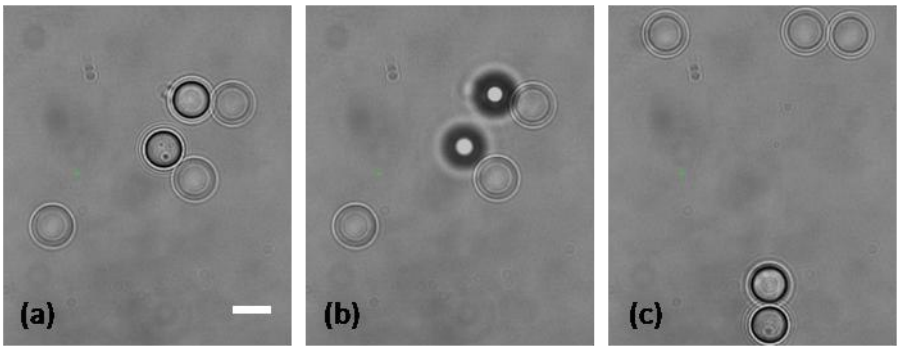

Figure 4.8: *Images showing the sorting of silica and glass microspheres (diameter ~5 µm) from a mixture of the two. (a) Bright-field image of the sample plane. (b) Glass particles were trapped and lifted to the upper plane while silica particles are in the bottom plane in the trap. (c) Sorted particles. The total time required for sorting is ~21 s and the movie is accelerated by 3×. Scale bar: ~5 µm.*

It is pertinent to note that the ~270 ms time required to compute the coordinates for the desired particles and display the first hologram to trap the particles in the sample plane

will limit the smallest size particles that can be sorted, because in this time window the smaller size particles may diffuse and move out of the trapping range. The diffusion constant is given by Stokes Einstein relation [121]

$$D = \frac{k_B T}{6\pi\eta r} \tag{4.6}$$

where η is the dynamic viscosity of the medium, r is the radius of the particle, k_B is the Boltzmann constant and T is absolute temperature. The mean square displacement is given by

$$\left\langle r^2 \right\rangle = 6Dt_D \tag{4.7}$$

where t_D is the diffusion time. In 270 ms, silica microspheres of diameter 1 and 2 μm suspended in water can diffuse to a distance of ~0.9 and ~0.6 μm. The spatial extent of the optical trap in the focal plane depends on both the size of the particle and on the focal spot size. For the particle sizes used in the experiments it will be approximately equal to the diameter of the particle. Because, for the 1 μm particles, the diffusion length is approximately equal to its size, there is a strong possibility that the particles would diffuse out over a distance so that the trap when generated by the first hologram would not be able to capture the particle. Therefore, the method should be suitable for manipulation and sorting of particles having diameters greater than 1 μm.

It is also pertinent to note that the sorting method makes use of a pattern matching technique to select the desired particles based on their bright-field images. A variation in the intensity pattern of the particles that may be caused for example by buoyancy of lighter particles will therefore influence the selectivity. While a higher threshold value will ensure 100% selectivity at a reduced separation factor, a lower threshold value will

compromise selectivity for the desired particles. While the effect of buoyancy was insignificant for silica and glass microspheres because of their larger density (≥2 g cm^{-3}), it was significant while working with polystyrene microspheres (density ~1.052 g cm^{-3}).

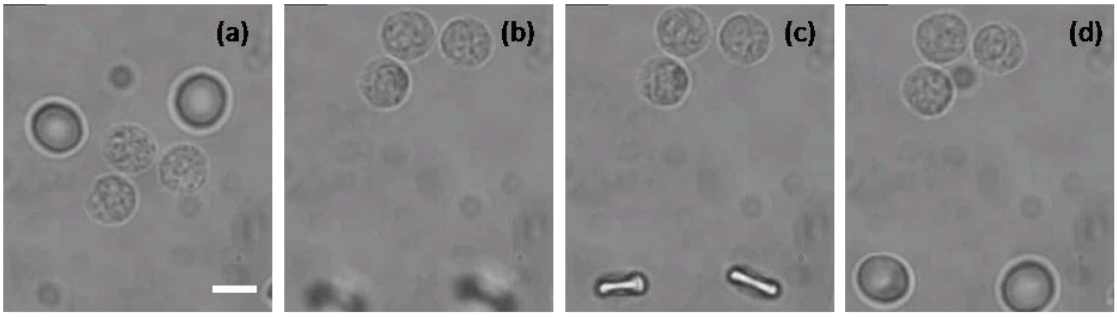

Figure 4.9: *Sorting of RBCs and WBCs from a mixture of the two. (a) Cells in the sample plane, this image have been taken for the kernel selection. (b) The cells were trapped and translated in opposite directions in their respective planes. (c) The RBCs in the upper plane were brought back to the lower plane. (d) After releasing the cells from the trap the RBCs took some time (~20 s) to move from the vertical orientation to the natural horizontal orientation. The total sorting time is ~30 s. Scale bar: ~8 µm,*

Furthermore, the heating of the medium due to the laser beam could also create some convective flow which may adversely affect the implementation of the scheme. However, it has been shown earlier that for transparent objects of sizes greater than a few hundred nanometers the effect of the convective flow is negligible as compared to the optical forces [19, 205].

As a demonstration of the proof of the concept for suitability of the approach for sorting of cells in a mixture, red blood cells (RBCs) and white blood cells (WBCs) were sorted from a given mixture of the two. Snaps of the videos of sorting of these has been shown in figure 4.9. Initially all the cells were trapped, and thereafter RBCs were lifted to the upper plane ~10 µm away from the bottom plane. Typical human RBCs are biconcave disk-shaped cells having disk diameters of ~6–8 µm and thicknesses of ~2–3 µm [206]. It is well known that when a RBC is trapped, it orients itself to the

vertical plane [207, 208] as this maximizes the overlap of the cell with the region of high beam intensity. Furthermore, if a linearly polarized beam is used for trapping, the orientation of the RBC in the vertical plane changes such that its symmetry axis becomes perpendicular to the electric vector of the trapping beam [99, 208]. Depending on the polarization state of the trap beam, the orientation of the symmetry axis of the trapped RBC can be different from that of the direction of translation. Therefore the projection of the RBC along the direction of translation will vary. Therefore, we used a smaller translation step size of R/5 (~0.8–0.9 μm) for the RBC while the WBC was translated with R/2 (~2.5 μm) translation step size. The cells were translated in two opposite directions in the respective Z planes and then the RBCs from the upper plane were brought back to the bottom plane. The time required for sorting was ~30 s and the cells could be translated up to a speed of ~12.5 μm s^{-1}.

4.2.4 Multi particle sorting

Most of the sorting approaches are suitable for sorting in a binary mixture [126, 127]. However, this is not the case with the pattern matching based sorting approach. The approach can easily be extended for samples containing four types of particles either varying in size of material. It is to be noted that as the region of interest is rectangular, it led to extension of the approach for four types of particles. The sorting process can be executed in two ways; **(A)** in semi sequential manner i.e. all the particles in the ROI were trapped and one type of particles was lifted to the upper plane and translated to bottom side of the ROI and thereafter brought down to the bottom plane as shown in figure 4.10(a)-(c). Similarly ~3μm polystyrene sphere (second type of particle) was sorted to the upper side of the ROI as shown in figure 4.10(d).

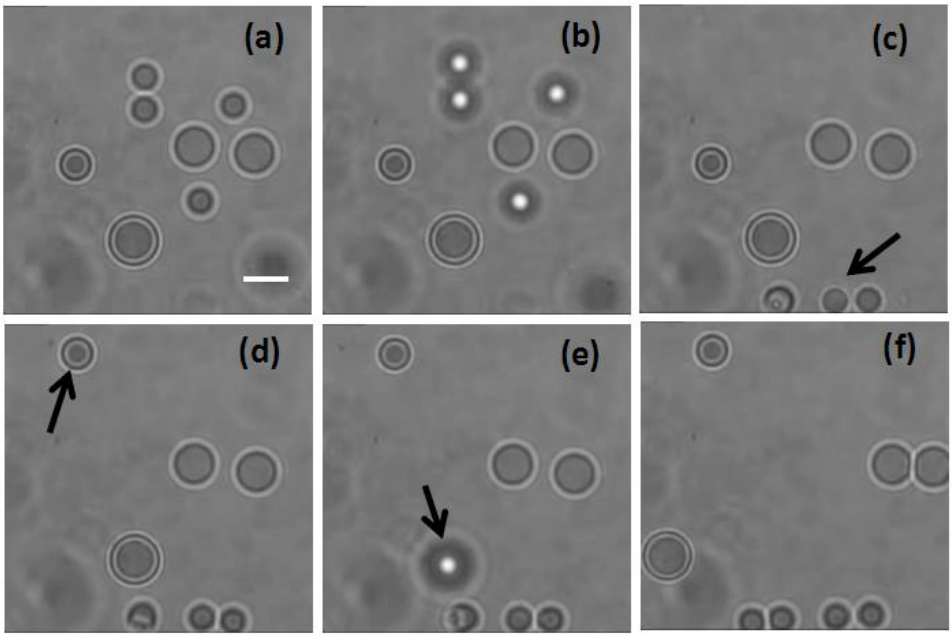

Figure 4.10: *Snapshots from a video showing sorting of particles in sequential manner using two Z planes (a) particle before the start of the sorting process (b) 2µm silica microspheres trapped and lifted to higher Z plane and (c) after translation to the bottom side of the ROI brought down to bottom side (black arrow shows the sorted particles on the bottom plane (d) ~3µm polystyrene sphere after getting sorted to upper side of the ROI (e) ~6µm polystyrene microsphere lifted to higher Z plane (black arrow shows the lifted particle) (f) all the particles sorted at four sides of the ROI; Scale bar: 5µm*

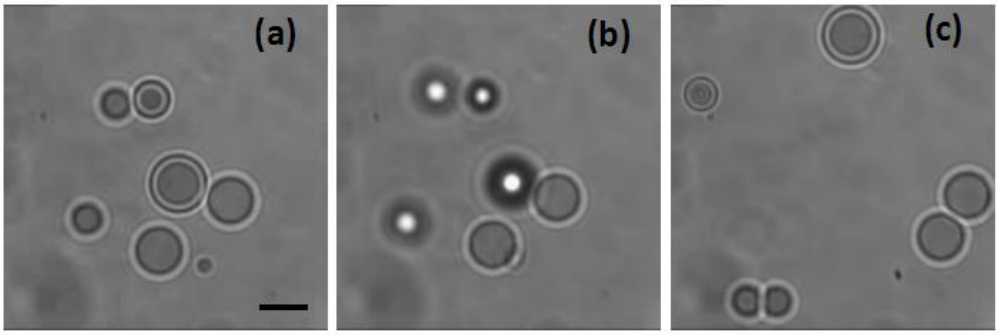

Figure 4.11: *Snapshots from a video showing sorting of particles in sequential manner using four Z planes (a) particle before the start of the sorting process (b) all the particles have been lifted in multiple Z planes leaving only one type of particle in the bottom plane (~5µm silica) (c) after translation to the pre defined sides of the ROI in their respective Z planes, all the particles were brought to the bottom plane. Scale bar: 5µm*

Thereafter among the leftover particles, 6µm polystyrene spheres were lifted to the upper plane and silica spheres and polystyrenes in the upper plane were translated in

opposite direction and sorted to the rest of the two sides of the ROI as shown in figure 4.9(f). (**B)** In parallel manner i.e. all the types of particles were trapped in the bottom plane and lifted to three different planes above the bottom plane leaving only ~5µm silica microsphere in the bottom plane and were translated in respective planes to the sides of the rectangular ROI as shown in figure 4.11. Furthermore these were brought down to the bottom plane. Though, feasibility of both the methods have been demonstrated, as the optical trap strength decreases as we go deeper inside the sample, implementing the sequential approach appears to be better as compared to the parallel approach.

4.3 Sorting of particles in low concentration

The presented approach is particularly suitable for sorting in low concentration poly disperse sample. An approach was developed which uses dynamically controllable holographic traps to trap the desired particles in the higher plane above to the sample plane and maintain these in the same plane during the change of field of view so effectively could collect many particles of one type which were rarely available in one field of view. Experiments were carried out to demonstrate the technique by sorting of ~3 µm silica micro-sphere in a mixture of ~3 and ~5 µm silica micro-spheres and the results obtained have been presented.

4.3.1. Method

The bright field images were acquired using a CCD interfaced with personal computer and controlled via a Lab-view program. One bright field image was recorded to estimate the typical pixel image size of different types of particles in the sample. Form the figure 4.4 we observe that the transverse optical force is at its peak typically up to a distance of the radius of the particle. Therefore the step size for the lateral

translation of the desired particle was taken as half of the particle size.

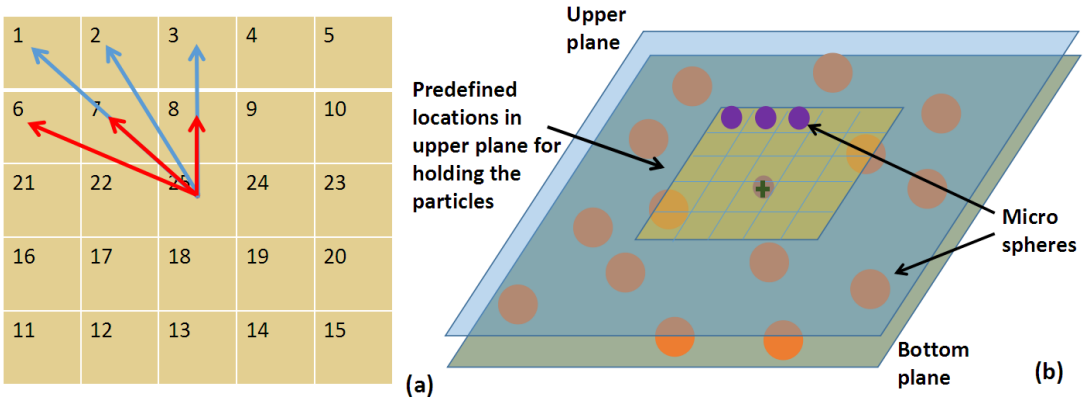

Figure 4.12: *Schematics of the (a) upper plane particle filling order and (b) bottom and upper plane appearance when three particles are in the upper plane while the fourth one is to be trapped.*

To hold the desired particles from the multiple ROIs, a plane above the sample plane was chosen such that if a particle is trapped in the upper plane, particles in the bottom plane is not affected by the trap beam. The minimum height has to be ~1.2 (R1+R2) i.e. the sum of the size of the desired particle and size of the other particle. However, even at this height if the trap beam focused in the upper plane affects the particles in the bottom plane, the trap height need to be increased and this will depend on the optical power used in the individual trap and the size of the other particle.

A height of ~12 µm was taken for the particles sizes used in the experiments. The step size for the vertical translation was taken as $1/4^{th}$ of the particle size. The upper plane has been pre-configured for the multiple particles with a spacing of 1.5 times of the size of the desired particle. The filling order as shown in figure 4.12a for the particles has been taken considering the fact that when a particle is being translated in the upper plane to a predefined location, the previously existed particles in the upper plane should not be hurdle in current particle movement. The phase hologram for all

the pre defined locations in the upper plane has already been calculated. Once the first desired particle is brought at the '+' mark in the sample plane (bottom plane), the left click of the mouse allows a phase hologram computed using a modified Gerchberg Saxton algorithm to generate a trap a predefined location in the sample plane (marked with +). The particle at the predefined location (at '+' in the sample plane) is trapped and translated to a predefined location in the upper plane. The sample is further scanned for next desired particle and the located particle is brought to the '+' position in the field of view. At this time a combined phase hologram is generated which generates traps for lifting/translation of the currently located particle and for holding the previously trapped particle in the upper plane. In the similar fashion more number of desired particles are trapped and transported to a predefined location in the upper plane. Figure 4.12(b) schematically shows a situation during the sorting process when three particles are in upper plane while the fourth one is in the bottom plane to be trapped. Similarly the selection of the desired particles can be done up to permissible limit depending on the total lower available for generating multiple traps and the size of the desired particles. A flow chart of the sorting process has been shown in figure 4.13. We prepared a sample of silica micro microspheres of sizes ~3 and 5 μm (Poly Sciences Inc.) by mixing aqueous suspension of these particles in a ratio so as to achieve a ratio of ~1:5 particle concentration in deionized water.

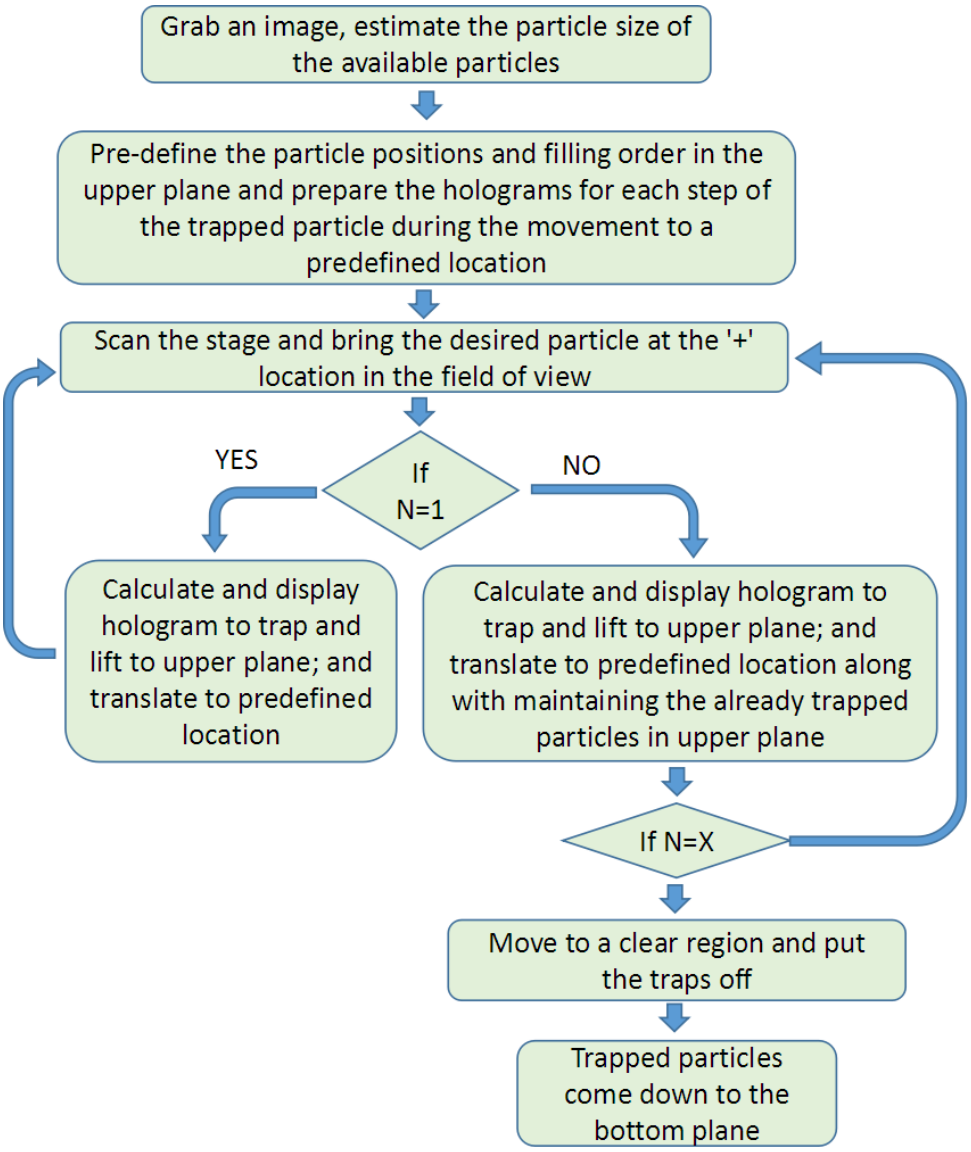

Figure 4.13*: Flow chart of the sorting process*

4.3.1 Results

A few snaps from the video of sorting of ~3 μm silica micro-sphere from a mixture of the silica microspheres of sizes ~3 and 5 μm is shown in figure 4.13. For the first time, a silica particle of size ~3μm was brought to the fixed point (shown by green colour '+' sign in the image) as shown in figure 4.14(a) and by left click of the mouse an optical trap is generated (using a Mat lab program) to trap the particle; lift to the upper plane and thereafter translate to a predefined location. Figure 4.14(b) shows a snap while the

particle is being translated in the upper plane to the predefined location and brought to the defined location as shown in figure 4.14(c). Further the sample was scanned by moving the sample stage for more number of desired particles and same procedure was followed.

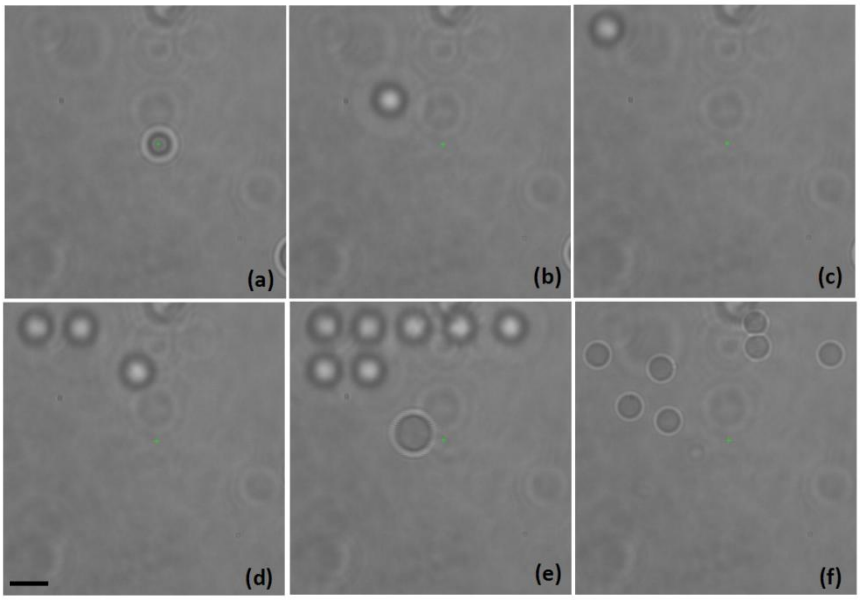

Figure 4.14: *Snapshots from a video of sorting ~3µm silica micro-sphere from a mixture of the silica microspheres of sizes ~3 and 5 µm; first silica particle (a) at the desired position in the field of view for getting trapped and translated (b) in the upper plane in the middle of its path (c) reached to the predefined location in the upper plane ; (d) third particle in the middle of its path to the predefined location in the upper plane while there are already two particle lying in the same plane (e) seven particles have been trapped and maintained in the upper plane in a predefined manner using optical traps (f) trapped particles in the bottom plane when the trap was off. The green colour '+' sign on the images is the location where the desired particle has to be brought during scanning of the sample. Scale bar: ~5µm.*

4.4 Conclusion

In summary, we showed that in a mixture containing a total of 18 particles of sizes ~2 and ~3 µm, covering ~28% of the area (~92 μm^2) of the ROI, could be sorted with 100% accuracy in ~27s. The sorting time mainly depends on the hologram computation time and the translation step and how far the particles need to be separated and not on the number of particles as the translation and uplifting of particles is done in parallel.

The applicability of the approach was also demonstrated for a sample consisting of four types of particles using multiple Z planes. Furthermore we also demonstrated an active optical sorting technique for sorting of particles in low concentration in the sample in flow less medium. The advantage of the approach is that it is not limited to the number of types of the particles in the mixture and can be easily integrated with other spectroscopic techniques like fluorescence and Raman spectroscopy for identification of the required type of particles.

5 Chapter 5: Micromanipulation of cells/ microparticles using Opto-electronic tweezers

In this chapter, we present the development of an Opto-electronic tweezers setup that makes use of light induced di-electrophoresis to trap and manipulate micro-particles. Thermal evaporation technique was used for coating of titanium oxide phthalocyanine (TiOPc) as a photo conductive layer on ITO coated glass slide. We demonstrate the use of the setup for sorting of cells / micro-particles using size as well as nature of DEP forces by suitably adjusting the frequency of the applied AC bias. We also present the development of digital light projector based OET setup and demonstrated its functionality by guiding, focusing etc. of cells.

5.1 Introduction

Throughput of a sorting approach for microscopic objects such as cells/colloids is an important parameter in many bio-medical and research applications.

Work discussed in this chapter has resulted in the following publication:

1. **R. S. Verma**, R. Dasgupta, N. Kumar, S. Ahlawat, A. Uppal and P. K. Gupta, "Manipulation of microparticles and red blood cells using opto-electronic tweezers", Proceedings of National Laser Symposium-21 held at BARC, Mumbai, India, Feb. 6-9, 2013, CP-11-17.

   The work was further selected for publication in special edition of Pramana J. Phys.

   R. S. Verma, R. dasgupta, N. Kumar, S. Ahlawat, A. Uppal and P. K. Gupta, "Manipulation of microparticles and red blood cells using opto electronic tweezers", Pramana J. Phys. **82**, 43-437, (2014).

2. **R. S. Verma**, N. Kumar, S. Ahlawat and P. K. Gupta, "Separation of micro particles in a concentrated sample using opto electronic tweezers", Proceedings of National Laser Symposium-22 held at Manipal University, Manipal, Karnataka, India, Jan 8-11, 2014,CP-11-23.

3. **R. S. Verma** and N. Kumar, "Opto electronic tweezers based smart sweeper for cells/micro-particles sorting", Proc. SPIE 10716, Saratov Fall Meeting 2017: Optical Technologies in Biophysics and Medicine XIX, 1071613.

Sorting approaches can be broadly classified as; one making use of optical field and the other making use of electric field. When the requirement of desired particle type is limited to typically 1000's of cells/particles, sorting in flow free medium is advantageous as it does not require any arrangement like microfluidic pumps, syringes for creating flow in medium. In samples with no microfluidic flow, sorting using optical field is performed by using HOTs [118], potential energy landscapes generated by multiple beam interference [136]. However, HOT based techniques could generate hardly a few 100s of traps, primarily limited by the laser power handling capability of the SLM and interference based techniques are prone to vibrations. In addition, since attractive forces are used for separation/sorting, these suffer from the inherent problem of particle collision and jamming which hinders the sorting process when working with concentrated samples. Among the approaches that make use of electric field, DEP has been widely used for sorting of microscopic objects [209-211]. The optically driven electro-kinetic approach known as Opto-electronic tweezers [63] have drawn considerable interest in this regard as it facilitates several advantages over the existing techniques such as manipulation of 1000's of particles using an optical power in ~mW range. Unlike the conventional dielectrophoresis, OET consists of one of the electrodes generated by projecting the sculpted light pattern onto a photo conductive substrate. As the illuminated region conductivity is higher than the non illuminated region, the illuminated region works like virtual electrode and can be dynamically generated anywhere in the region of interest by illuminating the region. This allows the use of the OET for development of sorting approaches in non flowing medium as well.

Here we present the development of an OET setup which consists of an OET chip with a photo conductive layer of TiOPc deposited by thermal evaporation on ITO

coated glass substrate. Working of the OET chip was shown by manipulating the polystyrene microspheres and RBCs. Using the setup, two sorting approaches were developed suitable for concentrated samples. These approaches were based on the fact that DEP force depends on the size of the particle and on the dielectric constant of the particle and increases with increase in the radius of the particle. Therefore for size based sorting, an array of circular intensity spots having spacing larger than the size of the smaller particle and smaller than the size of larger sized particle were scanned across a mixture of polystyrene microspheres (PMs) in low conductivity medium. PMs have negative DEP response in medium of conductivity ~100 μS/cm. During scanning, the larger sized particle will be carried away with scanning beam whereas the smaller size particles will have no DEP effect in inter spot region and will pass through the gaps. The method was used for separation of 6 μm PMs from a mixture of PMs of sizes 6μm and 15μm. For sorting between different types of particles, we exploited the fact that the DEP forces depend on the frequency of the applied a.c. field as the dielectric constant of the trapped particle varies with frequency of the a.c. field. Thus the frequency of the applied a.c. field could be tuned such that one type of particle (polystyrene) would experience strong repulsive DEP while the other particle (red blood cells) would not experience any significant DEP force. RBCs were sorted by scanning a line shaped intensity pattern across the sample (mixture of polystyrene and RBCs) and keeping frequency of the applied a.c. field close to the crossover frequency (frequency at which the DEP force becomes zero) of RBC.

Initially we describe the setup along with the functional demonstration for manipulation of the cells/micro-particles. Next the sorting approaches are discussed.

We also present the development of digital light projector based OET setup and demonstrate the ease of use by guiding, focusing etc. of cells.

5.2 OET chip development

Use of transparent conductive oxides like indium tin oxide (ITO) or fluorine-doped tin oxide (FTO) is common, considering their wide use in solar cell industry these are easily available commercially at reasonable cost and coating of these onto a glass is well established . Therefore, for making a functional OET chip for cell samples, the focus was to have a photo-conductive material film on ITO coated glass which should have properties like (i) good photo conductivity i.e. the material should exhibit high conductance in the presence of light and high resistance under no illumination condition (ii) good adherence to the ITO/FTO film for coating so that when a cell sample made in water is placed on the chip, the coating should not get dissolved (iii) less hygroscopic so that stable optical properties for at least a few days. Considering all these properties, several material and approaches were reported. In initial reports, Ohta et al. [63] used a layer of amorphous silicon (a:Si), a widely used photo conductor in solar cell fabrication, on ITO glass substrate by plasma-enhanced chemical vapor deposition (PECVD) process. For sustainability of the layer, a:Si also requires a thin layer of Aluminum/Molybdenum over the ITO coated glass slide as a passivasive coating on top side to protect contact from water. In some reports [63] even the hydrogenated amorphous Silicon (a:SiH) was used for better photo-conductivity. PECVD is a relatively costly system and the procedure for coating is very complex and involved. In view of this, several other approaches were explored to replace the a:Si layer with an appropriate alternative photo-conductive material to simplify the fabrication process of OET chips. Recently Wang et al. [143] used three thin films PEDOT:PSS/P3HT:

PCBM/LiF in sequence on a ITO coated glass substrate to use organic polymer P3HT:PCBM as a photo conductive layer by spin coating. The LiF layer was used to avoid any damage to the photo conductive substrate from water. Yang et al. [142] reported the use a single layer of titanium oxide phthalocyanine (TiOPc) as a photo conductive organic material by spin coating. Though spin coating of TiOPc on an ITO coated glass substrate is relatively easier process, for a good quality film a highly homogeneous solution of TiOPc is required. This is a tedious job as TiOPc is insoluble in inorganic solvents and has very low solubility in organic solvents. A technique which can use TiOPc in powder form will be more suitable for coating. We, therefore, fabricated the photo conductive TiOPc layer on to an ITO coated glass substrate by thermal evaporation technique and the appearance of the film is shown in figure 5.1(a). The thermally deposited photo conductive layer has very good adherence to the ITO film obviating the need for an intermediate layer of any material between ITO film and photo conductive layer to improve the adherence of the photo conductive material.

5.3 Experimental setup

A schematic of the OET chip is shown in figure 5.1(b). The liquid containing the sample is sandwiched between an ITO coated glass slide (top) and another ITO coated glass slide (bottom) containing a ~200 nm TiOPc layer. We used commercially available TIOPc (Y modification, Sigma Aldrich) which has absorption in the red side of the visible region as shown in figure 5.1(d). The OET chip was utilized for performing experiments using a setup shown in figure 5.2. As the photo conductor has strong absorption in the 650-750 nm and having a peak at ~720 nm, a 664 nm diode laser (ILX Lightwave) with output power of 150 mW was used to illuminate the liquid

crystal based spatial light modulator (SLM) (LCR 2500, Holoeye) for generation of the dynamically re-configurable multiple optical traps.

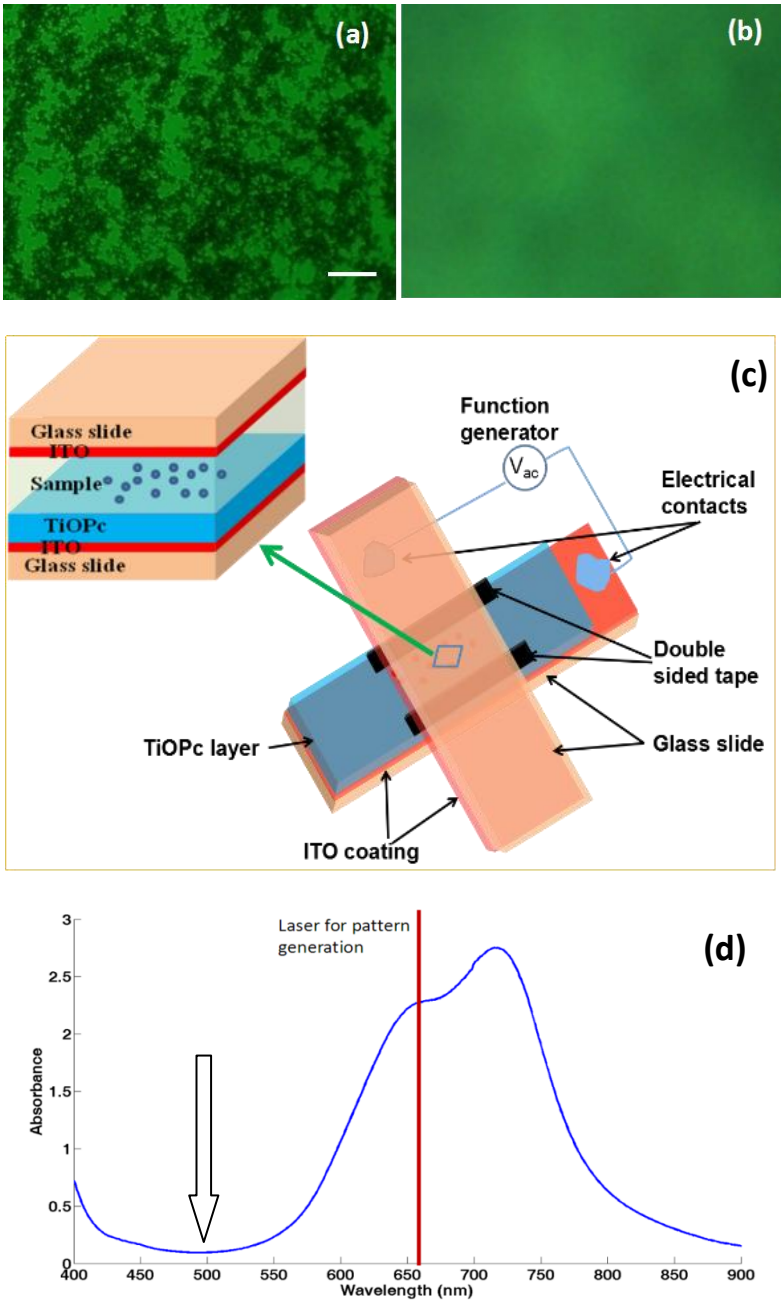

Figure 5.1: *(a) Image of the slide prepared using spin coating, (b) using thermal evaporation in bright filed illumination; Scale bar: 100µm, (c) Schematics of the OET chip and (d) the absorption spectra of titanium oxide pthalocynine.*

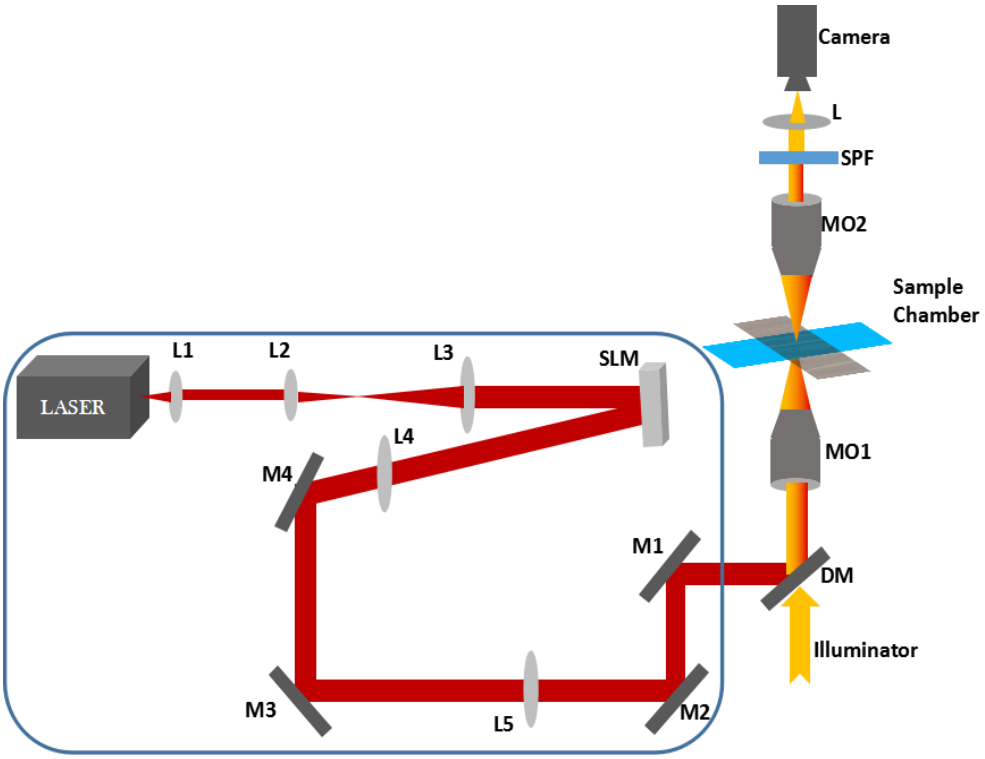

Figure 5.2: *Schematic of the experimental setup, the enclosed part is illumination unit.*

An aspheric lens was used to collimate the laser output. Spatially filtering was performed using a pair of lenses (L2, L3) and a pin hole aperture (A). Same lens pair was also used to expand the laser beam suitably before falling on the SLM. The SLM was placed in the conjugate plane to the input pupil of a 10X objective lens using a lens pair (L4, L5) of focal length 500 mm each. A fiber optic illumination source (Dolan Jenner) was used for bright field illumination. The images were collected using 25X objective lens and were focused on to a monochrome CCD(Oscar) using a lens (L6). A short pass filter (F) was used to suppress the laser light to the CCD. The a.c. biasing on the ITO electrodes was applied by a function generator (Agilent 3320).

For fabricating the OET chip, ITO coated BK7 glass slide (Vin Krola Instruments) of size 20 mm x 50 mm x 1.1mm were cleaned ultrasonically in sequential

manner in solutions of 2% Triton X100 in deionized water, deionized water, Acetone, Isopropyl alcohol for 10 min in each solution and at last dried using dry Nitrogen blow. These cleaned glasses were coated with TiOPc via thermal evaporation technique. The OET chip was made by placing these coated glass slides in cross position with another ITO coated glass slide of same size facing the conducting surface against each other as shown in the figure 5.1(c). The electrodes were glued with each other using a double sided tape working as a spacer of ~100μm and a channel region for manipulation of sample. The electrical connections were made using conducting silver paste on both the electrodes using copper wire and electrically soldered to the output of the function generator via a BNC cable for applying the a.c. electric field across the electrodes.

Unused part of the blood sample collected for screening and found healthy without disclosing the donor's identification were provided to us Choithram Hospital and Research Centre, Indore. The blood samples were collected from healthy volunteers. Blood was collected by vein-puncture from healthy volunteers in glass tubes containing EDTA (5.4 mg/3ml) as an anticoagulant. RBCs were separated from these anti coagulated blood samples by centrifugation at 3000 rpm for ~3 mins. The separated RBCs were then washed twice with phosphate buffer saline and at last washed with the low conductivity buffer. For experiments, ~10μm PMs (Poly sciences Inc.) and RBCs were suspended in an isotonic solution consisting of 8.5% sucrose (w/v), 0.3% dextrose (w/v) in deionized water and conductivity of the medium was adjusted by 0.1 molar solution of KCl. Human colon adenocarcinoma (Colo-205) cell line was purchased from National Centre for Cell sciences (NCCS), Pune, India. Cells were grown in a monolayer in Roswell Park Memorial Institute medium (HiMedia) supplemented with 10% FBS (Sigma-Aldrich), penicillin (50 units per ml,

Sigma-Aldrich) and streptomycin (50 μg ml^{-1}, Sigma-Aldrich) at 37 °C in a humidified incubator with 5% CO_2 atmosphere. At the time of experiments, the colon cells were washed twice with phosphate-buffered saline (PBS) and mixed with RBCs in low conductivity buffer with appropriate dilution and allowed to get adjusted with low conductivity buffer for ~30 min before the experiments. To reduce the non-specific interaction between the cells to glass bottom, 1% bovine serum albumin was also mixed in the low conductivity buffer sample.

5.4 Results

The developed system was validated by performing manipulation of cells and micro-particles. The applied a.c bias was 10 Vpp, 100 KHz and the total power at the sample plane was ~8μW. The polystyrene microspheres will always have negative DEP at these low conductivities as shown in figure 1.12. Therefore to trap these, annular intensity pattern (LG beam) was generated using the modified GS algorithm used for generating multiple optical traps [193]. The annular intensity pattern was generated encircling the particles and due to the negative DEP force, the polystyrene particle comes to the center of the annular pattern. Furthermore by translating the LG pattern (LG_{10}), the particles could be translated up to a speed of ~8μm/sec. At higher speed the particles were not following the translation of the intensity pattern due to the drag force. Further LG beam of variable mode orders were used for concentrating the particles as shown in figure 5.3. As the mode order of LG beam was changed from LG_{25} to LG_{10} in a sequential way, the microspheres being repelled by the intense region got concentrated to the dark central region of the LG beam intensity profile as shown in figure 5.3(a)-(c).

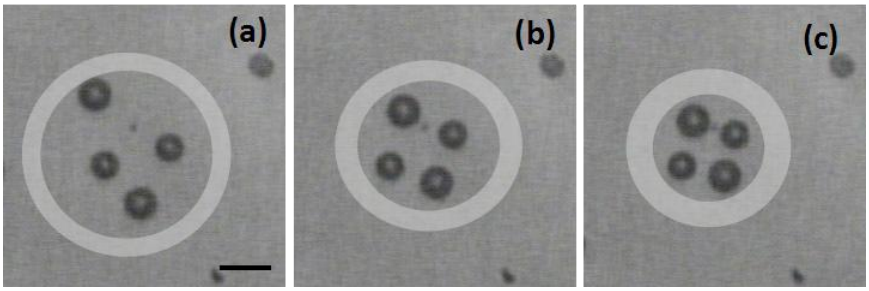

Figure 5.3: *Sequential images showing the particle concentration using varying mode of LG beam. The rings showing the schematic LG beam intensity pattern for (a) LG_{25} (b) LG_{18} and (c) LG_{10}. Scale bar: 30µm.*

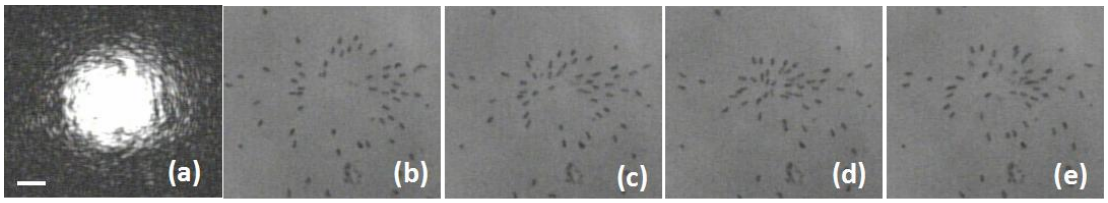

Figure 5.4: *Manipulation of RBCs (a) illumination intensity pattern, (b)-(d) RBCs getting attracted towards the illumination region (e) RBCs getting repelled from the illuminated region. Scale bar: 30 µm.*

The system was also used for demonstrating the suitability for biological particles like red blood cells. When a Gaussian intensity pattern, as shown in figure 5.4(a), was applied to manipulate the RBCs at 200 KHz, $10V_{pp}$, the cells were attracted towards the illuminated region as shown in figure 5.4 (b)-(d). During the process when the frequency of the applied bias was changed to 80 KHz, the cells started getting repelled slowly and at 40 KHz cell got repelled very fast from the illuminated region as shown in figure 5.4(e). By changing the frequency, the cells got repelled as the Clausius-Mossotti factor changes sign from positive to negative inducing a negative DEP force. It is to be noted that similar experiments have been shown in several other reports for demonstration purposes [64]. The developed system was used for the development of two sorting/separation approaches of cells/micro-particles suitable for very high packing density samples.

5.5 Separation of polystyrene micro-particles based on their size

We investigated the use of OET for separation of polystyrene micro spheres based on their size difference by scanning an intensity pattern consisting of linear array of equally spaced circular intensity spots across a concentrated sample. For this, an array of circular intensity spots having spacing larger than the size of the smaller particle and smaller than the size of larger sized particle were generated using the SLM and scanned across a mixture of polystyrene microspheres (PMs). PMs have negative DEP in low conductivity medium (~100μS/cm). When the particles interact with only one intensity spot particles of all sizes will be repelled. However, during scanning the larger sized particle lying between the two intensity spots will have negative DEP force and will be carried away with scanning beam whereas the smaller size particles will have no DEP effect and will pass through the gap. The step size for the scanning of the intensity pattern was chosen to be a fraction of the diameter of the larger sized particle as this ensures that these particles do not get repelled to the opposite direction of the scanning. Figure 5.5(a) schematically the sorting of the smaller sized particles separated after the scanning the intensity pattern. The method was used for separation 6μm PMs from a mixture of PMs of sizes 6μm and 15μm having ~100% packing density having conductivity ~100μS/cm. The spacing between the intensity spots was kept ~10 μm and the step size for scanning was ~5μm. The power used in the sample plane was ~75μW per spot and the scanning speed was ~ 4μm/s. PMs have negative DEP force at all the a.c. bias frequencies for medium conductivity ~100μS/cm so PMs will be repelled from the illuminated region. During scanning, initially all the particles were repelled in random directions away from the illuminated region in all direction. After a few steps of scanning, the 6μm particles lying between the intensity spots pass

through the gap while the 15 µm particles were carried away with the scanning beam as shown in figures 5.5(b).

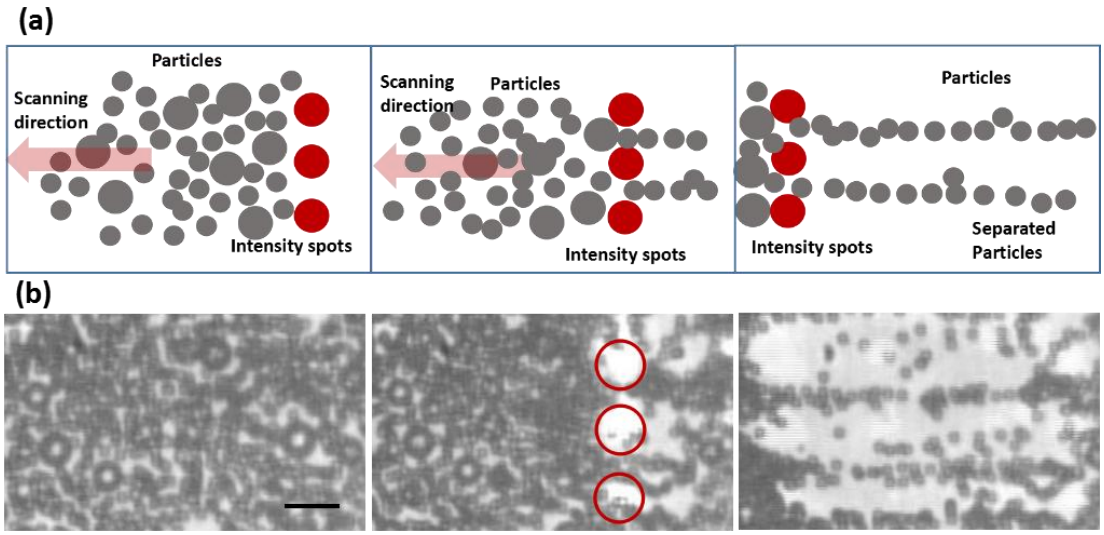

Figure 5.5: *(a) Schematics of the sorting approach showing shorting process while the intensity pattern scanned across the sample (b) sequential microscope images showing separation of 6 µm Polystyrene microspheres (PMs) from a mixture of PMs of sizes 6µm and 15 µm, Scale bar: 30 µm*

The 6 µm particles could be separated with a ~100 % purity and a throughput of ~20 particles/s. The separation efficiency which was less than 100 % as there will always be some smaller sized particles mixed with larger sized particles due to n-DEP can be enhanced by increasing the travel range of the intensity pattern. It is to be noted that we used n-DEP for the separation of the particles. When n-DEP is used particles get deflected to random directions away from the illuminated spots instead of getting attached to a fixed point which resolves the problem of colloidal jamming. Though the method was demonstrated on PMs which have only n-DEP forces for the given medium conductivity, concept can also be applied to particles/cells having frequency dependent DEP behavior. However, depending on the behavior of the two types of the particles the appropriate bias frequency can be selected to keep the n-DEP force on both types of particles.

5.6 Opto-electronic smart sweepers for cell/microparticle sorting

5.6.1 Scheme

In OET, the sculpted light intensity pattern is generated mainly by SLM along with coherent/incoherent light sources. These SLMs providing dynamic control over the generation of the projected light pattern are the diffractive optics having their own light intensity losses in addition to high cost of these systems. We, therefore, modified the illumination scheme in the OET for development of a simplified sorting approach, termed as opto-electronic smart sweepers, for sorting of cells/micro-particles in a flow free medium. The approach is based on the fact that the DEP response of cells is dependent on the frequency of the applied ac bias field. Therefore linear scanning/spinning of the line shaped intensity pattern, generated by a cylindrical lens, across the mixture could be used for sorting provided the applied a.c. bias electric field is kept on the n-DEP side, close to the crossover frequency of one of the particles. One type of particles whose cross over frequency is close to the applied bias frequency, will experience negligible negative DEP force, while the other will experience large repelling force due to negative DEP and will be forced to move along the scanning direction of the line shaped intensity profile. As a proof of concept, the working principle of opto-electronic smart sweepers was demonstrated by sweeping out the polystyrene microspheres from a mixture consisting of PSMs and RBCs. Further the approach was also demonstrated on a sample consisting of mixture of cells.

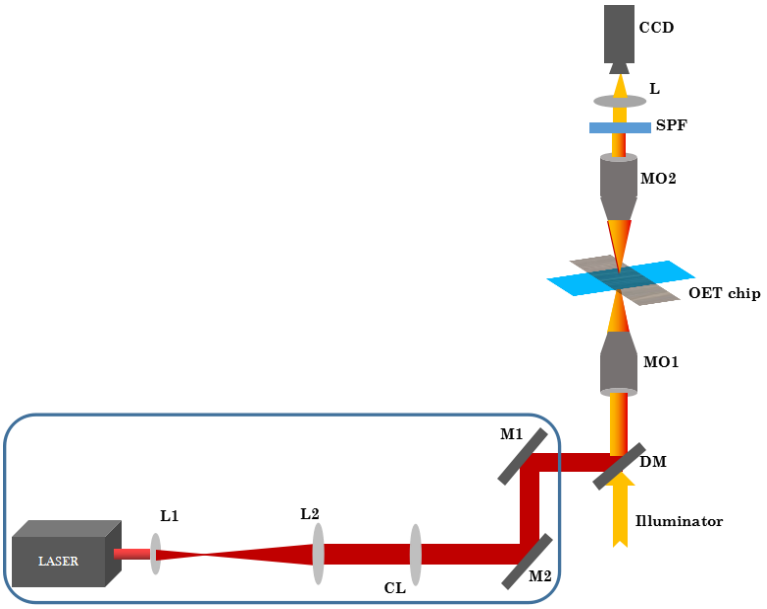

Figure 5.6*: Schematics of the OET setup having modified illumination scheme*

To achieve the illumination pattern, the setup described in the figure 1 was modified as shown in figure 5.6. As the approach only required a line shaped intensity profile, the use of SLM generates several ghost illumination spots which were effectively creating hindrance in applying the approach. Therefore the SLM based illumination part was just replaced by the scheme shown in figure 5.6. The cylindrical lens was fixed on a rotating mount.

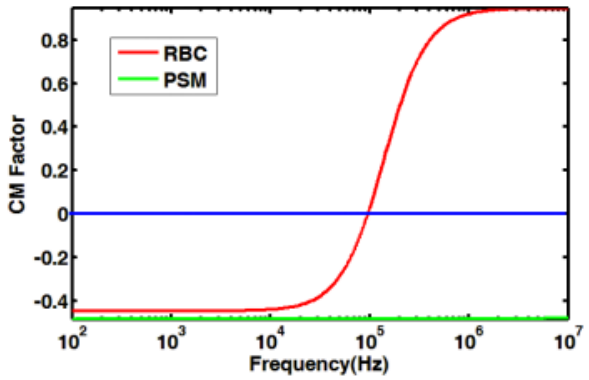

Figure 5.7: *Clausius-Mossotti factor frequency response of RBC and PSM*

The frequency dependence of the Clausius-Mossotti factor for PSM and the RBC is shown in figure 5.7. The dielectric permittivity of the medium (ε_m) has been taken as 80. Figure 5.7 shows that the PSM always have negative DEP forces for the used conductivity of the medium while the RBCs have negative as well as positive DEP response.

5.6.2 Results and discussion

The cross over frequency of RBCs is ~95 kHz. It is to be noted that the estimated DEP response is based on the average cell size whereas cells have some size variation. Considering this fact, if the applied a.c. bias frequency is slightly less than the crossover frequency, the negligible fraction of a type of cells will have positive DEP response. And the cells having negative DEP side will have negligible DEP force which will be overcome by appropriately choosing the scanning speed of the line electrode. The a.c. bias of frequency of 90 kHz with the bias voltage of $10V_{p\text{-}p}$ was applied. The optical power at the sample plane was ~500µW. The bias frequency was kept slightly less than the cross over frequency of RBCs which results in a negligible repelling force on the cells. A bias frequency higher than the crossover frequency may allow attract the cells which move along with the intensity profile leading to reduction in sorting efficacy.

The region of interest is circular area like microscope view; the spinning of the line intensity profile could sort the cells as well. The spinning speed of the line intensity profile was kept at ~2^o/s. At this speed, the PSM feel the negative DEP forces and after a few strokes during the rotation of the intensity profile, particles get deflected away from the center of the region as shown schematically in figure 5.8. Figure 5.9 shows the initial and the final view of of sorting of cells via spinning of the

line intensity profile in region of interest of ~0.2 mm^2. It may be noted that the particles which are near to the rotation axis of the intensity profile will take more time to be deflected to periphery of the region of interest.

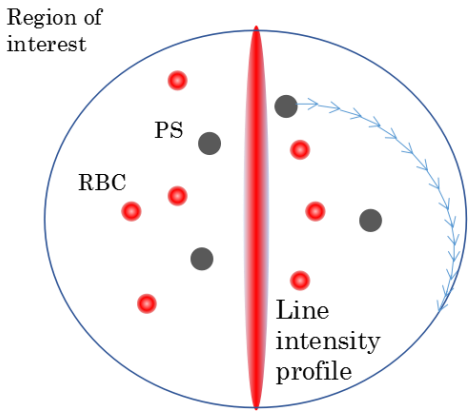

Figure 5.8: *Schematically showing a PSM interacting with the spinning intensity profile and getting repelled; resulting in these to move to the periphery of the circular region.*

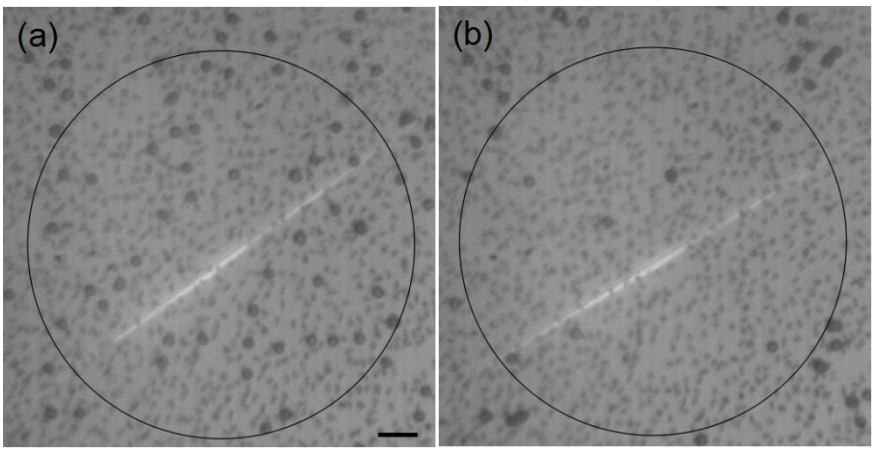

Figure 5.9: *Snapshots from a video showing the sorting of RBCs in a mixture of RBCs and PSMs by spinning the line shaped intensity profile (a) before spinning (b) after completing two spin; the black circle shows the region of interest. Scale bar: ~30 μm*

If the region of interest is rectangular area, the line shaped intensity profile can be scanned across the sample along the sides of the rectangular area. Here the line shaped intensity profile was scanned at a speed of ~ 6.5μm/s across the sample. Due to negative DEP force, the PSMs were forced to move along the scanning direction of

the line shaped intensity profile leaving the RBCs in the region of interest as shown in figure 5.10. Though there is no limit to area of linear scan for sorting, an area of ~0.36 mm^2 was scanned. Some cells are not moving or just budging in the sample plane while scanning the line profile were appeared to be adhered to the bottom plane. Although these reduce the efficacy of the sorting approach, as the opto-electronic tweezers can handle very dense sample [212], there is negligible effect on the sorting efficiency. Though the approach has been demonstrated in a mixture of PSMs and RBCs, it should also be suitable for sorting in a mixture of cells. In that case, the applied bias frequency of the electric field should be kept at close to the type of cells whose crossover frequency is less among the two. The approach can be made more controllable in terms of the scan speed and line intensity pattern thickness by replacing the laser and cylindrical lens with Multimedia projector.

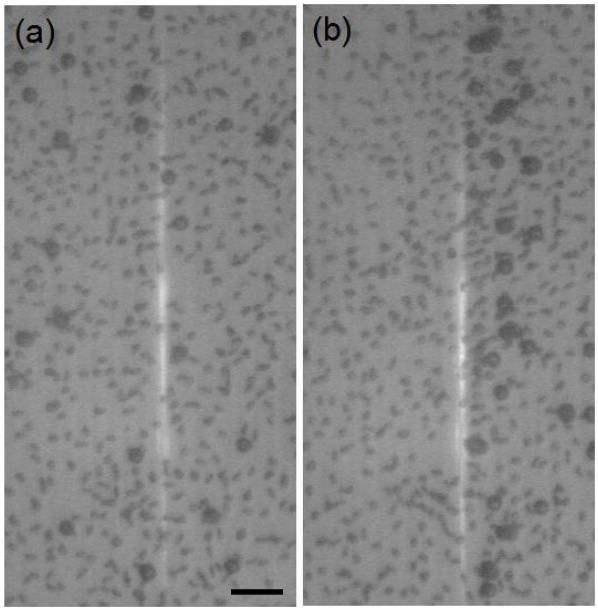

Figure 5.10: *Snapshot from a video demonstrating the operation of the Opto-electronic sweepers by sweeping out the PSMs and leaving only the RBCs in the region of interest by translating the shaped intensity profile across the sample, sample appearing (a) before scanning (b) after completing the scan; Scale bar: ~30 μm.*

5.7 Projector based OET setup for manipulation of cells

SLM is sensitive to the wavelength of the light being projected on it. Therefore a laser was used to generate the illumination pattern. However, the OET requires only a few mW of optical power to generate the illumination pattern, other incoherent light sources such as light emitting diodes, mercury lamp can also be used if the pattern generating device is not wavelength sensitive. Therefore in several reports, Digital micro mirror (DMD) device [63] has been used as pattern generating device. DMD is a Micro Electro mechanical system manufactured by Texas Instruments, USA and can be used as spatial light modulator [62]. It has two dimensional arrays of micro rectangular moving mirrors which are controlled by the underlying CMOS electronics [61]. These mirrors are made to flip in binary state termed as 'on' and 'off' state in ~20kHz rate and can direct the light on to or away from an intended target. These micro mirrors have different coating for reflecting the visible light and for the UV light.

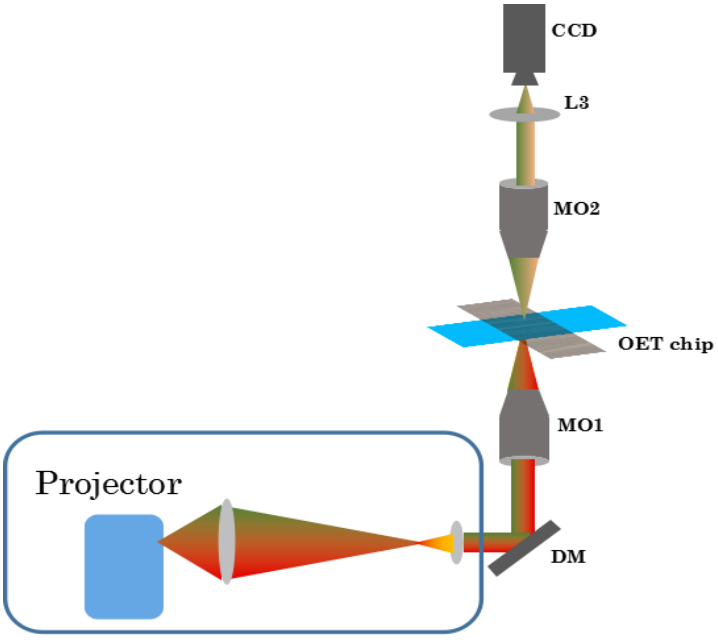

Figure 5.11: *Schematics of the OET setup using the DMD based multimedia projector*

In our setup, the pattern generation part has been replaced with a DLP based projector (Casio, Model No. XJ-A146) which has red, green, blue LED light sources for generating the colors. It is to be noted that the multimedia projectors have the 256 levels of intensity values for each color.

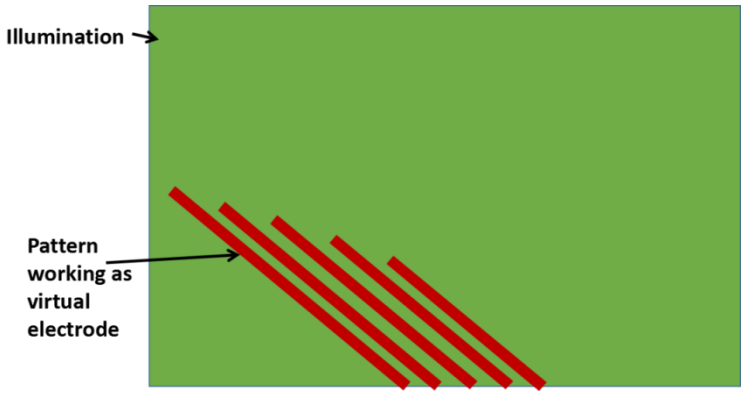

Figure 5.12: *A power point projection slide for generating ladder type virtual electrodes to guide the micro particles using negative DEP.*

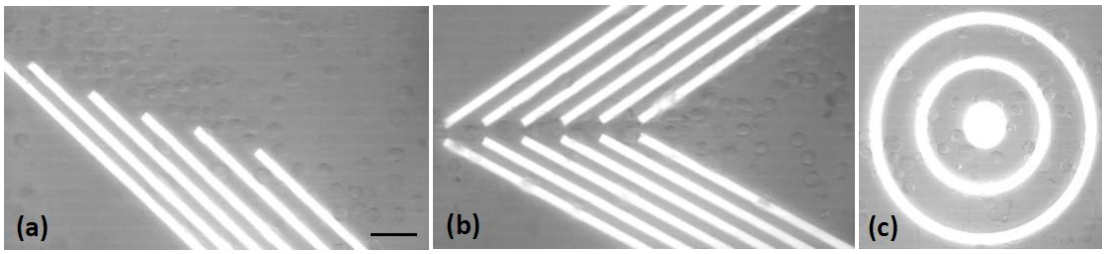

Figure 5.13: *Demonstration of the Projector based OET setup for guiding, focusing and patterning of colo 205 cells. Scale bar 50 µm.*

The red LED source (peak at ~660 nm) was chosen for the generation of the pattern because in this region the photo conductor has strong absorption while the green LED was chosen for illumination purpose because in this region the photo conductor has least absorption as shown by arrow in figure 5.1(d). The digital value for the blue LED was set as zero. This way a single light source served the purpose for the illumination as well as for pattern generation. The Projector is controlled via a desktop computer and the pattern is generated using the power point application. A power point slide image for the guiding of the cells in the OET chip is shown in figure 5.12

The colo 205 cells experiences the negative DEP forces at an a.c. bias of ~10V and the applied frequency of ~40 kHz and therefore repelled by the illumination region. The ladder kind of illumination pattern is generated to guide the cells by moving the sample stage. If these illumination pattern were mirror imaged, the arrangement starts working like a cell focusing arrangement which is often a requirement for performing single cell analysis in microfluidics. It is to be noted that the microfluidic arrangement in the 'Y' or 'X' can be made by appropriate input and output drills in the upper glass and connecting the micro bore tubing to these. Further applying an appropriate frequency of the bias field, cells can be deflected selectively. This reduces the complexity of fabricating the metal electrodes to a greater extent. Similarly the cell pattering is many a time required during the growth of cells. Therefore a light pattern as per the requirement of cell pattering can be generated and made to illuminate on the chip. As an example two circular ring have been illuminated on the chip and when the bias field is applied such that the cells experience negative DEP, the cells align in the non illuminated annular region as shown in figure 5.13(c). It is applied bias frequency is such that the cells experience positive DEP, the cells would align along the illuminated region.

5.8 Conclusion

We have presented the development and use of opto-electronic tweezers setup for manipulation and sorting of micro particles. We showed sorting approaches based on the fact that DEP depends on the size of the particle as well as on the frequency of applied field for sorting of red blood cells / polystyrene microspheres. A digital light projector based OET setup for guiding, focusing etc. of colon carcinoma cells was also presented.

6 *Chapter 6: Conclusion*

In this chapter we present the major accomplishments and an outline of future works that may be pursued based on the work presented in the thesis.

We developed a novel approach for focusing of cells in microfluidics for single cell Raman spectroscopic analysis. Such measurements in microfluidic chip require cell focusing i.e. a single line flow of cells through the analysis region. We made use of dual line optical tweezers arranged in the shape of 'Y' as an optical guide for focusing of the cells into a single line flow of cells in microfluidic chip. To generate dual line optical tweezers, we split a single laser in two parts using beam splitter and handled these separately and the Raman Excitation beam was placed at the tail of the optical guide. The resonance Raman effect was used to analyze the cells as they pass through the Raman excitation region without the need for trapping the cells. This arrangement has an advantage that it decouples the width of the cell stream and the cell flow speed in the microfluidic chip and facilitates independent control of the cell flow speed. The suitability of this approach for cytometry was demonstrated by identifying red blood cells (RBCs) in their met and normal form in a mixture of met-haemoglobin and normal haemoglobin RBCs in the ratio of 1: 9. The cell flow rate was ~500 cells/hour and was primarily limited by the integration time for acquiring Raman spectra.

Another application of multiple optical traps explored by us was development of various micro-scale sorting approaches suitable for flow less medium. We developed a multiple optical tweezers setup known as acousto-optic tweezers and utilized for passive optical sorting of the micro-particles. The approach exploits the fact that diffusion constant of a particle in a medium depends on its size. This enabled

sorting of large sized micro particles (which have higher residency time in the trap owing to slower diffusion) in a mixed sized population in a flow less medium. The method requires only a few mWs of optical power since single beam is used in time sharing mode and therefore the approach can be implemented using a low cost, compact diode lasers also.

To generate three dimensional manipulation capabilities with multiple optical traps we used SLM based approach, commonly referred to as holographic optical tweezers and developed two active optical sorting approaches based on use of multiple Z planes for trapping. In one of the approach, we first employed a cross correlation based pattern matching technique for selection of particle and then trapped these using HOT. Thereafter one set of particles is lifted axially to a higher plane and then both set of particles were translated simultaneously in respective planes without disturbing each other. The approach has improved throughput over the existing techniques for sorting in flow less medium. Another approach was developed for samples which contain low concentration of the desired particles in the ROI. In this approach the targeted particles are selected manually and moved to the upper plane at predefined position and maintained there by HOT while scanning the sample through multiple ROIs. Once the desired number of particles is collected, all the particles were brought down to bottom plane.

We developed another interesting tweezers setups based on light driven electro kinetic approach known as Opto-electronic tweezers. SLM was used for illumination pattern generation and hereafter it was replaced with multimedia projector for ease of pattern generation using power point. We presented application of this setup for manipulation and several approaches for sorting of micro particles such as RBCs,

polystyrene spheres etc. In one of the approach, we scanned an array of suitably spaced circular intensity spots across the sample for sorting the polystyrenes spheres based on their size. In another approach, we exploited the dependency of the DEP response of cell on the frequency of applied electric field for sorting of red blood cells from a mixture of RBCs and polystyrene microspheres. At the end, we demonstrated the projector based approach for guiding, focusing etc. of colon carcinoma cells.

The microfluidic flow cytometry approach developed for single cell Raman spectroscopy employs three channel input and one channel output. The same approach, if implemented in a microfluidic chip with three channel input and three channel output, can evolve as a label free cell sorter with the introduction of a suitable cell deflection technique as used elsewhere [148] to get the desired particles in one of the side channels.

Furthermore the sorting technique suitable for samples containing the desired particle in low concentration can be improved by making the particle selection by image based automated process so that a large number of ROIs could be scanned enabling the approach for sorting of rare cells in flow free medium.

The issue of getting a good quality photo conductive layer on the ITO coated glass was achieved by thermal deposition method. Therefore, a portable OET setup with an automated programming for required patterns for any specific application can be developed. For example a label free malaria diagnosis setup can be made as the setup can easily handle ~10000 cells, which is the standard number used in hospitals for fluorescence based detection, without requiring any flow.

REFERENCES

[1] A. Ashkin, J. M. Dziedzic, J. E. Bjorkholm and S. Chu, " Observation of a single beam gradient force optical trap for dielectric particles," *Opt. Lett.* , vol. 11, pp. 288-290, 1986.

[2] A. Ashkin, "Forces of a single-beam gradient laser trap on a dielectric sphere in the ray optics regime," *Biophy. J.* , vol. 61, pp. 569-582 , 1992.

[3] A. Ashkin, J. M. Dziedzic and T. Yamane, "Optical trapping and manipulation of single cells using infrared laser beams," *Nature* , vol. 330, pp. 769-771 , 1987.

[4] H. Zhang and K.Liu, "Optical tweezers for single cells," *J. R. Soc. Interface,* vol. 5, p. 671–690, 2008.

[5] S. C. Kuo and M. P. Sheet, "Optical tweezers in cell biology," *Trends Cell Biol.,* vol. 2, pp. 116-118, 1992.

[6] A. Ashkin and J. M. Dziedzic, " Optical trapping and manipulation of viruses and bacteria," *Science* , vol. 235, p. 1517–1520 , 1987.

[7] S. M. Block, D. F. Blair and H. C. Berg, "Compliance of baterial flagella measured using optical tweezers," *Nature* , vol. 338, p. 514–518 , 1989.

[8] R. M. Berry and H. C. Berg., "Absence of a barrier to backwards rotation of the bacterial flagellar motor demonstrated with optical tweezers," *Proc. Natl. Acad. Sci.* , vol. 94, p. 14433–14437 , 1997.

[9] R. Dasgupta, S. K. Mohanty and P. K. Gupta, "Controlled rotation of biological microscopic objects using optical line tweezers," *Biotechnol. Lett.,* vol. 25, pp. 1625-1628 , 2003.

[10] S. K. Mohanty, A. Uppal and P. K. Gupta, "Optofluidic stretching of RBCs using single optical tweezers," *J. Biophoton.,* vol. 1, pp. 522-525, 2008.

[11] S. K. Mohanty, A. Uppal and P. K. Gupta, "Self-rotation of red blood cells in optical tweezers: prospects for high throughput malaria diagnosis," *Biotechnol. Lett.* , vol. 26, pp. 971-974 , 2004.

[12] J. A. Dharmadhikari, S. Roy, A. K. Dharmadhikari, S. Sharma and D. Mathur, "Naturally occurring, optically driven, cellular rotor," *Appl. Phy. Let.,,* vol. 85, pp. 6048-6050, 2004.

[13] B. V. Nagesh, Yogesha, R. Pratibha, P. Parthasarathi, S. Curvaturehruthi, S. Iyengar, S. Bhattacharya and S. Ananthamurthy, "Birefringence of a normal human red blood cell and related optomechanics in an optical trap," *Biophys. J.,* vol. 19, pp. 115004-12, 2014.

[14] A. Ashkin and J. M. Dziedzic, "Internal cell manipulation using infrared laser traps," *Proc. Natl. Acad. Sci. USA* , vol. 86, p. 7914–7918, 1989.

[15] J. C. Maxwell, A Treatise on Electricity and Magnetism, vol. 2, Oxford: Clarendon press, Oxford, UK, 1873.

[16] P. N. Lebedev, “Experimental examination of light pressure,” *Ann. Phys.,* vol. 6, p. 433, 1901.

[17] E. Nichols and G. Hull, “A preliminary communication on the pressure of heat and light radiation,” *Phys. Rev.,* vol. 13, p. 307–320, 1901.

[18] E. Nichols and G. Hull, “The pressure due to radiation (second paper),” *Phys Rev (Series I),* vol. 17, p. 26–50, 1903.

[19] A. Ashkin., “Acceleration and Trapping of Particles by Radiation Pressure,” *Phys. Rev. Lett.,* vol. 24, pp. 156-159, 1970.

[20] A. Ashkin and J. M. Dziedzic, “Optical levitation by radiation pressure,” *Applied Physics Letters ,* vol. 19, pp. 283-285 , 1971.

[21] A. Ashkin and J. M. Dziedzic, “Optical levitation of liquid drops by radiation pressure,” *Science,* vol. 187, pp. 1073-1075, 1975.

[22] A. Ashkin, K. Schutze, J. M. Dziedzic, U. Euteneuer and M. Schliwa, “Force generation of organelle transport measured in vivo by an infrared laser trap,” *Nature,* vol. 348, pp. 346-348, 1990.

[23] T. N. Buican, M. J. Smyth, H. A. Crissman, G. C. Salzman, C. C. Stewart and J. C. Martin, “Automated single-cell manipulation and sorting by light trapping,” *Appl. Opt. ,* vol. 26 , p. 5311–5316 , 1987.

[24] Y. Harada and T. Asakura, “Radiation forces on a dielectric sphere in the Rayleigh scattering regime,” *Opt. Comm. ,* vol. 124, pp. 529-541, 1996.

[25] A. Ashkin, “History of optical trapping and manipulation of small-neutral particle, atoms, and molecules,” *IEEE J. Selected Topics in Quantum Electronics,* vol. 6, pp. 841-856, 2000.

[26] K. Svoboda and S. M. Block, “ “Biological applications of optical forces,,” *Annual Review of Biophysics and Biomolecular Structure,* vol. 23, p. 247–285 , 1994.

[27] D. V. Petrov, “Raman spectroscopy of optically trapped particles,” *J. Opt. A: Pure Appl. Opt. ,* vol. 9, pp. S139-S156 , 2007.

[28] R. Dasgupta, S. Ahlawat, R. S. Verma, A. Uppal and P. K. Gupta., “Hemoglobin degradation in human erythrocytes with long duration near infrared laser exposure in Raman optical tweezers,” *J. Biomed. Opt. ,* vol. 15, p. 055009 , 2010.

[29] R. Dasgupta, R. S. Verma, S. Ahlawat, A. Uppal and P. K. Gupta, “Studies on erythrocytes in malaria infected blood sample with Raman optical tweezers,” *J. Biomed. Opt. ,* vol. 16, p. 077009 , 2011.

[30] D. G. Grier, “A revolution in optical manipulation,” *Nature,* vol. 424, pp. 810-816, 2003.

[31] S. M. Block, L. S. B. Goldstein and B. J. Schnapp, “Bead movement by single kinesin molecules studied with optical tweezers,” *Nature ,* vol. 348, pp. 348-352, 1990.

[32] S. C. Kuo and M. P. Sheetz, "Force of single kinesin molecules measured with optical tweezers," *Science*, vol. 260, pp. 232-234, 1993.

[33] K. C. Neuman and A. Nagy, "Single-molecule force spectroscopy: optical tweezers, magnetic tweezers and atomic force microscopy," *Nature Methods*, vol. 5 , pp. 491-505 , 2008.

[34] K. Svoboda, C. F. Schmidt, B. J. Schnapp and S. M. Block, "Direct observation of kinesin stepping by optical trapping interferometry," *Nature*, vol. 365, pp. 721-727, 1993.

[35] G. Mie, "Beiträge zur Optik trüber Medien, speziell kolloidaler Metallösungen," *Annalen der physik,* , vol. 25, p. 377–452, 1908.

[36] G. Gouesbet, B. Maheu and G. Grehan, "Light scattering from a sphere arbitrarily located in a Gaussian beam, using a Bromwich formulation," *J. Opt. Soc. Amer. A*, vol. 5, p. 1427–1443, 1988.

[37] Y. K. Nahmias and D. J. Odde, "Analysis of radiation forces in laser trapping and laser-guided direct writing applications," *IEEE J. Quantum Electron.*, vol. 38, p. 131–41 , 2002.

[38] Y. Liu, G. J. Sonek, M. W. Berns and B. J. Tromberg, "Physiological monitoring of optically trapped cells: assessing the effects of confinement by 1064-nm laser tweezers using microfluorometry," *Biophys. J.* , vol. 71, p. 2158–21, 1996.

[39] Y. Lui, D. K. Cheng, G. J. Soneck, M. W. Berns, C. F. Chapman and B. Tromberg, "Evidence of localized cell heating induced by infrared optical tweezers," *Biophys. J.*, vol. 68, p. 2137 , 1995.

[40] K. König, H. Liang, M. W. Berns and B. J. Tromberg, "Cell damage in near-infrared multimode optical traps as a result of multiphoton absorption," *Opt Lett.*, vol. 21 , pp. 1090-1092 , 1996.

[41] K. C. Neuman and S. M. Block, "Optical trapping,," *Review of Scientific Instruments*, vol. 75, pp. 2787-2809, 2004.

[42] M. Capitanio, G. Romano, R. Ballerini, M. Giuntini, F. S. Pavonea, D. Dunlap and L. Finzi, "Calibration of optical tweezers with differential interference contrast signals," *Rev. Sci. Instrum.* , vol. 73, pp. 1687-1696 , 2002.

[43] J. Gelles, B. J. Schnupp and M. P. Sheetz, "Tracking kinesin-driven movements with nanometre-scale precision," *Nature* , vol. 331 , pp. 450-453 , 1988.

[44] M. K. Cheezum, W. F. Walker and W. H. Guilford, "Quantitative Comparison of Algorithms for Tracking Single Fluorescent Particles," *Biophys. J.* , vol. 81, p. 2378–2388 , 2001.

[45] R. M. Simmons, J. T. Finer, S. Chu and J. A. Spudich, "Quantitative Measurements of Force and Displacement Using an Optical Trap," *Biophys. J.*, vol. 70 , pp. 1813-1822, 1996.

[46] M. D. Wang, M. J. Schnitzer, H. Yin, R. Landick, J. Gelles and S. M. Block, "Force and velocity measured for single molecules of RNA polymerase," *Science* , vol. 282 , pp. 902-907 , 1998.

[47] H. Yin, M. D. Wang, K. Svoboda, R. Landick, S. M. Block and J. Gelles, "Transcription against an applied force," *Science* , vol. 270 , pp. 1653-1657, 1995 .

[48] M. M. Burns, J. Fournier and J. A. Golovchenko, “Optical matter: Crystallization and binding in intense optical fields,” *Science* , vol. 249, pp. 749-754, 1990.

[49] K. Visscher, S. P. Gross and S. M. Block, “Construction of multiplebeam optical traps with nanometer-resolution position sensing,” *IEEE J. Select. Topics Quant. Electr.* , vol. 2, p. 1066–1076, 1996.

[50] T. R. Strick, J. F. Allemand, D. Bensimon, A. Bensimon and V. Croquette, “The elasticity of a single supercoiled DNA molecule,” *Science* , vol. 271, pp. 1835-1837, 1996.

[51] J. F. Ortas, “Dynamic Optical Tweezers using Acousto-Optic Modulators,” 06 2015. [Online]. Available: http://diposit.ub.edu/dspace/bitstream/2445/67388/1/TFG-Ferrer-Ortas-Julia.pdf. [Accessed 27 08 2018].

[52] N. Matsumoto, T. Ando, T. Inoue, Y. Ohtake, N. Fukuchi and T. Hara, “Generation of high quality higher-order Laguerre–Gaussian beams using liquid-crystal-on-silicon spatial light modulators,” *J. Opt. Soc. Am. A,* vol. 25, pp. 1642-1651, 2008.

[53] “Phase spatial light Modulator LCOS-SLM,” Hamamatsu Photonics, [Online]. Available: https://www.hamamatsu.com/resources/pdf/ssd/e12_handbook_lcos_slm.pdf. [Accessed 27 08 2018].

[54] E. R. Dufresne, G. C. Spalding, M. T. Dearing, S. A. Sheets and D. G. Grier, “Computer-generated holographic optical tweezer arrays,” *Rev Sci Instrum,* vol. 72, p. 1810–1816, 2001.

[55] J. Liesener, M. Reicherter, T. Haist and H. J. Tiziani, “Multifunctional optical tweezers using computer-generated holograms,” *Opt. Commun.,* vol. 185, p. 77– 82, 2000.

[56] M. Meister and R. J. Winfield, “Novel approaches to direct search algorithms for the design of diffractive optical elements,” *Opt. Commun.* , vol. 203, p. 3949 , 2002.

[57] J. E. Curtis, B. A. Koss and D. G. Grier, “Dynamic holographic optical tweezers,” *Opt. Comm.* , vol. 207, pp. 169-175 , 2002.

[58] G. C. Spalding, J. Courtial and R. D. Leonardo, “Holographic optical tweezers,” [Online]. Available: https://sun.iwu.edu/~gspaldin/HOTsReview.pdf. [Accessed 28 08 2018].

[59] R. W. Gerchberg and W. O. Saxton, “A Practical Algorithm for the Determination of Phase from Image and Diffraction Plane Pictures,” *OPTIK,* vol. 35 , pp. 237 -246, 1972.

[60] R. D. Leonardo, F. Ianni and G. Ruocco, “Computer generation of optimal holograms for optical trap arrays,” *Opt. Express* , vol. 15, pp. 1913-1922, 2007.

[61] D. Dudley, W. M. Duncan and J. Slaughter, “Emerging digital micromirror device (DMD) applications,” in *MOEMS Display and Imaging Systems*, San Jose, 2003.

[62] B. Lee, “Introduction to ±12 Degree Orthogonal Digital Micromirror Devices,” [Online]. Available: http://www.ti.com/lit/an/dlpa008b/dlpa008b.pdf . [Accessed 27 08 2018].

[63] P. Y. Chiou, A. T. Ohta and M. C. Wu, “Massively parallel manipulation of single cells and

microparticles using optical images," *Nature,* vol. 436, pp. 370-372, 2005.

[64] A. T. Ohta, P. Y. Chiou, T. H. Han, J. C. Liao, U. Bhardwaj, E. R. B. McCabe, R. S. F. Yu and M. C. Wu, "Dynamic cell and microparticle control via optoelectronic tweezers," *J. Microelectromech. Syst.,* vol. 16 , p. 491–499, 2007.

[65] S. B. Huang, M. H. Wu, Y. H. Lin, C. H. Hsieh, C. L. Yang, H. C. Lin, C. P. Tseng and G. B. Lee, ""High-purity and label-free isolation of circulating tumor cells (CTCs) in a microfluidic platform by using optically-induced dielectrophoretic (ODEP) force," *Lab chip,* vol. 13, pp. 1371-1383, 2013.

[66] A. Jamshidi, P. J. Pauzauskie, P. J. Schuck, A. T. Ohta, P.-Y. Chiou, J. Chou, P. Yang and M. C. Wu, "Dynamic manipulation and separation of individual semiconducting and metallic nanowires," *Nature Photonics,* vol. 2, p. 86–89, 2008.

[67] Y. H. Lin and G. B. Lee, "An optically-induced cell lysis device using dielectrophoresis,"," *Appl. Phys. Lett.,* vol. 94, p. 033901, 2009.

[68] C. H. Wang, Y. H. Lee, H. T. Kuo, W. F. Liang, W. Li and G. B. Lee., "Dielectrophoretically-assisted electroporation using light-activated virtual microelectrodes for multiple DNA transfection," *Lab on a Chip,* vol. 14, p. 592–601, 2014.

[69] H. A. Pohl, Dielectrophoresis, Cambridge, U.K.: Cambridge Univ. Press, 1978.

[70] R. Pethig, "Review Article—Dielectrophoresis: Status of the theory, technology, and applications," *Biomicrofluidics,* vol. 4, p. 022811, 2010.

[71] J. Voldman, "Dielectrophoretic Traps for Cell Manipulation," in *BioMEMS and Biomedical Nanotechnology*, Boston, MA,, Springer, 2006, pp. 159-186.

[72] P. R. Gascoyne, X. B. Wang, Y. Huang and F. F. Becker, "Dielectrophoretic Separation of Cancer Cells from Blood," *IEEE Trans. Ind. Appl.,* vol. 33, p. 670–678, 1997.

[73] J. K. Valley, A. Jamshidi, A. T. Ohta, I. Y. Hsu and M. C. Wu, "Operational Regimes and Physics Present in Opto-electronic Tweezers," *J. Microelectromech Syst.,* vol. 17, p. 342–350, 2008.

[74] A. Ashkin and J. M. Dziedzic, "Observation of light scattering from nonspherical particles using optical levitation," *Appl. Opt. ,* vol. 19, pp. 660-668, 1980.

[75] J. T. Finer, R. M. Simmons and J. A. Spudich, "Single myosin molecule mechanics: pico-newton forces and nanometre steps," *Nature,* vol. 368, p. 113–119 , 1994.

[76] J. E. Molloy, J. E. Burns, J. K. Jones, R. T. Tregear and D. C. S. White, "Movement and force produced by a single myosin head," *Nature ,* vol. 378, p. 209–212, 1995.

[77] K. Sasaki, M. Koshioka, H. Misawa, N. Kitamura and H. Masuhara, "Laser-Scanning Micromanipulation and Spatial Patterning of Fine Particles," *Jpn. J. Appl. Phys.,* vol. 30, pp. L907-L909, 1991 .

[78] K. Sasaki, M. Koshioka, H. M. M, N. Kitamura and H. Masuhara, "Pattern formation and flow

control of fine particles by laser-scanning micromanipulation," *Opt. Lett.* , vol. 16, pp. 1463-1465, 1991.

[79] H. Misawa, K. Sasaki, M. Koshioka and N. Kitamura, "Multibeam laser manipulation and fixation of microparticles," *Appl. Phys. Lett.* , vol. 60, pp. 310-312, 1992.

[80] K. Sasaki, M. Koshioka, H. Misawa and N. Kitamura, "Optical trapping of a metal particle and a water droplet by a scanning laser beam," *Appl. Phys. Lett.* , vol. 60, pp. 807-809, 1992.

[81] K. Visscher, G. J. Brakenhoff and J. J. Krol, "Micromanipulation by multiple optical traps created by a single fast scanning trap integrated with the bilateral confocal scanning laser microscope," *Cytometry*, vol. 14 , p. 105–114, 1993.

[82] P. J. H. Bronkhorst, G. J. Streekstra, J. Grimbergen, E. J. Nijhof, J. J. Sixma and G. J. Brakenhoff, "A New Method to Study Shape Recovery of Red Blood Cells Using Multiple Optical Trapping," *Biophys. J.* , vol. 69, pp. 1666-1673, 1995 .

[83] J. E. Molloy, "Optical chopsticks: digital synthesis of multiple optical traps," *Methods Cell Biol.* , vol. 55, p. 205–216, 1998.

[84] J. Sleep, D. Wilson, R. Simmons and W. Gratzer, "Elasticity of the Red Cell Membrane and Its Relation to Hemolytic Disorders: An Optical Tweezers Study," *Biophys. J.*, vol. 77, p. 3085–3095, 1999 .

[85] H. D. Ou-Yang, "Design and applications of oscillating optical tweezers for direct measurements of colloidal forces," in *Farinato RS and Dubin PL (eds) Colloid Polymer Interactions: From Fundamentals to Practice* , New York, Wiley, 1999, pp. 385-405.

[86] M. J. Lang, C. L. Asbury, J. W. Shaevitz and S. M. Block, "An Automated Two-Dimensional Optical Force Clamp for Single Molecule Studies," *Biophys. J.*, vol. 83, p. 491–501, 2002 .

[87] E. A. Abbondanzieri, W. J. Greenleaf, J. W. Shaevitz, R. Landick and S. M. Block, "Direct observation of base-pair stepping by RNA polymerase," *Nature,* vol. 438 , pp. 460-465, 2005.

[88] R. T. Dame, M. C. Noom and G. J. L. Wuite, "Bacterial chromatin organization by H-NS protein unravelled using dual DNA manipulation,," *Nature,* vol. 444, pp. 387-390, 2006 .

[89] G. B. Liao, P. B. Bareil, Y. Sheng and A. Chiou, "One-dimensional jumping optical tweezers for optical stretching of bi-concave human red blood cells," *Opt. Exp.*, vol. 16, pp. 1996-2004, 2008.

[90] R. L. Eriksen, V. R. Daria and J. Glückstad, "Fully dynamic multiple-beam optical tweezers," *Opt. Exp.* , vol. 10 , pp. 597-602, 2002.

[91] E. R. Dufresne and D. G. Grier, "Optical tweezer arrays and optical substrates created with diffractive optics," *Rev. Sci. Instrum.*, vol. 69, p. 1974 –1977, 1998.

[92] J. Leach, G. Sinclair, P. Jordan, J. Courtial, M. J. Padgett, J. Cooper and Z. J. Laczik, "3D manipulation of particles into crystal structures using holographic optical tweezers," *Opt. Exp.*, vol. 12, pp. 220-226, 2004.

[93] G. Sinclair, P. Jordan, J. Courtial, M. Padgett, J. Cooper and Z. J. Laczik, "Assembly of 3-dimensional structures using programmable holographic optical tweezers," *Opt. Exp.* , vol. 12, pp. 5475-5480 , 2004.

[94] A. Jesacher, C. Maurer, A. Schwaighofer, S. Bernet and M. Ritsch-Marte, "Near-perfect hologram reconstruction with a spatial light modulator," *Opt. Exp.*, vol. 16, p. 2597–2603 , 2008.

[95] N. Matsumoto, T. Ando, T. Inoue, Y. Ohtake, N. Fukuchi and T. Hara, "Generation of high quality higher-order Laguerre–Gaussian beams using liquid-crystal-on-silicon spatial light modulators," *J. Opt. Soc. Am. A* , vol. 25, pp. 1642-1651, 2008.

[96] N. Chattrapiban, E. A. Rogers, D. Cofield, W. T. Hill and R. Roy, "Generation of nondiffracting Bessel beams," *OPTICS LETTERS,* vol. 28, 2003.

[97] S. H. Tao, W. M. Lee and X. C. Yuan, "Dynamic optical manipulation with a higher-order fractional Bessel beam generated from a spatial light modulator," *Opt. Lett.,* vol. 28, 2003.

[98] M. Duocastella and C. B. Arnold, "Bessel and annular beams for materials processing," *Laser Photonics Rev.,* vol. 6 , p. 607–621, 2012.

[99] R. Dasgupta, S. Ahlawat, R. S. Verma and P. K. Gupta, "Optical orientation and rotation of trapped RBCs with Laguerre-Gaussian mode," *Opt. Exp.* , vol. 19, pp. 7680-7688, 2011.

[100] S. K. Mohanty, R. S. Verma and P. K. Gupta, "Trapping and controlled rotation of low-refractive-index particles using dual line optical tweezers," *Appl. Phys. B* , vol. 87, p. 211–216 , 2007.

[101] R. Dasgupta, S. Ahlawat, R. S. Verma, S. Shukla and P. K. Gupta, "Optical trapping of spermatozoa using Laguerre-Gaussian laser modes," *J. Biomed. Opt.* , vol. 15, p. 065010 , 2010.

[102] R. Dasgupta, R. S. Verma, S. Ahlawat, D. Chaturvedi and P. K. Gupta, "Long distance axial trapping with Laguerre-Gaussian beams," *Appl. Opt.* , vol. 50, pp. 1469-1476, 2011.

[103] C. Bechinger, M. Brunner and P. Leiderer, "Phase behavior of two-dimensional colloidal systems in the presence of periodic light fields," *Phys. Rev. Lett.* , vol. 86, pp. 930-933, 2001.

[104] M. Bechinger and C. Brunner, "Phase behavior of colloidal molecular crystals on triangular light lattices," *Phys. Rev. Lett.,* vol. 88, p. 248302, 2002.

[105] C. Reichhardt and C. J. Olson, "Novel colloidal crystalline states on two-dimensional periodic substrates," *Phys. Rev. Lett.* , vol. 88, p. 248301, 2002.

[106] K. Mangold, P. Leiderer and C. Bechinger., "Phase transitions of colloidal monolayers in periodic pinning arrays," *Physical Review Letters,,* vol. 90, p. 158302, 2003.

[107] J. Baumgart, M. Brunner and C. Bechinger, "Locked-floating-solid to locked-smectic transition in colloidal systems," *Phys. Rev. Lett.,* vol. 93, p. 168301, 2004.

[108] C. J. O. Reichhardt and C. Reichhardt, "Directional locking effects and dynamics for particles driven through a colloidal lattice," *Physical Review E,* vol. 69, p. 041405, 2004.

[109] C. Reichhardt and C. J. O. Reichhardt, "Cooperative behavior and pattern formation in mixtures of driven and nondriven colloidal assemblies," *Phys. Rev. E,* vol. 74, p. 011403, 2006.

[110] X. Wang, S. Chen, M. Kong, Z. Wang, K. D. Costa, R. A. Li and e. al., "Enhanced cell sorting and manipulation with combined optical tweezers and microfluidic chip technologies," *Lab Chip,* vol. 11, pp. 3656-3662, 2011.

[111] P. T. Korda, M. B. Taylor and D. G. Grier, "Kinetically locked-in colloidal transport in an array of optical tweezers," *Phys. Rev. Lett.,* vol. 89, p. 128301, 2002.

[112] H. Little, C. T. A. Brown, V. G. Chavez, W. Sibbett and K. Dholakia, "Optical guiding of microscopic particles in femtosecond and continuous wave Bessel light beams," *Opt. Exp.* , vol. 12, pp. 2560-2565, 2004.

[113] P. Fischer, A. E. Carruthers, K. V. Sepulveda, E. M. Wright, C. T. A. Brown, W. Sibbett and K. Dholakia, "Enhanced optical guiding of colloidal particles using a supercontinuum light source," *Opt. Exp.* , vol. 14, pp. 5792-5802 , 2006.

[114] S. Ahlawat, R. S. Verma, R. Dasgupta and P. K. Gupta, "Long distance optical guiding of colloidal particles using holographic axilens," *Appl. Opt.* , vol. 50, pp. 1933-1940 , 2011.

[115] A. Y. Lau, L. P. Lee and J. W. Chan, "An integrated optofluidic platform for Raman-activated cell sorting," *Lab Chip* , vol. 8, p. 1116–1120, 2008.

[116] B. A. Koss and D. G.Grier, "Optical peristalsis," *Appl. Phy. Lett.,* vol. 82, pp. 3985-3987, 2003.

[117] K. Xiao and D. G. Grier, "Sorting colloidal particles into multiple channels with optical forces: Prismatic optical fractionation," *Phys. Rev. E,* vol. 82, pp. 051407-9 , 2010.

[118] S. C. Chapin, V. Germain and E. R. Dufresne, "Automated trapping, assembly, and sorting with holographic optical tweezers," *Opt. Exp.,* vol. 14, p. 13095–13100, 2006.

[119] P. J. Rodrigo, R. L. Eriksen, V. R. Daria and J. Glückstad, "Interactive light-driven and parallel manipulation of inhomogeneous particles," *Opt. Exp.,* vol. 10, pp. 1550-1556, 2002.

[120] B. Landenberger, H. H. Femann, S. Wadle and A. Rohrbach, "Microfluidic sorting of arbitrary cells with dynamic optical tweezers," *Lab Chip,* vol. 12, p. 3177–3183, 2012.

[121] R. Dasgupta, S. Ahlawat and P. K. Gupta, "Microfluidic sorting with a moving array of optical traps," *Appl. Opt.,* vol. 51 , pp. 4377-4387, 2012.

[122] K. Xiao and D. G. Grier, "Multidimensional Optical Fractionation of Colloidal Particles with Holographic Verification," *Phy. Rev. Lett.,* vol. 104, pp. 028302-4, 2010.

[123] S. Ahlawat, R. Dasgupta, R. S. Verma, V. N. Kumar and P. K. Gupta, "Optical sorting in holographic trap arrays by tuning the inter-trap separation," *J. Opt.,* vol. 14 , p. 125501 (12pp), 2012.

[124] C. S. Guo, Y. N. Yu and Z. Hong, "Optical sorting using an array of optical vortices with fractional topological charge," *Opt. Comm.,* vol. 283, p. 1889–1893, 2010.

[125] I. P. Nielsen, D. Palima, J. S. Dam and J. Gluckstad, “Parallel particle identification and separation for active optical sorting,” *J. Opt. A: Pure Appl. Opt.,* vol. 11, p. 034013 (6pp), 2009.

[126] L. Paterson, E. Papagiakoumou, G. Milne, V. G. Chávez, T. Briscoe, W. Sibbett, K. Dholakia and A. C. Riches, “Passive optical separation within a ’nondiffracting’ light beam,” *J. Biomed. Opt.* , vol. 12, pp. 054017-13, 2007.

[127] L. Paterson, E. Papagiakoumou, G. Milne, V. G. Chávez, S. A. Tatarkova, W. Sibbett, F. J. G. Moore, P. E. Bryant, A. C. Riches and K. Dholakia, “Light induced cell separation in a tailored optical landscape,” *Appl. Phy. Lett.,* vol. 87, pp. 123901-3, 2005.

[128] K. Ladavac, K. Kasza and D. G. Grier, “Sorting mesoscopic objects with periodic potential landscapes: Optical fractionation,” *Phys. Rev. E* , vol. 70, pp. 010901-4, 2004.

[129] J. Gluckstad, “Sorting particles with light,” *Nature Mat.,* vol. 3, pp. 9-10, 2004.

[130] P. M, K. Ladavac and D. G. Grier, “Transport and fractionation in periodic potential-energy landscapes,” *Phys. Rev. E,* vol. 70, pp. 031108-10, 2004.

[131] S. Ahlawat, N. Kumar, R. Dasgupta, R. S. Verma, A. Uppal and P. K. Gupta, “Raman spectroscopic investigations on optical trap induced deoxygenation of red blood cells,” *Appl. Phys. Let.,* vol. 103 , pp. 183704 1-5, 2013.

[132] S. Ahlawat, A. Chowdhury, N. Kumar, A. Uppal and R. S. V. P. K. Gupta, “Polarized Raman spectroscopic investigations on hemoglobin ordering in red blood cells,” *J. Biomed. Opt.,* vol. 19, pp. 087002 1-9, 2014.

[133] M. P. MacDonald, G. C. Spalding and K. Dholakia, “Microfluidic sorting in an optical lattice,” *Nature,* vol. 426, pp. 421-424, 2003.

[134] R. L. Smith, G. C. Spalding, K. Dholakia and M. P. MacDonald, “Colloidal sorting in dynamic optical lattices,” *J. Opt. A,* vol. 9 , p. S134, 2007.

[135] G. Milne, D. Rhodes, M. MacDonald and K. Dholakia, “Fractionation of polydisperse colloid with acousto-optically generated potential energy landscapes,” *Opt. Lett.* , vol. 32, pp. 1144-1146, 2007.

[136] T. Cizmar, M. Siler, M. Sery and Z. a. P, “Optical sorting and detection of submicrometer objects in a motional standing wave,” *Phy. Rev. B* , vol. 74 , p. 035105, 2006.

[137] I. R. Vargas, P. R. Montero, R. R. García and K. V. Sepúlveda, *Appl. Phys. Lett.* , vol. 88, p. 121116 , 2006.

[138] K. W. Huang, Y. C. Wu, J. A. Lee and P. Y. Chiou, “Microfluidic integrated optoelectronic tweezers for single-cell preparation and analysis,” *Lab on a Chip,* vol. 13, p. 3721–3727, 2013.

[139] S. B. Huang, M. H. Wu, Y. H. Lin, C. H. Hsieh, C. L. Yang, H. C. Lin, C. P. Tseng and G. B. Lee, “High-purity and label-free isolation of circulating tumor cells (CTCs) in a microfluidic platform by using optically-induced dielectrophoretic (ODEP) force,” vol. 13, pp. 1371-1383, 2013.

[140] P. Y. Chiou, A. T. Ohta, A. Jamshidi, H. Y. Hsu and M. C. Wu, “Light-actuated AC electroosmosis

for nanoparticle manipulation," *J. Microelectromech. Syst.,* vol. 17, p. 525–531, 2008.

[141] Y. H. Lin and C. T. Y. K. S. Ho, "Set-up for an optically induced dielectrophoresis platform and its application to micro- and nanoscale material manipulation," *International journal of automation and smart technology,* vol. 4, pp. 208-215, 2014.

[142] S. M. Yang, T. M. Yu, H. P. Huang, M. Y. Ku, S. Y. Tseng, C. L. Tsai, H. P. Chen, L. Hsu and C. H. Liu, "Light-driven manipulation of picobubbles on a titanium oxide phthalocyanine-based optoelectronic chip,," *Appl. Phys. Lett.,* vol. 98, p. 153512 , 2011.

[143] W. Wang, Y. H. Lin, R. S. Guan, T. C. Wen, T. F. Guo and G. B. Lee, "Bulk-heterojunction polymers in optically-induced dielectrophoretic devices for the manipulation of microparticles,," *Opt. Exp.,* vol. 17, pp. 17603-17613, 2009.

[144] M. Eisenstein, "Divide and conquer," *Nature,* vol. 441, p. 1179–1185 , 2006.

[145] J. Guo, X. Liu, K. Kang, Y. Ai, Z. Wang and Y. Kang, "A Compact Optofluidic Cytometer for Detection and Enumeration of Tumor Cells," *J. of Lightwave Tech.,* vol. 33, pp. 3433-3438 , 2015.

[146] G. M. Whitesides, "The origins and the future of microfluidics," *Nature,* vol. 442, p. 368–373 , 2006.

[147] J. Guo, X. Ma, N. V. Menon, C. M. Li, Y. Zhao and Y. Kang., "Dual fluorescence-activated study of tumor cell apoptosis by an optofluidic system," *IEEE J. Sel. Top. Quantum Electron.,* vol. 21, pp. 392-398 , 2015.

[148] M. M. Wang, D. E. R. E. Tu, J. M. Yang, H. C. Zhang, N. Hagen, B. Dees, E. M. Mercer, A. H. Forster, I. Kariv, P. J. Marchand and W. F. Butler, "Microfluidic sorting of mammalian cells by optical force switching," *Nature Biotechnol.,* vol. 23, p. 83–87 , 2005.

[149] J. W. Chan, "Recent advances in laser tweezers Raman spectroscopy (LTRS) for label-free analysis of single cells," *J. Biophotonics,* vol. 6, pp. 36-48 , 2013.

[150] J. Sun, Y. Kang, E. M. Boczko and X. Jiang, "A Microfluidic Cell Size/Density Sensor by Resistive Pulse Detection," *Electroanalysis,* vol. 25, pp. 1023-1028 , 2013.

[151] J. Guo, L. Chen, Y. Ai, Y. Cheng, C. M. Li, Y. Kang and Z. Wang, "Numerical and experimental characterization of solid-state micropore-based cytometer for detection and enumeration of biological cells," *Electrophoresis,* vol. 36, pp. 737-743 , 2015.

[152] J. Guo, L. Chen, X. Huang, C. M. Li, Y. Ai and Y. Kang, "Dual Characterization of Biological Cells by Optofluidic Microscope and Resistive Pulse Sensor," *Electrophoresis,* vol. 36, p. 420–423 , 2015.

[153] J. Guo, X. Huang and Y. Ai, "On-demand lensless single cell imaging activated by differential resistive pulse sensing," *Anal. Chem.,* vol. 87, pp. 6516-6519 , 2015.

[154] J. Guo, X. Huang, D. Shi, H. Yu, Y. Ai, C. M. Li and Y. Kang, "Portable resistive pulse-activated lens-free cell imaging system," *RSC Advances,* vol. 4, pp. 56342-56345 , 2014.

[155] Y. Song, H. Yin and W. E. Huang, "Raman activated cell sorting," *Curr. Opinion in Chemical Biology*, vol. 33, pp. 1-8 , 2016.

[156] Q. Zhang, P. Zhang, H. Gou, C. Mou, W. E. Huang, M. Yang, J. Xu and B. Ma, "Towards High-throughput Microfluidic Raman-activated Cell Sorting," *Analyst,* vol. 140, p. 6163–6174, 2015.

[157] S. Dochow, C. Krafft, U. Neugebauer, T. Bocklitz, T. Henkel, G. Mayer, J. Albert and J. Popp, "Tumour cell identification by means of Raman spectroscopy in combination with optical traps and microfluidic environments," *Lab Chip,* vol. 11, p. 1484–1490, 2011.

[158] S. Dochow, C. Beleites, T. Henkel, G. Mayer, J. Albert, J. Clement, C. Kraft and J. Popp, "Quartz microfluidic chip for tumour cell identification by Raman spectroscopy in combination with optical traps," *Anal. Bioanal. Chem.*, vol. 405, p. 2743–2746 , 2013.

[159] Z. Pilát, J. Ježeka, J. Kaňka and P. Zemáneka, "Raman tweezers in microfluidic systems for analysis and sorting of living cells," in *Imaging, Manipulation, and Analysis of Biomolecules, Cells, and Tissues XII*, San Francisco, California, United States, 2014.

[160] S. Casabella, P. Scully, N. Goddarda and P. Gardner, "Automated analysis of single cells using Laser Tweezers Raman Spectroscopy," *Analyst,* vol. 141, pp. 689-696 , 2016.

[161] K. C. Neuman, E. H. Chadd, G. F. Liou, K. Bergman and S. M. Block., "Characterization of Photodamage to Escherichia coli in Optical Traps," *Biophy. J.*, vol. 77, p. 2856 –2863, 1999.

[162] S. Ahlawat, N. Kumar, A. Uppal and P. K. Gupta., "Visible Raman excitation laser induced power and exposure dependent effects in red blood cells," *J. Biophotonics,* vol. 10, pp. 415-422, 2017.

[163] P. Zhang, L. Ren, X. Zhang, Y. Shan, Y. Wang, Y. Ji, H. Yin, W. E. Huang, J. Xu and B. Ma, "Raman-Activated Cell Sorting Based on Dielectrophoretic Single-Cell Trap and Release," *Anal. Chem.*, vol. 87, pp. 2282-2289, 2015, .

[164] L. Yang, P. P. Banada, A. K. Bhunia and R. Bashir, "Effects of Dielectrophoresis on growth, viability and immuno-reactivity of Listeria monocytogenes," *J. of Bio. Eng.* , vol. 2, pp. 1-14 , 2008.

[165] U. C. Schroder, A. Ramoji, U. Glaser, S. Sachse, C. Leiterer, A. Csaki, U. Hubner, W. Fritzsche, W. Pfister, M. Bauer, J. Popp and U. Neugebauer, "A combined dielectrophoresis-Raman setup for the classification of pathogens recovered from the urinary tract," *Anal. Chem.,* vol. 85, pp. 10717-10724, 2013.

[166] R. M. Jarvis, N. Law, I. T. Shadi, P. O'Brien, J. R. Lloyd and R. Goodacre., "Surface-enhanced Raman scattering from intracellular and extracellular bacterial locations," *Anal. Chem.*, vol. 80, p. 6741–6746 , 2008.

[167] P. D. maker and R. W. Terhune., "Study of optical effects due to an induced polarization third order in the electric field strength," *Phys. Rev.*, vol. 137, pp. A801-A818 , 1965.

[168] C. L. Evans and X. S. Xie, "Coherent Anti-Stokes Raman Scattering Microscopy: Chemical Imaging for Biology and Medicine," *Annu Rev Anal Chem. (Palo Alto Calif),* vol. 1, p. 883–909 ,

2008.

[169] E. Ploetz, S. Laimgruber, S. Berner, W. Zinth and P. Gilch, “Femtosecond stimulated Raman microscopy,” *Appl. Phys. B,* vol. 87, p. 389–393 , 2007.

[170] C. W. Freudiger, W. Min, B. G. Saar, S. Lu, G. R. Holtom, C. He, J. C. Tsai, J. X. Kang and X. S. Xie, “Label-free biomedical imaging with high sensitivity by Stimulated Raman Scattering Microscopy,” *Science,* vol. 322, p. 1857–1861, 2008.

[171] D. A. Watson, L. O. Brown, D. F. Gaskill, M. Naivar, S. W. Graves, S. K. Doorn and J. P. Nolan, “A Flow Cytometer for the Measurement of Raman Spectra,” *Cytometry A,* vol. 73A, pp. 119-128 , 2008.

[172] I. Freitag, C. Beleites, S. Dochow, J. H. Clement, C. Krafft and J. Poppa, “Recognition of tumor cells by immuno-SERS markers in a microfluidic chip at continuous flow,” *Analyst,* vol. 141, pp. 5986-5989 , 2016.

[173] A. Pallaoro, M. R. Hoonejani, G. B. Braun, C. D. Meinhart and M. Moskovits, “Rapid identification by Surface Enhanced Raman Spectroscopy of cancer cells at low concentrations flowing in a microfluidic channel,” *ACS Nano,* vol. 9, p. 4328–4336, 2015.

[174] W. Lei, W. Jiankang and C. Bo, “Analytic Solution of Liquid flow in rectangular PDMS-GLASS microchannel with wall slip and electroviscous effects,” *Appli. Math. Sc.,* vol. 3, pp. 20195-2214, 2009.

[175] C. A. Lieber and A. M. Jansen, “Automated method for subtraction of fluorescence from biological Raman spectra,” *Appl. Spectrosc.,* vol. 57, p. 1363–1367 , 2003.

[176] D. McIlvenna, W. E. Huang, P. Davison, A. Glidle, J. Coopera and H. Yin, “Continuous cell sorting in a flow based on single cell resonance Raman spectra,” *Lab chip,* vol. 16, pp. 1420-1429, 2016.

[177] J. He and A. Karlsson, “Light scattering by multiple red blood cells,” *J. Opt. Soc. Am. A,* vol. 21, pp. 1953-1961, 2004.

[178] R. C. Gauthier, “Optical trapping: a tool to assist optical machining,” *Opt. & Las. Tech.,* vol. 29, pp. 389-399 , 1997.

[179] I. Sraj, A. C. Szatmary, D. W. M. Marr and C. D. Eggleton, “Dynamic ray tracing for modeling optical cell manipulation,” *Opt. Exp.,* vol. 18, pp. 16702-16714 , 2010.

[180] W. H. Wright, G. J. Sonek and M. W. Berns, “Parametric study of the forces on microspheres held by optical tweezers,” *Appl. Opt. ,* vol. 33, pp. 1735-1748 , 1994.

[181] K. Ramser, J. Engera, M. Goksöra, D. Hanstorp, K. Logg and M. Käll, “A microfluidic system enabling Raman measurements of the oxygenation cycle in single optically trapped red blood cells,” *Lab Chip,* vol. 5, pp. 431-436 , 2005.

[182] C. L. Evans, E. O. Potma, M. P. Haag, D. Coˆte, C. P. Lin and X. S. Xie, “Chemical imaging of tissue in vivo with video-rate coherent anti-Stokes Raman scattering microscopy,” *Proc. Nat.*

Acad. Sci., vol. 102, p. 16807–16812, 2005.

[183] C. H. C. Jr, Y. J. Lee, J. M. Heddleston, C. M. Hartshorn, A. R. H. Walker, J. N. Rich, J. D. Lathia and M. T. Cicerone., "High-speed coherent Raman fingerprint imaging of biological tissues," *Nature Photonics,* vol. 8, pp. 627-634, 2014.

[184] B. G. Saar, C. W. Freudiger, J. Reichman, C. M. Stanley, G. R. Holtom and X. S. Xie., "Video-Rate molecular imaging in vivo with stimulated Raman scattering," *Science,* vol. 330, pp. 1368-1370 , 2010.

[185] K. M. Marzec, D. P. Guaita, M. d. Veij, D. McNaughton, M. Baranska, M. W. A. Dixon, L. Tilley and B. R. Wood, "Red blood cells polarize green laser light revealing Hemoglobin's enhanced non-fundamental Raman modes," *Chem. Phys. Chem.*, vol. 15, p. 3963–3968, 2014.

[186] H. Andersson and A. v. d. Berg, "Microfluidic devices for cellomics: a review," *Sensors and Actuators B,* vol. 92, pp. 315-325 , 2003.

[187] I. R. Vargas, P. R. Montero, R. R. Garcia and K. V. Sepulveda, "Modulated optical sieve for sorting of polydisperse microparticles," *Appl. Phys. Lett.* , vol. 88 , p. 121116, 2006.

[188] P. Jakl, T. Čižmár, M. Šerý and P. Zemánek, "Static optical sorting in a laser interference field," *Appl. Phys. Lett.*, vol. 92, p. 161110 , 2008.

[189] H. C. Berg, Random Walks in Biology, Princeton University Press, 1993.

[190] "MODEL DTD-274HA6 2-AXIS ACOUSTO-OPTIC DEFLECTION SYSTEM," IntraAction Corp., 3719 Warren Avenue, Bellwood, IL. 60104, [Online]. Available: https://intraaction.com/wp-content/themes/Divi/pdf/DTD-274HA6.pdf. [Accessed 02 09 2018].

[191] S. Roy, "Calibration and interfacing of the acousto-optic deflector with LabVIEW for generating optical tweezers array," Indore, 2012.

[192] C. D. a. A. K. P. Schiro, "Large capture-range of a single-beam gradient optical trap," *Opt. Exp.*, vol. 11, pp. 3485-3489 , 2003.

[193] R. Dasgupta, R. S. Verma and P. K. Gupta, "Microfluidic sorting with blinking optical traps," *Opt. Lett.*, vol. 37, pp. 1-4, 2012.

[194] T. Čižmár, M. Šiler, M. Šerý and P. Zemánek, "Optical sorting and detection of submicrometer objects in a motional standing wave," *Phy. Rev. B,* vol. 74, p. 035105, 2006.

[195] R. W. Applegate, J. Squier, T. Vestad, J. Oakey, D. W. M. Marr, P. Bado, M. A. Dugan and A. A. Said, "Microfluidic sorting system based on optical waveguide integration and diode laser bar trapping," *Lab. Chip,* vol. 6, p. 422–426, 2006.

[196] J. R. Kovac and J. Voldman, "Intuitive, image-based cell sorting using opto-fluidic cell sorting," *Anal Chem.*, vol. 79, p. 9321–9330, 2007.

[197] P. H. Biwole, W. Yan, Y. Zhang and J. J. Roux, "A complete 3D particle tracking algorithm and its applications to the indoor airflow study," *Meas. Sci. Technol.*, vol. 20, p. 115403, 2009.

[198] A. A. R. Neves, A. Fontes, C. L. Cesar, A. Camposeo, R. Cingolani and D. Pisignano, "Axial optical trapping efficiency through a dielectric interface," *Phys. Rev. E*, vol. 76, p. 061917, 2007.

[199] S. U. Hwang, Y. H. Park and Y. G. Lee, "Interactive Control of Holographic Optical Traps with Fast Hologram Generation," in *Proc. of IEEE Int. Symp. on Assembly and Manufacturing*, Suwon, Korea, 2009.

[200] M. M. Usategui, E. Pleguezuelos, J. Andilla and E. M. Badosa, "Fast generation of holographic optical tweezers by random mask encoding of Fourier components," *Opt. Exp.*, vol. 14, pp. 2101-2107, 2006.

[201] M. A. Seldowitz, J. P. Allebach and D. W. Sweeney, "Synthesis of digital holograms by direct binary search," *Appl. Opt.*, vol. 26, pp. 2788-2798, 1987.

[202] U. R. Corona, V. M. Arrizon, J. C. Ramirez-San-Juan and R. R. Garcia, "Sorting of microparticles by optical landscapes generated with a spatial light modulator," in *Optical Trapping and Optical Micromanipulation V*, 2008.

[203] G. Sinclair, J. Leach, P. Jordan, G. Gibson, E. Yao, Z. J. Laczik, M. J. Padgett and J. Courtial, " Interactive application in holographic optical tweezers of a multi-plane Gerchberg-Saxton algorithm for three-dimensional light shaping," *Opt. Exp.*, vol. 12, pp. 1665-1670, 2004.

[204] G. C. Spalding, J. Courtial and R. D. Leonardo, "Holographic optical tweezers," in *Structured Light and Its Applications*, Burlington, MA, Academic press, 2008, pp. 139-168.

[205] R. T. Schermer, C. C. Olson, J. P. Coleman and F. Bucholtz, "Laser-induced thermophoresis of individual particles in a viscous liquid," *Opt. Exp.*, vol. 19, pp. 10571-10586, 2011.

[206] K. K. Y. Kim and Y. Park, "Measurement Techniques for Red Blood Cell Deformability: Recent Advances," in *Blood Cell - An Overview of Studies in Hematology* , Rijeka, Croatia, Intech, 2012, p. 168.

[207] S. C. Grover, A. G. Skirtach, R. C. Gauthier and C. P. Grover, "Automated single-cell sorting system based on optical trapping," *J. Biomed. Opt*, vol. 6, pp. 14-22, 2001.

[208] S. K. Mohanty, K. S. Mohanty and P. K. Gupta, "Dynamics of interaction of RBC with optical tweezers," *Opt. Exp.*, vol. 13, pp. 4745-4751, 2005.

[209] X. Hu, P. H. Bessette, J. Qian, C. D. Meinhart, P. S. Daugherty and H. T. Soh, "Marker-specific sorting of rare cells using dielectrophoresis," *PNAS*, vol. 102, p. 15757–15761, 2005.

[210] P. R. C. Gascoyne and J. Vykoukal., "Particle separation by dielectrophoresis," *Electrophoresis* , vol. 23, p. 1973–1983, 2002.

[211] C. Iliescu, G. Tresset and G. Xu, "Dielectrophoretic field-flow method for separating particle populations in a chip with asymmetric electrodes," *Biomicrofluidics* , vol. 3, p. 044104 , 2009.

[212] R. S. Verma, N. Kumar, S.Ahlawat and G. P. K., "Separation of micro particles in a concentrated sample using opto electronic tweezers," in *National Laser Symposium-22*, 2014.

[213] J. A. Dharmadhikari, S. Roy, A. K. Dharmadhikari, S. Sharma and D. Mathur, "Torque-generating malaria-infected red blood cells in an optical trap," *Opt. Exp.,* , vol. 12, pp. 1179-1184 , 2004.

[214] P. Parthasarathi, B. V. Nagesh, Y. Lakkegowda, S. S. Iyengar, S. Ananthamurthy and S. Bhattacharya, "Orientational dynamics of human red blood cells in an optical trap," *J. of Bio-med. Opt.* , vol. 18, p. 025001 , 2013.

[215] A. Ashkin, "Optical trapping and manipulation of neutral particles using lasers," *Proc Natl Acad Sci USA* , vol. 94, pp. 4853-4860, 1997.

[216] K. O. Roberts, T. McKellar, J. Fekete, A. Rakonjac, A. B. Deb and N. Kjærgaard, "Steerable optical tweezers for ultracold atom studies," *Opt. Lett.,* vol. 39, pp. 2012-2015, 2014.